

โครงสร้างและอันตรกิริยาของเกสต์โมเลกุลกับหมู่ซิลานอลบนพื้นผิว (010) ของซีทิกาไลต์-1:  
การคำนวณ โดยวิธีทางเคมีควอนตัม



นางสาวอรพรรณ แสงสว่าง

สถาบันวิทยบริการ  
จุฬาลงกรณ์มหาวิทยาลัย

วิทยานิพนธ์นี้เป็นส่วนหนึ่งของการศึกษาตามหลักสูตรปริญญาวิทยาศาสตรมหาบัณฑิต

สาขาวิชาเคมี ภาควิชาเคมี

คณะวิทยาศาสตร์ จุฬาลงกรณ์มหาวิทยาลัย

ปีการศึกษา 2547

ISBN 974-17-5981-9

ลิขสิทธิ์ของจุฬาลงกรณ์มหาวิทยาลัย

STRUCTURES AND INTERACTIONS OF GUEST MOLECULES WITH  
THE SILANOL GROUPS ON THE (010) SURFACE OF SILICALITE-1  
: QUANTUM CHEMICAL CALCULATIONS



Miss Oraphan Saengsawang

สถาบันวิทยบริการ

จุฬาลงกรณ์มหาวิทยาลัย  
A Thesis Submitted in Partial Fulfillment of the Requirements  
for the Degree of Master of Science in Chemistry

Department of Chemistry

Faculty of Science

Chulalongkorn University

Academic year 2004

ISBN 974-17-5981-9

**Thesis Title** Structures and Interactions of Guest Molecules with the  
Silanol Groups on the (010) Surface of Silicalite-1:  
Quantum Chemical Calculations

**By** Miss Oraphan Saengsawang

**Field of Study** Chemistry

**Thesis Advisor** Associate Professor Supot Hannongbua, Ph. D.

**Thesis Co-advisor** Assistant Professor Tawan Sooknoi, Ph. D.

---

Accepted by the Faculty of Science, Chulalongkorn University in Partial  
Fulfillment of the Requirements for the Master's Degree

..... Dean of the Faculty of Science  
(Professor Piamsak Menasveta, Ph. D.)

THESIS COMMITTEE

..... Chairman  
(Associate Professor Sirirat Kokpol, Ph. D.)

..... Thesis Advisor  
(Associate Professor Supot Hannongbua, Ph. D.)

..... Thesis Co-advisor  
(Assistant Professor Tawan Sooknoi, Ph. D.)

..... Member  
(Associate Professor Vudhichai Parasuk, Ph. D.)

..... Member  
(Amarawan Intasiri, Ph. D.)

อรพรรณ แสงสว่าง: โครงสร้างและอันตรกิริยาของเกสต์โมเลกุลกับหมู่ซิลานอลบนพื้นผิว (010) ของซิลิกาไลต์-1: การคำนวณโดยวิธีทางเคมีควอนตัม (STRUCTURES AND INTERACTIONS OF GUEST MOLECULES WITH THE SILANOL GROUPS ON THE (010) SURFACE OF SILICALITE-1: QUANTUM CHEMICAL CALCULATIONS) อาจารย์ที่ปรึกษา: รศ. ดร. สุพจน์ หารหนองบัว, อาจารย์ที่ปรึกษาร่วม: ผศ. ดร. ตะวัน สุขน้อย, 91 หน้า. ISBN 974-17-5981-9

ได้ทำการศึกษาโครงสร้างและอันตรกิริยาระหว่างเกสต์โมเลกุลซึ่งได้แก่น้ำและมีเทน กับ หมู่ซิลานอลบนพื้นผิวของซิลิกาไลต์-1 โดยวิธีการทางกลศาสตร์ควอนตัม ทั้งนี้ ได้เลือกใช้พื้นผิว (010) ซึ่งเป็นพื้นผิวที่ตั้งฉากกับท่อตรง เลือกแฟรกเมนต์จากส่วนต่าง ๆ ของพื้นผิว เป็นตัวแทนของ ซิลิกาไลต์-1 และการคำนวณด้วยวิธีทางกลศาสตร์ควอนตัม ในระดับต่าง ๆ คือ HF/6-31G(d,p), B3LYP/6-31G(d,p), HF/6-31++G(d,p), B3LYP/6-31++G(d,p) รวมถึง MP2/6-31++G(d,p) สำหรับ มีเทน โดยให้มีการปรับทั้งโครงสร้างของพื้นผิวและโครงสร้างของเกสต์โมเลกุล ผลการศึกษาพบว่า โครงสร้างที่เสถียรที่สุดของน้ำคือ การเกิดพันธะไฮโดรเจน 2 พันธะกับหมู่ซิลานอล 2 หมู่บนพื้นผิว โดยซิลานอล 1 หมู่อยู่บนปากของท่อตรง มีพลังงานเสถียร -13.84 กิโลแคลอรีต่อโมล ข้อมูลข้างต้น ทำให้คาดการณ์ได้ว่า บริเวณดังกล่าวเป็นส่วนแรกของพื้นผิวที่ถูกปกคลุมด้วยโมเลกุลน้ำ เมื่อมี ปริมาณน้ำมากขึ้นบริเวณที่น้ำปกคลุมจะกระจายออกไปอยู่โดยรอบบริเวณปากท่อตรงโดยมีค่าของ พลังงานเสถียรประมาณ -8 กิโลแคลอรีต่อโมล ในรูปของความถี่ของการสั่นของพันธะ O-H ของซิลานอล พบว่า ความถี่มีค่าสั้นลงหลังจากเกิดสารประกอบเชิงซ้อน นอกจากนี้ยังพบว่า พลังงานกีด ขวางในการเคลื่อนโมเลกุลน้ำเข้าสู่ท่อตรงของซิลิกาไลต์ มีค่า 9.08 กิโลแคลอรีต่อโมล สำหรับ โมเลกุลมีเทน ผลที่ได้จะแตกต่างอย่างชัดเจนจากกรณีของน้ำ กล่าวคือ พลังงานการยึดเกาะกับพื้นผิว มีค่าน้อยกว่าการสั่นที่เนื่องมาจากอุณหภูมิ ดังนั้นจึงนำไปสู่ข้อสรุปที่ว่าโมเลกุลมีเทน ไม่ยึดเกาะกับ พื้นผิว (010) ของซิลิกาไลต์-1 นอกจากนี้ยังพบว่า การเคลื่อนที่เข้าสู่ท่อตรงของซิลิกาไลต์-1 สำหรับ โมเลกุลมีเทนไม่มีพลังงานกีดขวาง

ภาควิชา.....เคมี.....ลายมือชื่อนิสิต.....  
 สาขาวิชา.....เคมี.....ลายมือชื่ออาจารย์ที่ปรึกษา.....  
 ปีการศึกษา.....2547.....ลายมือชื่ออาจารย์ที่ปรึกษาร่วม.....

## 4572574323: MAJOR CHEMISTRY

ORAPHAN SAENGSAWANG: STRUCTURES AND INTERACTIONS OF GUEST MOLECULES WITH THE SILANOL GROUPS ON THE (0,1,0) SURFACE OF SILICALITE-1: QUANTUM CHEMICAL CALCULATIONS. THESIS ADVISOR: ASSOC. PROF. SUPOT HANNONGBUA, Ph.D., THESIS CO-ADVISOR: ASST. PROF. TAWAN SOOKNOI, Ph.D., 91 pp. ISBN 974-17-5981-9

Quantum mechanical calculations have been carried out to investigate structural properties and interaction between guest molecules, water and methane, and silanol group on the surface of silicalite-1. The (010) surface which perpendicular to the straight channel, has been selected and represented by three fragments taken from different parts of the surface. Calculations have been performed using different levels of accuracy: HF/6-31G(d,p), B3LYP/6-31G(d,p), HF/6-31++G(d,p), and B3LYP/6-31++G(d,p), including MP2/6-31++G(d,p) for methane. Geometry of the silanol groups as well as those of guest molecules have been fully optimized. The results show that the most stable conformation takes place when a water molecule forms two hydrogen bonds with two silanols, only one lies on the opening pore of the straight channel. The corresponding binding energy is -13.84 kcal/mol. These areas are supposed to be the first binding sites which have to be covered when water molecule approaches the surface. When water loading increases, the next favorable silanols are those of the opening pore in which the four possible complex conformations yield the binding energy of approximately -8 kcal/mol. In terms of vibrational frequency, complexation leads to red shift of the O-H stretching of the silanol group. The estimated energy barrier for water molecule to enter into the silicalite-1's pore is amount to 9.08 kcal/mol. For methane molecule, situation is different. The calculated binding energies are within thermal fluctuation at room temperature. This leads to a clear conclusion that methane molecule does not absorb on the (010) surface of silicalite-1. In addition, the entering process for methane molecule is observed to be barrier free.

Department.....Chemistry.....Student's signature.....  
 Field of study.....Chemistry.....Advisor's signature.....  
 Academic year.....2004.....Co-advisor's signature.....

## ACKNOWLEDGEMENTS

First of all, I would like to give all gratitude affectionately to my beloved parents for all their love, support and encouragement during the whole period of my study. These keep my life always going.

I am truly grateful to Associate Professor Dr. Supot Hannongbua, my advisor, for his multifarious understanding, useful guidance, kind suggestions and encouragement throughout this study. Gratefully thanks to Associate Professor Dr. Tawan Sooknoi, my co-advisor, for good advise. I pass my sincere thanks to Privatdozent Dr. rer. nat. habil. Siegfried Fritzsche, Prof. Dr. rer. nat. habil. Reinhold Haberlandt for all the help and valuable suggestions. I would like to special thanks to Associate Professor Dr. Sirirat Kokpol, Associate Professor Dr. Vudhichai Parasuk and Dr. Amarawan Intasiri who act as the thesis committee. I also would like to thank Dr. Teerakiat Kerdcharoen, Dr. Tawun Remsungnen and Mr. Arthorn Loisruangsin for kind suggestions and discussions.

Finally, I gratefully acknowledge the Computational Chemistry Unit Cell (CCUC) and Computer Center for Advance Research at the Faculty of Science, Chulalongkorn University for computer resources and other facilities. I also gratefully acknowledge the Thailand Research Fund (TRF) and the National Research Council of Thailand (NRCT), the Deutsche Forschungsgemeinschaft (DFG) for financial support during the study.

สถาบันวิทยบริการ  
จุฬาลงกรณ์มหาวิทยาลัย

# CONTENTS

	Pages
<b>ABSTRACT IN THAI</b> .....	iv
<b>ABSTRACT IN ENGLISH</b> .....	v
<b>ACKNOWLEDGEMENTS</b> .....	vi
<b>CONTENTS</b> .....	vii
<b>LIST OF FIGURES</b> .....	x
<b>LIST OF TABLES</b> .....	xii
<b>NOTATIONS</b> .....	xiv
<b>CHAPTER 1 INTRODUCTION</b> .....	1
1.1. Research Rationale.....	1
1.2. Zeolites.....	2
1.2.1. What is a Zeolite?.....	2
1.2.2. Classification of Zeolites.....	3
1.2.3. Applications.....	5
1.2.4. Silicalite-1.....	9
1.3. Silanols.....	10
1.3.1. What is a Silanol?.....	10
1.3.2. Role of Silanol.....	10
1.4. Hydrocarbon and Water in Zeolites.....	12
1.5. Aim of this Study.....	13
<b>CHAPTER 2 THEORY</b> .....	14
2.1. Quantum Mechanics.....	14
2.1.1. Introduction: Basic Molecular Quantum Mechanics.....	14
2.1.2. The Schrödinger Equation.....	15
2.1.3. Born-Oppenheimer Approximation.....	16
2.1.4. <i>Ab initio</i> Methods.....	17
2.1.4.1. Hartree-Fock Theory.....	18

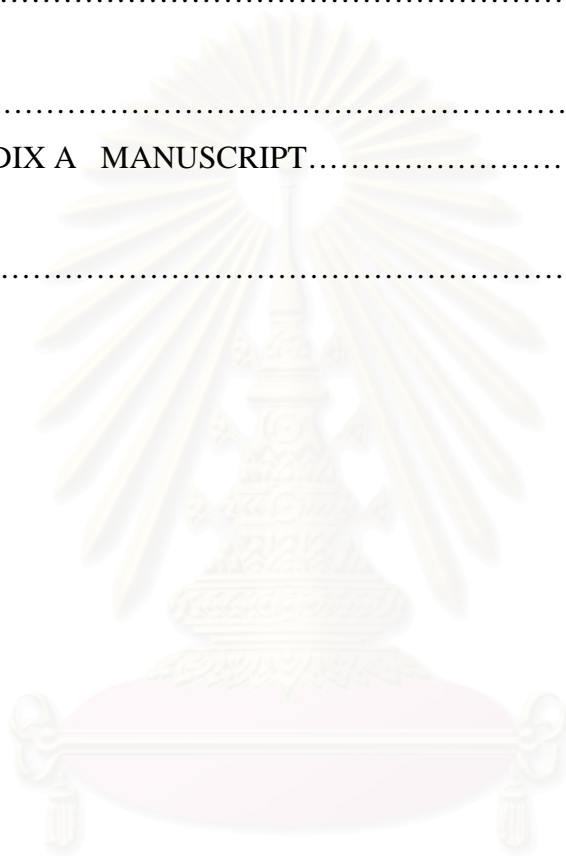
## CONTENTS (cont.)

	Pages
2.1.4.2. Basis Sets.....	22
2.1.5. Møller-Plesset Perturbation Theory.....	27
2.2. Density Functional Theory.....	31
2.2.1. Basic Theory.....	32
2.2.2. Local Density Methods .....	37
2.2.3. Gradient Corrected Methods.....	38
2.2.4. Hybrid Methods.....	40
<b>CHAPTER 3 CALCULATIONS DETAILS .....</b>	<b>42</b>
3.1. Naked Cluster Models.....	42
3.2. Geometries, Interaction Energies and Vibrational Frequencies of the Complexes.....	43
3.2.1. Water Molecules.....	43
3.2.2. Methane Molecules.....	46
3.3. Estimate Energy Barrier.....	48
<b>CHAPTER 4 RESULTS AND DISCUSSIONS.....</b>	<b>51</b>
4.1. Water-Silanol Complexes.....	51
4.1.1. Complexes with Single Silanol.....	51
4.1.1.1. Optimal Method, Basis set and Interaction Energies..	51
4.1.1.2. Geometries and Vibrational Frequencies.....	56
4.1.2. Double Complexes.....	58
4.1.2.1. Interaction Energies.....	58
4.2. Methane-Silanol Complexes.....	61
4.3. The Energy Barrier for Guest Molecules to Enter into Silicalite-1's channel.....	62



**CONTENTS (cont.)**

	Pages
<b>CHAPTER 5 CONCLUSION.....</b>	64
<b>REFERENCES.....</b>	66
<b>APPENDIX.....</b>	73
APPENDIX A MANUSCRIPT.....	74
<b>VITAE.....</b>	91



สถาบันวิทยบริการ  
จุฬาลงกรณ์มหาวิทยาลัย

## LIST OF FIGURES

		Pages
<b>Figure 1.1</b>	From $[\text{SiO}_4]^{4-}$ or $[\text{AlO}_4]^{5-}$ tetrahedral to three-dimensional structures of zeolites.....	2
<b>Figure 1.2</b>	The FAU framework structure .....	3
<b>Figure 1.3</b>	Secondary building units and their symbols where the number in the parenthesis stands for frequency of occurrence [23].....	4
<b>Figure 1.4</b>	Separation of linear hydrocarbons from the mixtures using zeolite A.....	6
<b>Figure 1.5</b>	Shape selectivity of zeolites.....	8
<b>Figure 1.6</b>	Structure and channel system of ZSM-5 and its analogue, silicalite-1.....	9
<b>Figure 1.7</b>	Four types of silanol groups.....	10
<b>Figure 2.1</b>	An acceptable representation of a STO at least 3 GTO's.....	24
<b>Figure 3.1</b>	The (010) surface of silicalite-1 (a) and the three $\text{Si}_4\text{O}_{13}\text{H}_{10}$ (b), $\text{Si}_7\text{O}_{22}\text{H}_{16}$ (c) and $\text{Si}_9\text{O}_{27}\text{H}_{18}$ (d) clusters, used to represent the surface in the quantum chemical calculations to evaluate interactions between guest molecules and single (S1), double-near and double-far silanol groups (S1 and S2), respectively ....	43
<b>Figure 3.2</b>	Four investigated conformations representing interaction between single silanol and one (a-c) and two (d) water molecules.....	44
<b>Figure 3.3</b>	Investigated conformations representing interaction between water molecule and double silanol group: Double-near (a-c) and Double-far (d-e).....	44
<b>Figure 3.4</b>	Investigated conformations representing interaction between methane molecules and the single (a) and double (b) silanol groups on the silicalite-1's surface.....	47

## LIST OF FIGURES (cont.)

		Pages
<b>Figure 3.5</b>	Interaction energy versus water-silicalite-1 distance (a) when a water molecule moves through the center of the straight channel (b) in the four configurations shown in the insert. The dot solid-line represents the optimal route. The results were calculated using the HF method with the 6-31G* basis set and BSSE corrections and taken from Ref. [65].....	49
<b>Figure 3.6</b>	Binding energy when the guest molecule coordinates to the silanol group outside the channel ( $\Delta E_{\text{bind-out}}$ ) and at the center of the channel ( $\Delta E_{\text{bind-in}}$ ) as well as their differences ( $\Delta\Delta E$ ) which were used to estimate the energy barrier ( $\Delta E_{\text{barrier}}$ ) for guest molecule to enter into the straight channel of the silicalite-1 via the (010) surface.....	50
<b>Figure 4.1</b>	(a) The (010) surface of silicalite-1 and (b) with the initial configuration shown in Figure 3d, the B3LYP/6-31++G(d,p) fully optimization procedure brings the water molecule to the new configuration where water molecule prefers more to coordinate to S3 (see Figure 1d) than that to S2.....	60
<b>Figure 4.2</b>	Binding energy when the guest molecule coordinates to the silanol group outside the channel ( $\Delta E_{\text{bind-out}}$ ) and at the center of the channel ( $\Delta E_{\text{bind-in}}$ ) as well as their differences ( $\Delta\Delta E$ ) which were used to estimate the energy barrier ( $\Delta E_{\text{barrier}}$ ) for water (a) and methane molecule (b) to enter into the straight channel of the silicalite-1 via the (010) surface.....	63

## LIST OF TABLES

		Pages
<b>Table 1.1</b>	Characteristics of some typical porous materials.....	5
<b>Table 4.1</b>	Interaction and deformation energies (kcal/mol) representing complexation between water and single silanol groups in the configurations shown in Figure 3.2 where the surface geometry (Figure 3.1b) was optimized using the HF/3-21G* while the energy was calculated using different levels of accuracy.....	52
<b>Table 4.2</b>	Optimal geometry, O-H bond length (Å) and Si-O-H bond angle (in degree), and atomic net charges (in atomic unit), $q_i$ where $i$ denotes H, O and Si atoms, of the single silanol in free form yielded from different calculations.....	53
<b>Table 4.3</b>	Interaction and deformation energies (kcal/mol) representing complexation between water and single silanol groups in the configurations shown in Figure 3.2 where the surface optimization and the energy calculations were performed using the same levels of accuracy.....	55
<b>Table 4.4</b>	Bond length, bond angle and stretching frequency ( $\nu$ ) of water, naked surface and complex between water and single silanol group (Figure 2) using different methods of calculation where subscript “s” and “w” stand for surface and water molecule, respectively. The B3LYP/6-31++G(d,p) data, bold line, were proposed to be the optimal values.....	56
<b>Table 4.5</b>	The deformation energy and binding energy (kcal/mol) representing interaction between water and two silanol groups in the configurations shown in Figure 3 where the surface optimization and the energy calculations were performed using B3LYP/6-31++G(d,p).....	59

## LIST OF TABLES (cont.)

		Pages
<b>Table 4.6</b>	The deformation energy and binding energy (kcal/mol) representing interaction between methane and silanol group in the configurations shown in Figure 3.2 where the surface optimization and the energy calculations were performed using HF/6-31G(d,p), B3LYP/6-31++G(d,p) and MP2/6-31G(d).....	61
<b>Table 4.7</b>	Optimal binding energy (kcal/mol) on the surface ( $\Delta E_{\text{bind-out}}$ ), optimal binding energy inside the pore ( $\Delta E_{\text{bind-in}}$ ), $\Delta\Delta E$ (see Figure 3.6) and the estimated energy barrier ( $\Delta E_{\text{barrier}}$ ) for H <sub>2</sub> O and CH <sub>4</sub> molecules to enter into the straight channel via the (010) surface of the silicalite-1.....	62

# NOTATIONS

## Sections

### INTRODUCTION

FAU	Faujasite	1.1
MFI	Mobile Five zeolite	1.1
ZSM-22	Zeolite Socolony Mobile-22	1.1
FTIR	Fourier Transform Infrared	1.1
IZA	International Zeolite Association	1.2.2
SBU	Secondary building unit	1.2.2
ZSM-5	Zeolite Socolony Mobile-5	1.2.4
HF	Hartree-Fock	1.5
DFT	Density Functional Theory	1.5
MP2	second-order Møller-Plesset Perturbation Theory	1.5

### THEORY

#### QUANTUM MECHANICS

$\Psi$	Wave function	2.1.2
$t$	Time	2.1.2
$m$	Mass of the particle	2.1.2
$h$	Planck's constant	2.1.2
$V$	Potential field	2.1.2
$\hat{H}$	Hamiltonian	2.1.2
$E$	Total energy	2.1.2
$M_A$	Ratio of mass of nucleus $A$ to the mass of an electron	2.1.2
$Z_A$	Atomic number of nucleus $A$	2.1.2
BO	Born-Oppenheimer	2.1.3
$\hat{H}_{elec}$	Electronic Hamiltonian	2.1.3

## NOTATIONS (cont.)

		<b>Sections</b>
$\Psi_{elec}$	Electronic wave function	2.1.3
$E_{elec}$	Electronic energy	2.1.3
HF-SCF	Hartree-Fock self consistent field	2.1.4
$\varphi_i$	One-electron space wave functions	2.1.4.1
$\alpha, \beta$	Spin functions	2.1.4.1
$\hat{H}^{eff}$	Hartree-Fock Hamiltonian	2.1.4.1
$\hat{f}$	Fock operator	2.1.4.1
$\hat{J}$	Coulomb operator	2.1.4.1
$\hat{K}$	Exchange operator	2.1.4.1
$\varepsilon_i$	Orbital energy of the electron	2.1.4.1
$E^{HF}$	Energy of the molecule in term of the Hartree-Fock	2.1.4.1
$\phi_\mu$	Atomic orbitals	2.1.4.1
LCAO	Linear combination of atomic orbitals	2.1.4.1
$\mu$	Specific atomic orbital wavefunction	2.1.4.1
$i$	Specific molecular orbital	2.1.4.1
$c_{\mu i}$	Coefficients of the contribution	2.1.4.1
$F_{\mu\nu}$	Fock matrix	2.1.4.1
$S_{\mu\nu}$	Overlap matrix	2.1.4.1
C	Matrix of molecular orbital expansion coefficients	2.1.4.1
SCF	self-consistent field	2.1.4.1
STO's	Slater-type orbitals	2.1.4.2
$e^{-\zeta r}$	Radial part of orbital	2.1.4.2
$N$	Normalization constant	2.1.4.2
$\zeta$	Exponent	2.1.4.2
$r, \theta, \phi$	Spherical coordinates	2.1.4.2

## NOTATIONS (cont.)

		<b>Sections</b>
$Y_{lm}$	Angular momentum part	2.1.4.2
$n, l, m$	principal, angular momentum, magnetic quantum numbers	2.1.4.2
GTO's	Gaussian-type orbitals	2.1.4.2
$x, y, z$	Cartesian coordinates	2.1.4.2
DZ	Double-zeta basis set	2.1.4.2
3-21G	Split valence basis sets	2.1.4.2
6-311G	Triple split valence basis sets	2.1.4.2
DZP	Double-zeta plus polarization basis set	2.1.4.2
6-31G*	split valence double-zeta plus polarization basis set	2.1.4.2
<i>CI</i>	Configuration Interaction	2.1.4.2
<i>MPn</i>	Møller-Plesset Perturbation	2.1.4.2
$H_0$	Unperturbed Hamiltonian	2.1.5
$\lambda$	Formal parameter	2.1.5

### DENSITY FUNCTIONAL THEORY

$V_{\text{ext}}(\mathbf{r})$	External potential	2.2.1
$\rho(\mathbf{r})$	Electron density	2.2.1
$T(\rho)$	Kinetic energy	2.2.1
$V(\rho)$	Potential energy	2.2.1
$E(\rho)$	Total energy	2.2.1
$E_{\text{NE}}[\rho]$	Electron-nuclei attraction potential energy	2.2.1
$E_{\text{ee}}[\rho]$	Electron-electron repulsion energy	2.2.1
$F_{\text{HK}}$	Universal functional	2.2.1
$E_{\text{ncl}}$	Non-classical contribution to electron-electron interaction	2.2.1
$\tilde{\rho}$	Trial density	2.2.1



## NOTATIONS (cont.)

		<b>Sections</b>
$F[\rho]$	Universal functional	2.2.1
$\psi_i$	Orbitals of the non-interacting system	2.2.1
$E_{XC}$	Exchange-correlation energy	2.2.1
$\psi_i(r)$	Single-particle wave function	2.2.1
LDA	Local Density Approximation	2.2.2
LSDA	Local Spin Density Approximation	2.2.2
VWN	Vosko, Wilk and Nusair	2.2.2
GGA	Generalized Gradient Approximation	2.2.3
PW86	Perdew and Wang	2.2.3
LYP	Lee, Yang and Parr	2.2.3
ACF	Adiabatic Connection Formula	2.2.4
ACM	Adiabatic Connection Model	2.2.4
B3	Becke 3 parameter functional	2.2.4

## CALCULATION DETAILS

$\Delta E_{\text{bind}}$	Binding energy	3.2.1
$\Delta E_{\text{deform}}$	Deformation energy	3.2.1
$\Delta E_{\text{interact}}$	Interaction energy	3.2.1
$\Delta E_{\text{bind-in}}$	Optimal binding energy when guest molecules locate inside the straight channel of the silicalite-1	3.3
$\Delta E_{\text{bind-out}}$	Optimal binding energy outside the channel	3.3
$\Delta E_{\text{barrier}}$	Energy barrier	3.3
$\Delta \Delta E$	Energetic difference between the $\Delta E_{\text{bind-in}}$ and $\Delta E_{\text{bind-out}}$	3.3

## RESULTS AND DISCUSSION

$\nu$	Stretching frequency	4.1.1.2
-------	----------------------	---------

# CHAPTER 1

## INTRODUCTION

### 1.1. Research Rationale

Zeolites are microporous aluminosilicate materials which have numerous properties that are appropriate for catalysis and separation. The high porosity and the very regular system of pores lead to beneficial characteristics of these materials as for example shape selectivity and catalytic properties. However, before the activities in the pore can take place, the guest molecules have to diffuse into the pore opening of the zeolite that means they have to interact with the external surface. Only very recently the problem of approach and penetration of guest molecules at the zeolite surface started to be investigated. There exists experimental evidence which shows the significant role of external and internal surfaces and the very complicated nature of their interplay in the shape-size selective catalysis. Turro and coworkers used a combination of different spectroscopic techniques to show the very complicated nature of the shape-size selected catalysis of photolysis reactions of many ketone molecules by FAU and MFI as caused by the external and internal surface [1,2]. Isomerization of 1, 2, 4-trimethylbenzene over zeolite NU-87 was observed to take place mainly on the external surface [3] while alkylation of biphenyl over various zeolites was observed only on the external surfaces [4,5]. The external surface also contributes to adsorption of C<sub>6</sub>-C<sub>9</sub> *n*-alkanes on Pt/H-ZSM-22 [6].

It is known that the key elements determining the adsorption and diffusion behavior of guest molecules on the external surfaces are silanol groups. Most of the information regarding characteristics of silanol on the external surface of zeolites arises from FTIR experiments [7]. It was found that the open surfaces of most of the zeolitic and amorphous silica materials are covered by the silanol groups.

Non-cationic zeolites, in particular silicalite-1 are widely used in the separation of mixtures of light hydrocarbons with water or other polar solvents. It should be noted that the internal surface of perfect silicalite-1 is hydrophobic whereas

the external surface is hydrophilic attributable to terminal silanol groups which can interact with guest molecules. Several FTIR experiments expose that the O-H bond of silanol groups is softened when interacting with nitriles [8-11], alcohols [12], water [13], pyridine [14] and even with aliphatic and aromatic hydrocarbons [10]. However, most of the experimental and theoretical works focus on the internal surface that means the pore or channel whereas much less is known about the details of the external surface.

## 1.2. Zeolites

### 1.2.1. What is a Zeolite?

A zeolite was first discovered in 1756s by a Swedish mineralogist, named Cronstedt [15]. Zeolites [16-18] are crystalline and micro-porous aluminosilicates of the alkali or alkali earth metals (predominantly sodium, potassium, magnesium and calcium) that are built up from an infinitely extending three-dimensional network arising from framework of  $[\text{SiO}_4]^{4-}$  and  $[\text{AlO}_4]^{5-}$  tetrahedral linked to each other by the sharing of oxygen atom.

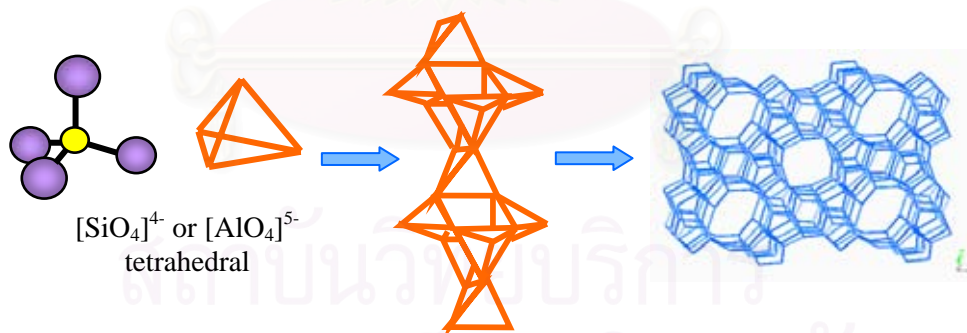


**Figure 1.1** From  $[\text{SiO}_4]^{4-}$  or  $[\text{AlO}_4]^{5-}$  tetrahedral to three-dimensional structures of zeolites.

This (-Si-O-Al-) linkages form pores of uniform diameter and enclose regular internal cavities and channels of different sizes and shapes, depending on the chemical composition and the crystal structure of the specific zeolite involved. These

cavities can be occupied by cations, water or other molecules. The cations can be mobile and may usually be exchanged by other cations.

The presence of  $[\text{AlO}_4]^{5-}$  tetrahedral in the framework introduces negative charges into the structure of zeolites, which are usually compensated by protons, metal cations or  $\text{NH}_4^+$ . The presence of different compensation cations leads to different redox or acidic and basic properties of zeolites which can be used as potential catalytic materials for oxidation, reduction or acid (base)-catalyzed reactions.

### 1.2.2. Classification of Zeolites

Zeolites [19] are a well-defined class of crystalline naturally occurring aluminosilicate materials. Approximately 40 natural zeolites have been found and more than 150 zeolites were synthesized [20,21]. Originally, zeolites are named by Framework Type Codes which are an identification by three capital letters used by the International Zeolite Association (IZA). The codes only describe and define the framework based on their overall topology. A list of framework codes for zeolites can be found in the *Atlas of Zeolite Structure Types* by Meier et al. 1996 [22]. An example of framework code was shown in Figure 1.2 where faujasite and all other zeolites that have the same topology were named as FAU.

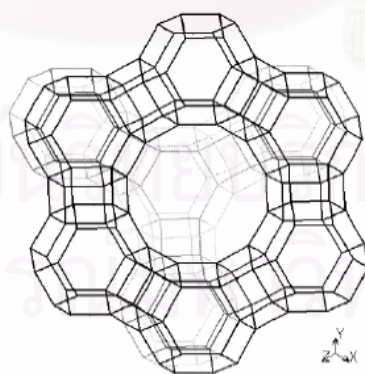


**Figure 1.2** The FAU framework structure.

Principally, zeolites can be classified according to structural building units called “secondary building unit” (SBU) with the primary building unit being the

tetrahedron. The SBU is the geometric arrangement of the primary unit tetrahedron. There are nine such building units, which can be used to describe all of the known zeolite structures. These secondary building units consist of 4, 6, and 8-member single rings, 4-4, 6-6, and 8-8-member double rings, and 4-1, 5-1, and 4-4-1 branched rings. Some topologies of these units are shown in Figure 1.3. The tetrahedron units can be arranged in rings, chains, sheets or complex frameworks taking into account various types and sizes of cavities that lead to their different properties for each zeolite.

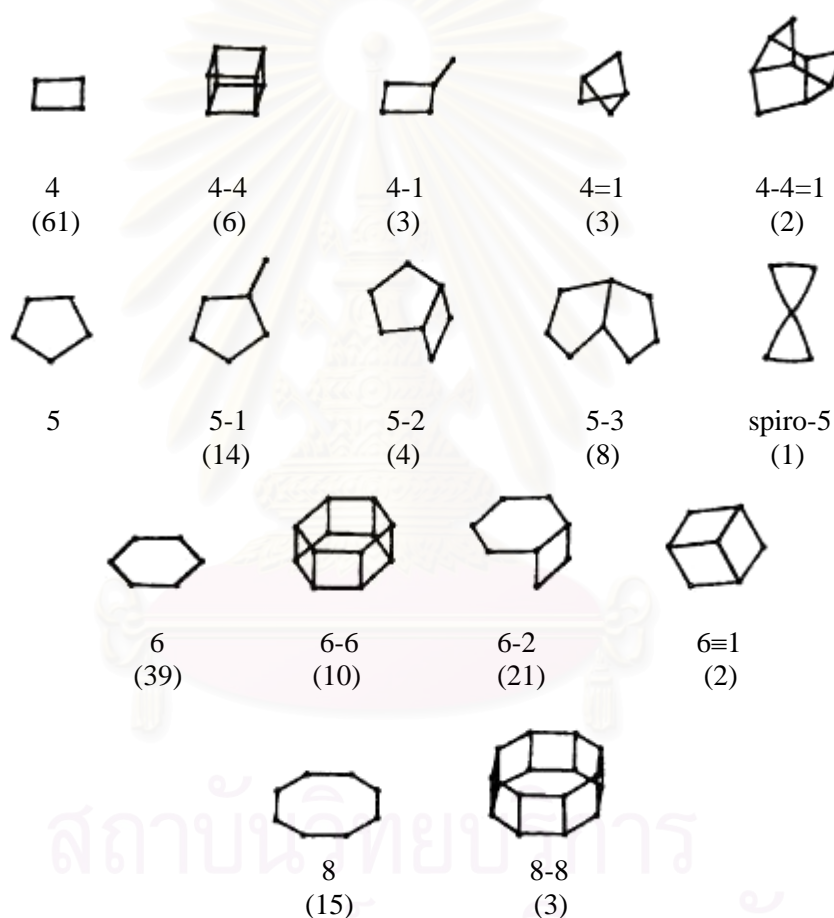


**Figure 1.3** Secondary building units and their symbols where the number in the parenthesis stands for frequency of occurrence [23].

Generally, zeolites can also be classified, according to their pore sizes, into small, medium, large and ultralarge pore systems. The corresponding number of tetrahedral (membered ring) are 6, 8, 9 for small; 10 for medium; 12 for large; and 14,

18, 20 for untrularge structures. The characteristics of some typical zeolites are listed in Table 1.1 [24].

**Table 1.1** Characteristics of some typical porous materials.

Zeolite	Number of rings	Pore size ( $\text{\AA}^2$ )	Pore/channel structure
<b>8-membered oxygen ring</b>			
Erionite	8	3.6x5.1	Intersecting
<b>10-membered oxygen ring</b>			
ZSM-5	10	5.1x5.6	Intersecting
ZSM-11	10	5.3x5.4	Intersecting
<b>Dual pore system</b>			
Ferrierite	10,8	4.2x5.4 3.5x4.8	One dimensional 10:8 intersecting
Mordenite	12 8	6.5x7.0 2.6x5.7	One dimensional 12:8 intersecting
<b>12-membered oxygen ring</b>			
ZSM-12	12	5.5x5.9	One dimensional
Faujasite	12	7.4 7.4x6.5	Intersecting 12:12 intersecting
<b>Mesoporous system</b>			
VPI-5	18	12.1	One dimensional
MCM41-S	-	16-100	One dimensional

### 1.2.3. Applications

For comprehensive applications of zeolitic materials, they show remarkable advantages over other solid materials:

- (i) Zeolites are well defined structures which can be clearly related to the activity and selectivity.
- (ii) Zeolites have well defined inner pores in which active species can be occupied.
- (iii) Zeolites can adjust framework composition and cations associated with different stability, hydrophilicity / hydrophobicity and acid-base properties.

- (iv) Zeolites are of various structure types which can be chosen as shape-selective catalysts for different reactions.

Principally, the comprehensive applications of zeolites regarding to their basis properties can be categorized in three groups:

### 1. Molecular sieve

A “molecular sieve” [25] is a material with selective adsorption properties capable of separating components of a mixture on the basis of a difference in molecular size and shape. Molecular sieves include clays, porous glasses, microporous charcoals, active carbons, etc. Zeolite are selective, high-capacity adsorbents because of their high intracrystalline surface area and strong interactions with adsorbates. Molecules of different size generally have different diffusion properties in the same sieve. Molecules are separated on the basis of size and structure relative to the size and geometry of the apertures of the sieve. An example of this is the separation of linear hydrocarbons from the mixtures of branch and cyclic hydrocarbons as shown in Figure 1.4 [14]. Molecular sieves adsorb molecules, in particular those with a permanent dipole moments, and exhibit other interactions not found in other sorbents. Different polar molecules have a different interaction with the molecular sieve framework and may thus be separated by a particular molecular sieve. This is one of the major uses of zeolites. An example is the separation of  $N_2$  and  $O_2$  in the air on zeolite A, by exploiting different polarities of the two molecules [16].

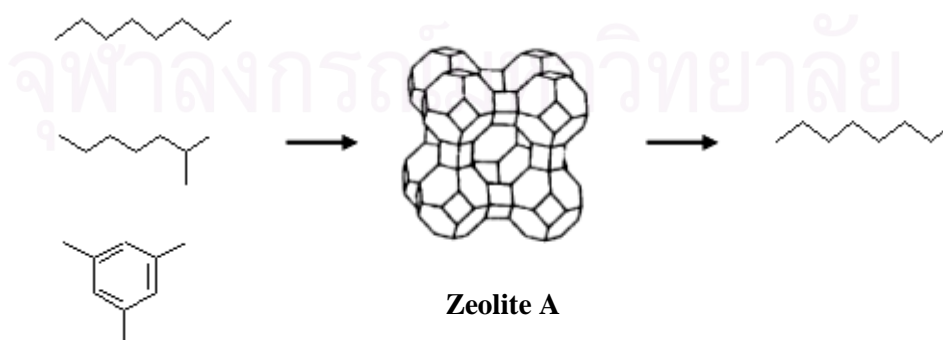


**Figure 1.4** Separation of linear hydrocarbons from the mixtures using zeolite A.

## 2. Ion exchanger

Zeolites with low Si/Al ratios have strongly polar anionic frameworks. The exchangeable cations create strong local electrostatic fields and interact with highly polar molecules such as water. The cation-exchange behavior of zeolites depends on (i) the nature of the cation species, the cation size (both anhydrous and hydrated) and cation charge, (ii) the temperature, (iii) the concentration of the cationic species in the solution, (iv) the anion associated with the cation in solution, (v) the solvent (most exchange has been carried out in aqueous solutions, although some work has been done in organics), and (vi) the structural characteristics of the particular zeolite.

Cation exchange in a zeolite is accompanied by an alteration of stability, adsorption behavior, catalytic activity and other properties. In some cases, the introduction of a larger or smaller cation will decrease or enlarge the pore opening. The location of cation within the crystal will also contribute to the size of pore opening. For example, the  $\text{Na}^+$  form of zeolite A has a smaller effective pore dimension than would be expected for its 8-membered ring framework opening. This is due to sodium ion occupancy of sites where it will partially block the 8-membered ring window. When the  $\text{Na}^+$  is exchanged for the larger  $\text{K}^+$ , the pore diameter is reduced so that only the very small polar molecules will be adsorbed. If the divalent  $\text{Ca}^{2+}$  is used to balance of the framework charge, the effective pore opening widens, as only half the number of cations are needed. These ions occupy sites within the voids of the zeolite and do not reduce the effective pore diameter of the 8-membered ring. Highly and purely siliceous molecular sieves have virtually neutral frameworks, exhibit a high degree of hydrophobicity and no ion-exchange capacity.

## 3. Heterogeneous catalysis

The most important application of zeolites is as catalysts. Zeolites combine high acidity with shape selectivity, high surface area and high thermal stability and have been used to catalyse a variety of hydrocarbon reactions, such as cracking, hydrocracking, alkylation and isomerisation. The reactivity and selectivity of



zeolites as catalysts are determined by the active sites arising from a charge imbalance between the silicon and aluminium atoms in the framework. Each framework aluminium atom induces a potential active acid site called Lewis acid site. Moreover, there exist also the Brønsted acid sites which have weak acidity on the external surface of the zeolite.

In addition, shape selectivity, including reactant, product and transition-state shape selectivity [26], which are described in Figure 1.5, play a very important role in zeolite catalysis.

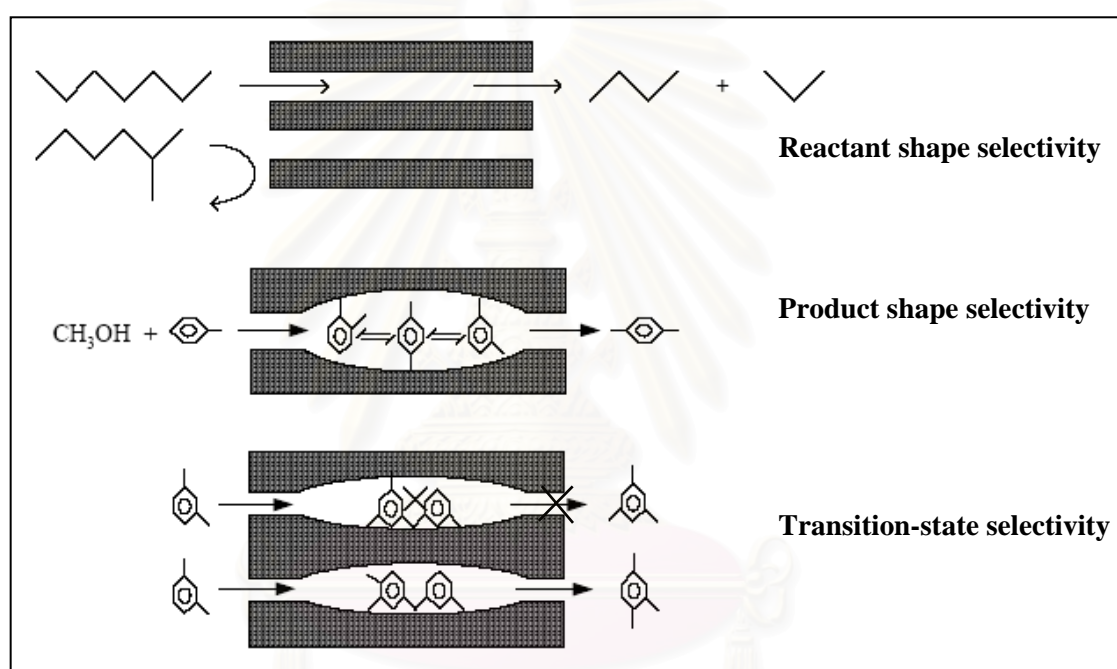


**Figure 1.5** Shape selectivity of zeolites.

Different sizes of channels and cages may therefore promote the diffusion of different reactants, products and transition-state species. High crystallinity and the regular channel structure are the principal features of catalysts. Reactant shape selectivity results from the limited diffusivity of some of the reactants, which cannot effectively enter and diffuse inside the crystal. Product shape selectivity occurs when slowly diffusing product molecules cannot rapidly escape from the crystal, and undergo secondary reactions. Restricted transition-state shape selectivity is a kinetic effect arising from the local environment around the active site. The rate constant for a

certain reaction mechanism is reduced if the necessary transition state is too bulky to form readily.

#### 1.2.4. Silicalite-1

Silicalite-1 is a pure silica analogue of zeolite ZSM-5 which is an MFI type material. The symmetry group of silicalite-1 is  $Pnma$  with cell parameters  $a = 20.07 \text{ \AA}$ ,  $b = 19.92 \text{ \AA}$  and  $c = 13.42 \text{ \AA}$ . The structure of the ZSM-5 zeolite and its analogue, silicalite-1, shown in Figure 1.6, has 10-membered oxygen rings and contains two types of channel systems with similar size: straight channels ( $5.4 \times 5.6 \text{ \AA}^2$ ) and sinusoidal (zigzag) channels ( $5.1 \times 5.4 \text{ \AA}^2$ ) [27]. The diameters of these channels are about  $5.4 \text{ \AA}$ . These two different channels are perpendicular to each other and generate intersection areas which have  $8.9 \text{ \AA}$  of diameter. The difference between zeolites and silicalite-1 is that zeolite has a  $\text{SiO}_2/\text{Al}_2\text{O}_3$  ratio with at least one aluminium per unit cell, whereas, silicalite-1 contains only silica and oxygen atoms. Silicalite-1 is thus an effective adsorbent for organic molecules, whereas ZSM-5 is less effective in this aspect [28]. Accordingly, silicalite-1 can not be considered as a zeolite, by definition, but rather as a silica molecular sieve. Silica molecular sieves such as silicalite-1 have a neutral framework which are hydrophobic in nature and have no ion exchange or catalytic properties. Silicalite-1 is widely used to separate paraffin or aromatics from water or other polar solvent as well as to sieve the molecules having different shapes [29-31].

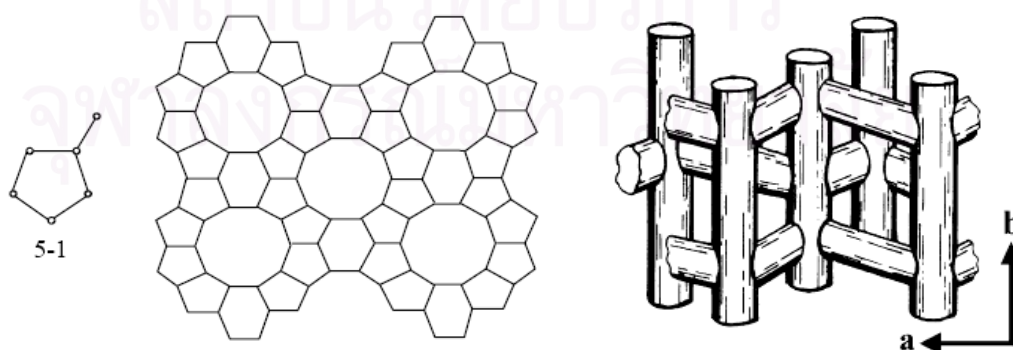


**Figure 1.6** Structure and channel system of ZSM-5 and its analogue, silicalite-1.

### 1.3. Silanols

#### 1.3.1. What is a Silanol?

Silanol is a hydroxyl group that is connected with a silicon atom (Si-OH). Silanols are usually classified into four types [32], namely, (i) the isolated silanol groups, (ii) the vicinal pair, where silanol groups can form hydrogen bonds with each other, (iii) the geminal species, where two hydroxyls sit on the same Si atom and (iv) the silanol groups that can form a hydrogen bond through a bridging water molecule. (see Figure 1.7)

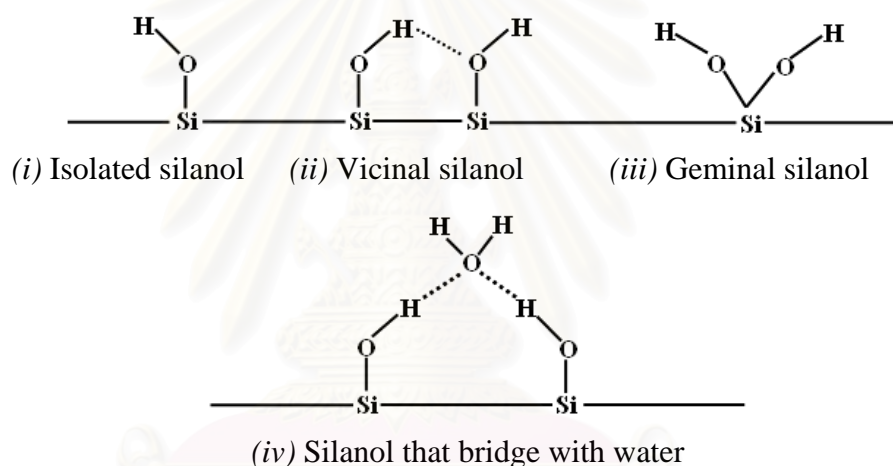


**Figure 1.7** Four types of silanol groups.

For the aluminosilicate zeolite, principally, two types of terminal silanol groups are detected, the normal (Si-OH) and bridging silanols (Si-OH-Al).

#### 1.3.2. Role of Silanol

Many experimental works proposed that the bridging silanols have a tendency to exist only inside the pore [3-6]. Trombetta and coworkers suggest a scheme demonstrating the preference of normal silanols over the bridging one at the external surface which can explain the unusual acidity of these terminal silanol groups [8]. In contrast, it is under discussion whether the normal silanols, which usually cover

the external surface of zeolites and open surface of silica and alumina-silica materials, also exist inside the pore too. It must be noted that spectral analysis of the vibrational frequencies seem to be the only prime evidence. Therefore, drawing conclusion from this limited information resource can be incorreced. For examples, previous vibrational spectra of terminal silanols of silicalite even suggest that there is no silanol group at the external surface (this was based on the assumption [7] that silanol groups of zeolites have the same OH stretching frequency as amorphous silica at  $3747\text{ cm}^{-1}$ ) [33]. In that work, the lower stretching frequency of  $3735\text{ cm}^{-1}$  was assigned to silanol groups inside the pore since this peak does not disappear after probing with water. However, recent experiment assigns this peak to silanols at the external surface according to its disappearance after probing with different nitriles that can not penetrate into the pores [9]. The same peak observed in the previous work is therefore attributed to the silanols at the extraframework of silicalite, not inside the internal pores. Unfortunately, they can not explain why the peak has unusually low frequency ( $3735\text{ cm}^{-1}$  versus  $3747\text{ cm}^{-1}$  for the amorphous silica). Based on this new perspective, there would be no silanol group inside the pore of pure silica zeolites.

At this step, the proposal that there is no normal silanol group in the internal pores of pure silica zeolites is well supported. In the case of the alumina-containing zeolites, FTIR studies on H-ZSM5 zeolites observed a small shoulder at  $3730\text{ cm}^{-1}$  and it was assigned to free silanol in the pores [10,14]. Later, it turns out to be only a misinterpretation biased in order to coincide with earlier experiments. In fact, this almost negligible band comes from the silanols at the external surface but it is not yet clear why this shoulder emerges [9,11]. One of the explanation is according to the extraframework defects.

At this moment, studies on the structure and dynamics of silanol groups are rare. Based on the available data, the silanols tend to be flexible and mostly free of adsorption. Weak interactions between the adjacent silanol groups via soft H-bonding is also observed [9]. Provided a proper geometry, the adjacent silanol groups can form hydrophobic hydroxyl nest as those found in a defect Faujasite undergoing hydrothermal and acid treatment [34].

#### 1.4. Hydrocarbon and Water in Zeolites

Zeolites are most widely used for catalysts in industry and have become extremely successful catalysts for oil refining, petrochemistry and organic synthesis in the production of fine and special chemicals especially when dealing with molecules having kinetic diameters below 10 Å [35]. The application of zeolites in petrochemical processes occurs in two main areas: the production of olefins and derived products and the production of aromatics. In many production lines for important commodities such as styrene and related polymers, nylon, polyurethane plastics and foams and polyesters, zeolite catalysts could help in improving performances and reducing environment impact, for instance by substituting mineral acid catalysts [36].

Alkanes in zeolites play an important role in many industrial applications [17] because the effectivity of the technical processes is usually limited by the slow migration of guest molecules through the channels and cavities of the zeolites. Numerous investigations of the diffusive properties of alkanes in zeolites have been reported using both experimental and theoretical approaches [17,37-42]. Such studies are a challenge to fundamental research because discrepancies between results obtained from different experimental methods are not yet understood.

Regarding to the fact that even small amounts of water, one of the most common substances found in zeolites, can significantly influence properties of zeolite like materials during some technological processes [43,44]. Interest in the water-zeolite interaction arises from the fact that water plays a strong and essential role for both adsorption and catalytic properties of zeolites [45,46] as it is known that all natural zeolites are hydrated. In addition, water molecules assist the exchange of the charge-compensating cations, which are essential for the industrial catalysts.

### 1.5. Aim of this Study

In this study, interaction between silanol group on the external (010) surface which is perpendicular to the straight channel of silicalite-1 and guest molecules which are water and methane molecules have been investigated. The energetic and geometric properties have been calculated using quantum chemical methods at the Hartree-Fock (HF), density functional theory (DFT) and second-order Møller-Plesset perturbation theory (MP2) levels. The calculated vibrational frequencies have been additionally evaluated for water molecules and compared with the experimental data. In addition, the energy barrier for guest molecules to enter into silicalite-1's channel have been estimated.

The obtained results provide basic knowledge in molecular level on the adsorption and transport of guest molecule leading to a clear understanding of molecule behavior in moving from the external surface to the pore of zeolite. This will benefit directly to the research and development and, hence, an application of zeolite in the catalytic as well as separation processes.



สถาบันวิทยบริการ  
จุฬาลงกรณ์มหาวิทยาลัย

## CHAPTER 2

### THEORY

#### 2.1. Quantum Mechanics

##### 2.1.1. Introduction: Basic Molecular Quantum Mechanics

The classical mechanics, which is founded on the laws of Newton, is the laws of motions of macroscopic objects [47]. In the late nineteenth century, the physicists found that classical mechanics does not correctly describe the behavior of very small particles such as the electrons and nuclei of atoms and molecules. The various phenomena, for instance black-body radiation, heat capacity of solids at low temperature, atomic spectra, and the structure of the hydrogen atom, could not be explained by classical mechanics but they had to be treated by new physics schemes. Since the electrons and other microscopic “particles” show wave-like as well as particle-like behavior, which implies that electrons do presently obey classical mechanics, the fusion of the apparently complementary concepts of waves and particles was started by De Broglie and carried to fulfillment in the quantum mechanics [48-52] of Heisenberg and Schrödinger. Nevertheless, the uncertainty principle of Heisenberg, which is authentically the limitation of the obtained microscopic information of a system, seems to be essential as the consequences of the wave-particle duality.

The first part of this chapter provides an introductory overview of the theory underlying the Schrödinger equation and the Born-Oppenheimer approximation. The second part describes the molecular quantum mechanics methods comprising *ab initio* method and Møller-Plesset perturbation theory. Moreover, the density functional theory also has been taken into account within this part.

### 2.1.2. The Schrödinger Equation

Quantum mechanics explains how entities like electrons have both particle-like and wave-like characteristics. The state of a quantum mechanical system is described by a state function or wave function  $\Psi$  of the particle, which is a function of the coordinates of all the particles in the system as well as the time,  $t$ . The state function changes with time according to the time-dependent Schrödinger equation, which for a one-particle, one-dimensional system is Equation (2.1).

$$\left\{ \frac{-h^2}{8\pi^2 m} \nabla^2 + \mathbf{V} \right\} \Psi(\bar{\mathbf{r}}, t) = \frac{i\hbar}{2\pi} \frac{\partial \Psi(\bar{\mathbf{r}}, t)}{\partial t} \quad (2.1)$$

In this equation,  $\Psi$  is the wave function,  $m$  is the mass of the particle,  $h$  is Planck's constant, and  $\mathbf{V}$  is the potential field in which the particle is moving. The product of  $\Psi$  with its complex conjugate ( $\Psi^* \Psi$ , often written as  $|\Psi|^2$ ) is interpreted as the probability distribution of the particle. The energy and many other properties of the particle can be obtained by solving the Schrödinger equation for  $\Psi$ , subject to the appropriate boundary conditions. Many different wavefunctions are solutions to it, corresponding to different stationary states of the system.

If  $\mathbf{V}$  is not a function of time, the Schrödinger equation can be simplified using the mathematical technique known as separation of variables. Frequently, the time-dependent wavefunction can be written as the product of a time-independent wavefunction,  $\Psi(\bar{\mathbf{r}})$  and a time function,  $\tau(t)$ .

$$\Psi(\bar{\mathbf{r}}, t) = \Psi(\bar{\mathbf{r}}) \tau(t) \quad (2.2)$$

and, then, new functions as in Equation (2.2) are substituted into Equation (2.1), the results obtain two equations, one of which depends on the position of the particle independent of time and the other of which is a function of time alone. For the problems in which this separation is valid, the familiar time-independent Schrödinger equation is performed:



$$\hat{H} \Psi(\vec{r}) = E \Psi(\vec{r}) \quad (2.3)$$

Equation (2.3) is an *eigenvalue equation* in which the Hamiltonian ( $\hat{H}$ ), acts upon the wave function ( $\Psi$ ) and returns the wave function multiplied by the total energy ( $E$ ) corresponding to the different stationary states of the system. Generally, in atomic units, for a molecule system, the Hamiltonian operator for  $N$  electrons and  $M$  nuclei is

$$\hat{H} = -\sum_{i=1}^N \frac{1}{2} \nabla_i^2 - \sum_{A=1}^M \frac{1}{2M_A} \nabla_A^2 - \sum_{i=1}^N \sum_{A=1}^M \frac{Z_A}{r_{iA}} + \sum_{i=1}^N \sum_{j>i}^N \frac{1}{r_{ij}} + \sum_{A=1}^M \sum_{B>A}^M \frac{Z_A Z_B}{R_{AB}} \quad (2.4)$$

In the above equation,  $M_A$  is the ratio of mass of nucleus  $A$  to the mass of an electron, and  $Z_A$  is the atomic number of nucleus  $A$ . The Laplacian operators  $\nabla_i^2$  and  $\nabla_A^2$  involve differentiation with respect to the coordinates of the  $i$ th electron and the  $A$ th nucleus. The first term in Equation (2.4) is the operator for the kinetic energy of the electrons; the second term is the operator for the kinetic energy of the nuclei; the third term represents the coulomb attraction between electrons and nuclei; the fourth and fifth terms represent the repulsion between electrons and nuclei, respectively.

The various solutions to Equation (2.3) correspond to different stationary states of the particle (molecule). Equation (2.3) is a non-relativistic description of the system. The separation is not valid when the velocities of particles approach the speed of light. Thus, Equation (2.3) does not give an accurate description of the core electrons in large nuclei.

### 2.1.3. Born-Oppenheimer Approximation

The Born-Oppenheimer (BO) approximation is based on the fact that the masses of the nuclei are much greater than that of the electrons, they move more slowly. Hence, to a good approximation, one can consider the electrons in a molecule to be moving in the field of fixed nuclei. Within this approximation, the second term of (2.4), the kinetic energy of the nuclei, can be neglected and the last term of (2.4), the repulsion between the nuclei, can be considered to be constant. Any constant added to

an operator only adds to the operator eigenvalues and has no effect on the operator eigenfunctions. The remaining terms in (2.4) are called the electronic Hamiltonian or Hamiltonian describing the motion of  $N$  electrons in the field of  $M$  point charges which becomes to:

$$\hat{H}_{elec} = -\sum_{i=1}^N \frac{1}{2} \nabla_i^2 - \sum_{i=1}^N \sum_{A=1}^M \frac{Z_A}{r_{iA}} + \sum_{i=1}^N \sum_{j>i}^N \frac{1}{r_{ij}} \quad (2.5)$$

The solution of the Schrödinger equation with the electronic Hamiltonian ( $\hat{H}_{elec}$ ) is the electronic wave function  $\Psi_{elec}$  and the electronic energy  $E_{elec}$ .

$$\hat{H}_{elec} \Psi_{elec} = E_{elec} \Psi_{elec} \quad (2.6)$$

Notice the both  $\hat{H}_{elec}$  and  $\Psi_{elec}$  depend parametrically on the positions of nuclei. Normally the solution of the electronic Schrödinger equation is represented in term of the total potential energy which is the sum of the total electronic energy of the molecular system  $E_{elec}$  and the nuclear repulsion term  $E_{nuc}$ .

$$E_{tot} = E_{elec} + E_{nuc} \quad (2.7)$$

where

$$E_{nuc} = \sum_{A=1}^M \sum_{B>A}^M \frac{Z_A Z_B}{R_{AB}} \quad (2.8)$$

#### 2.1.4. *Ab initio* Methods

The term “*ab initio*” means “from the beginning” in Latin. Ideally, this means the integrals implicated in the Schrödinger equation for the system are explicitly solved without the use of empirical parameters. An exact solution to the Schrödinger equation is not possible for any but the most trivial molecular systems. However, a number of simplifying assumptions and procedures do make an approximate solution possible for a large size of systems.

The first assumption is the Born-Oppenheimer approximation as described in the section 2.1.3. which reduces the Schrödinger equation for a molecule system to only the electronic motion for a particular nuclear configuration. This reduces the number of computational cycles needed to find the equilibrium geometry and, then, energy of the molecule. The next step is the Hartree-Fock self consistent field (HF-SCF) approximation as first introduced by Hartree and further improved by including electron exchange by Fock and Slater. The HF-SCF approach assumes that any one electron moves in a potential that is a spherical average due to the other electrons and the nucleus. The spherically averaged potential for an electron is expressed as a single charge that is centered on the nucleus and varies with the position  $r$  in the potentially averaged sphere. The Schrödinger equation is then solved numerically for that electron in the spherically averaged potential.

#### 2.1.4.1. Hartree-Fock Theory

The Hartree-Fock (HF) approximation results in separation of the electron motions resulting (together with the Pauli principle) in the ordering of the electrons into the molecular orbitals. Therefore, it is assumed that the many-electron wavefunction  $\Psi$  for N-electron molecule is represented in terms of one-electron space wavefunctions,  $\varphi_i$ , and spin functions,  $\alpha$  or  $\beta$ . At this stage it is assumed that the N-electron molecule is a closed-shell molecule (all the electrons are paired in the occupied molecular orbitals).

$$\Psi = |\varphi_1(1)\alpha\varphi_2(2)\beta \cdots \varphi_{N/2}(N)\beta\rangle \quad (2.9)$$

As described for a multi-electron atom, the HF-SCF approach assumes that any one electron moves in a potential that is a spherical average due to the other electrons and the nuclei of the molecule. The potential from the nuclei is set by the initial configuration of the molecule, and the potential from the other electrons is determined from initial approximate wavefunctions resulting in the Hartree-Fock Hamiltonian,  $\hat{H}^{eff}$  or Fock operator,  $\hat{f}$ .

$$\hat{f}(1) = -\frac{1}{2}\nabla^2 - \sum_A \frac{Z_A}{r_{1A}} + \sum_j^{N/2} [2\hat{J}_j(1) - \hat{K}_j(1)] \quad (2.10)$$

The first two terms in Equation (2.10) correspond to the one-electron part comprising the kinetic energy operator of the electron and the attraction between one electron and the nuclei of the molecule. These first two terms represent the core Hamiltonian which has no interactions from other electrons. Interesting is the last term which is the electron-electron interaction, and describes the whole electrons mean potential. Those consist of two terms that are respectively *Coulomb operator*,  $\hat{J}_j(1)$ , and *Exchange operator*,  $\hat{K}_j(1)$ .

$$\hat{J}_j(1) = \int |\varphi_j(2)|^2 \frac{1}{r_{12}} d\tau_2 \quad (2.11)$$

The Coulomb operator accounts for the smeared-out electron potential with an electron density of  $|\varphi_j(2)|^2$ . The factor of 2 results from two electrons in each spatial orbital.

$$\hat{K}_j(1) = \int \frac{\varphi_j^*(2)\varphi_i(2)}{r_{12}} d\tau_2 \quad (2.12)$$

The exchange operator has no physical interpretation as it takes into account the effects of spin correlation.

The Schrödinger equation is now solved for the one electron,  $\varphi_i(1)$ .

$$\hat{f}(1)\varphi_i(1) = \varepsilon_i\varphi_i(1) \quad (2.13)$$

The term  $\varepsilon_i$  corresponds to the orbital energy of the electron attributed by  $\varphi_i(1)$ . The molecular orbital wavefunctions,  $\varphi_i$ , are eigenfunctions of the Fock operator,  $\hat{f}$ , and can be chosen to be orthogonal causing many integrals in the expression to vanish.

The true Hamiltonian and wavefunction of a molecule include the coordinate of all  $N$  electrons, but the Hartree-Fock Hamiltonian includes the coordinates of only one electron and is a differential equation in terms of only one electron. Therefore, in the case of multi-electron atoms, the solution of the Hartree-Fock equations must be done in an iterative process. The energy of the molecule in term of the Hartree-Fock approach,  $E^{HF}$ , is resolved like this:

$$E^{HF} = 2 \sum_i^{N/2} \varepsilon_i - \sum_i^{N/2} \sum_j^{N/2} (2J_{ij} - K_{ij}) + \sum_{A>B}^{nuclei} \sum_B^{nuclei} \frac{Z_A Z_B}{R_{AB}} \quad (2.14)$$

The first summation in Equation (2.14) is over all the orbital energies of the occupied molecular orbitals. For the factor 2, arises from there exists two electrons in each molecular orbital. The term  $J_{ij}$  and  $K_{ij}$  are determined by operating the Coulomb and Exchange operator on  $\varphi_i(1)$  and multiplying the result by  $\varphi_i^*(1)$  and integrating over the whole space. The last summation term in Equation (2.14) refers to the inter-nuclear repulsion potential for a particular nuclear configuration.

The spatial one-electron wavefunctions,  $\varphi_i$ , are represented as a linear combination of atom-centered functions such as atomic orbitals,  $\phi_\mu$ , called the linear combination of atomic orbitals (LCAO) approximation. The functions  $\phi_\mu$  constitute a basis set.

$$\varphi_i = \sum_{\mu=1}^K c_{\mu i} \phi_\mu \quad \mu = 1, 2, 3, \dots, K \quad (2.15)$$

The index  $\mu$  refers to the specific atomic orbital wavefunction, whereas index  $i$  refers to its contribution to a specific molecular orbital. The best representation of the molecular orbital arises when an infinite sum of atomic orbitals is made, but practically, only a finite  $K$  sum is used. The coefficients  $c_{\mu i}$  correspond to the contribution of each atomic orbital to the corresponding molecular orbital.

The energy of a given electron in a molecular orbital of the molecule,  $\varepsilon_i$ , is calculated as a function of the coefficients for that molecule orbital,  $c_{\mu i}$ . These equations are called the *Roothaan-Hall equations*.

### ***Roothaan-Hall Equations***

Roothaan's method utilizes the basis set expansion technique to represent the spatial orbitals and thus is able to convert the set of Hartree-Fock differential equations into a set of algebraic equations. The spatial one-electron wavefunctions,  $\varphi_i$ , then can be expanded in terms of basis functions as defined in Equation (2.15). Substituting this expansion into the Hartree-Fock equation (Equation (2.13)) one obtains:

$$\hat{f} \sum_{\nu} c_{\nu i} \phi_{\nu} = \varepsilon_i \sum_{\nu} c_{\nu i} \phi_{\nu} \quad (2.16)$$

In order to calculate  $\hat{f}$ , an initial "guess" to the coefficient for the other molecular orbitals  $\varphi_i$  must be made. Multiplying Equation (2.16) by  $\phi_{\mu}^*$ , where  $\mu = 1, 2, 3, \dots, K$  and integrating yields the following expression.

$$\sum_{\nu} F_{\mu\nu} c_{\nu i} = \varepsilon_i \sum_{\nu} S_{\mu\nu} c_{\nu i} \quad (2.17)$$

The terms  $F_{\mu\nu}$  form the so called *Fock matrix*.

$$F_{\mu\nu} = \langle \phi_{\mu} | \hat{f} | \phi_{\nu} \rangle \quad (2.18)$$

The terms  $S_{\mu\nu}$  form the *overlap matrix*.

$$S_{\mu\nu} = \langle \phi_{\mu} | \phi_{\nu} \rangle \quad (2.19)$$

The Roothaan-Hall equation as shown in Equation (2.17) can be rewritten in a matrix form.

$$\mathbf{FC} = \mathbf{SC}\boldsymbol{\varepsilon} \quad (2.20)$$

where

- $\mathbf{C}$  is an  $M \times M$  square matrix of molecular orbital expansion coefficients  $c_{vi}$  ;
- $\mathbf{F}$  is the Fock matrix, which is the sum of a term representing the energy of a single electron in the field of the bare atomic nuclei and a term describing electron–electron repulsion within an averaged field of electron density ;
- $\mathbf{S}$  is a matrix describing the overlap of molecular orbitals and
- $\boldsymbol{\varepsilon}$  is a diagonal matrix of the orbital energies  $\varepsilon_i$  containing the one-electron energies of each molecular orbital.

Since the terms within the Fock matrix,  $\mathbf{F}$ , depend upon the electron density, which in turn, depends upon molecular wave functions defined by the matrix of molecular orbital expansion coefficients,  $\mathbf{C}$ , the Roothan-Hall equations are nonlinear, and must be solved by an iterative procedure and thus the Hartree-Fock theory is also known as the *self-consistent field* (SCF) method. The optimized coefficients for each molecular orbital in turn are then compared to the initial “guess” for the coefficients. If there is a difference, the computation is repeated with the new optimized coefficients. If there is no significant difference or enough computational cycles have been completed so that there is no significant difference, the computation is terminated. Upon convergence of the SCF method, the minimum-energy molecular orbitals produce the electric field which generate the same orbitals (hence, the self-consistency).

#### 2.1.4.2. Basis Sets

*Ab initio* electronic structure computations are almost always carried out numerically using a *basis set* of orbitals. It is important to choose a basis set that is large enough to give a good description of the molecular wavefunction. Typically, the basis functions are centered on the atoms, and so sometimes they are called “atomic orbitals”. A basis set is a set of basis function which is the mathematical description of the orbitals within a system which in order combine to approximate the total electronic wavefunction used to perform the theoretical calculation.

One reasonable choice for a set of basis functions are Slater-type orbitals (STO's) from the hydrogen atom but with different exponents due to different nuclear charges. They are described by the function depending on spherical coordinates. The radial part of orbital ( $e^{-\zeta r}$ ) is an exponentially decaying function:

$$\Phi_{STO}(\zeta, n, l, m; r, \theta, \phi) = Nr^{n-1} e^{-\zeta r} Y_{lm}(\theta, \phi) \quad (2.21)$$

where  $N$  is a normalization constant,  $\zeta$  is called “exponent”. The  $r$ ,  $\theta$  and  $\phi$  are spherical coordinates, and  $Y_{lm}$  is the angular momentum part which is a function describing the “shape”. The  $n$ ,  $l$  and  $m$  are principal, angular momentum and magnetic quantum numbers, respectively. Due to using STO's, two-electron integrals are difficult and time consuming to evaluate. In modern practice, these atom-centered basis functions are usually chosen to be Gaussian-type orbitals (GTO's). These orbitals decay as functions of  $e^{-\alpha r^2}$ . The functional form for GTO's is expressed as:

$$g(\alpha, l, m, n; x, y, z) = Ne^{-\alpha r^2} x^a y^b z^c \quad (2.22)$$

where  $N$  is a normalization constant,  $\alpha$  is called “exponent”.  $x$ ,  $y$ ,  $z$  are Cartesian coordinates.  $a$ ,  $b$  and  $c$  are simply integral exponents at Cartesian coordinates ( $r^2 = x^2 + y^2 + z^2$ ). The GTO's do not have the correct behavior for  $r$  approaching zero and infinity or it can be said that the GTO's do not have radial nodes. However, radial nodes can be obtained by *combining* different GTO's to represent STO's (STO-nG). An example of an acceptable representation of a STO at least 3 GTO's is shown in Figure 2.1. Quite frequently, an atomic basis function is actually a fixed linear combination of GTO's; this is called a *contracted Gaussian basis function*.



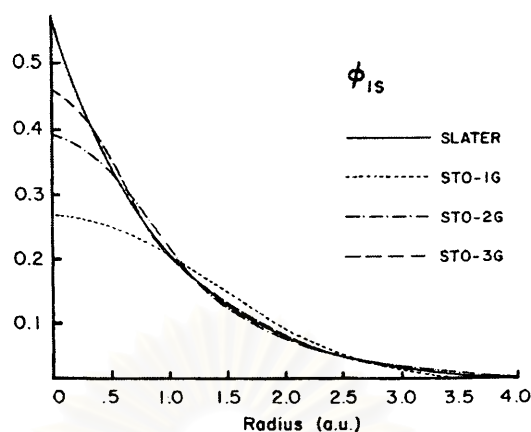


**Figure 2.1** An acceptable representation of a STO at least 3 GTO's.

The advantage of such an approach is that two-electron integrals can be solved analytically thus reducing the computational time because two Gaussian functions centered at two different nuclei are equal to a single Gaussian centered at a third point. By the LCAO approximation, not only, the type of function (STO/GTO), but also the number of functions to be used need to be determined for an appropriate basis set. Below are the descriptions of several widely used basis set.

**Minimal Basis Set:** The STO- $n$ G basis sets are minimal basis sets, where each Slater Type Orbital is approximated by  $n$  Gaussian primitive functions. In these basis sets, only a minimal number of basis functions for all orbitals in a given shell needed to accommodate all electrons in the system as in these examples:

H: 1s

C: 1s, 2s, 2p<sub>x</sub>, 2p<sub>y</sub>, 2p<sub>z</sub>

The STO-3G basis is a very well-known minimal basis set which contracts 3 Gaussian functions to approximate the more accurate Slater type orbitals. For example, the minimal basis set for H<sub>2</sub>O would be a 1s orbital for each hydrogen atom plus a 1s, 2s, 2p<sub>x</sub>, 2p<sub>y</sub> and 2p<sub>z</sub> orbitals for oxygen atom. The only advantage of using a minimal basis set is its low computational cost. Although a contracted GTO might give a good approximation to an atomic orbital, it lacks any flexibility to expand or shrink of the orbitals. Hence, a minimal basis set such as STO-3G is not capable of giving highly accurate results.

**Extended Basis Sets:** The first way that a basis set can be made larger is to increase the number of basis functions per atom. One solution is adding extra basis functions beyond the minimum number required to describe each atom. If each orbital is represented by two basis function, this is called *a double-zeta basis set* which is often denoted DZ (the zeta,  $\zeta$ , comes from the exponent in the GTO). Hence, a double-zeta basis set for hydrogen would have two functions, and a true double-zeta basis set for carbon would have 10 functions as described like this:

H: 1s, 1s'

C: 1s, 1s', 2s, 2s', 2p<sub>x</sub>, 2p<sub>y</sub>, 2p<sub>z</sub>, 2p<sub>x</sub>', 2p<sub>y</sub>', 2p<sub>z</sub>'

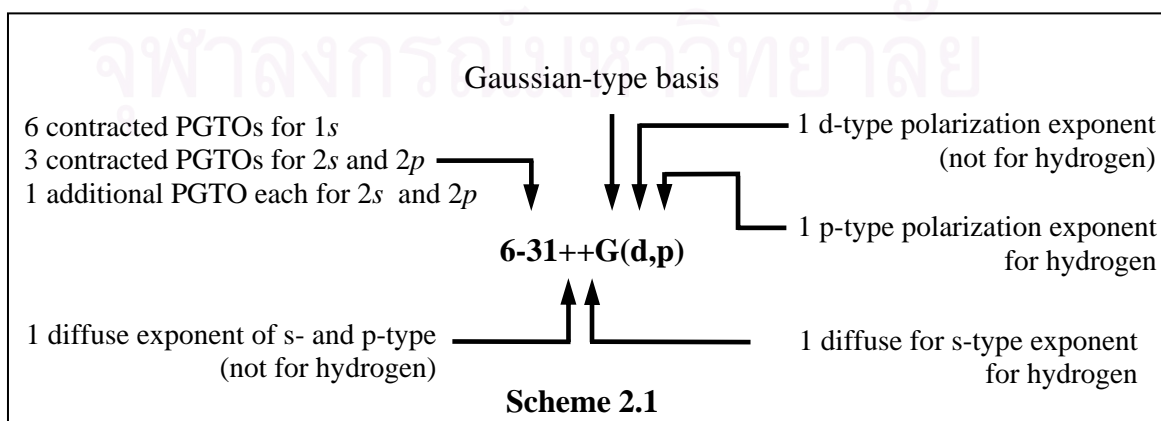
Consequently, for most chemical properties only electrons in the valence shell are important. Thus the more cost effective way to improve the basis set is to have more flexibility for the valence electrons only. For the carbon atom, only a single orbital for the core (1s) and 9 functions (1s, 2s, 2s', 2p<sub>x</sub>, 2p<sub>y</sub>, 2p<sub>z</sub>, 2p<sub>x</sub>', 2p<sub>y</sub>', 2p<sub>z</sub>') are used. This basis sets are said to be the *double-zeta in the valence* and they are also called the *split valence basis sets*. The inner-shell orbitals are represented by minimal basis set whereas the valence shell orbitals are represented by more than one basis function such as the 3-21G basis set which has one contracted Gaussian function that is a linear combination of three primitive Gaussian functions for each inner-shell atomic orbital and two basis functions, one contracted Gaussian function that is a linear combination of two primitive Gaussians and one primitive Gaussian function, for each valence orbital. Similarly, *triple split valence basis sets*, like 6-311G, use three sizes of contracted functions for each orbital-type.

**Polarized Basis Sets:** Split valence basis sets allow orbitals to change size, but not to change shape. Often additional flexibility is built in by adding higher-angular momentum basis functions which have an  $l$  quantum number greater than the maximum value of the valence orbitals in the ground state atom. Since the highest angular momentum orbital for carbon is a  $p$  orbital, the polarization of the atom can be described by adding a set of  $d$  functions. A hydrogen atom would use a set of 3  $p$  functions as polarization functions. A double-zeta plus polarization basis set might be designated DZP. The most famous example of a split valence double-zeta plus polarization basis set is Pople's so-called 6-31G\* basis. This notation means that the

core orbital is described by a contraction of 6 Gaussian orbitals, while the valence is described by two orbitals, one made of a contraction of 3 Gaussians, and one a single Gaussian function. The star (\*) indicates polarization functions which are *d* functions added to each non-hydrogen atom in the second or third row atoms. If for the polarization also *p* functions were added to hydrogen atoms, this basis would be called 6-31G\*\*. The confusing nature of this nomenclature has caused some chemists to start switching to slightly improved notation such as 6-31G(d,p), where the polarization functions are listed explicitly. There is no limit on the number of polarization functions included in the basis set, however, it does increase the computational demand significantly.

**Diffuse Functions:** Diffuse functions are large-size versions of *s*- and *p*-type functions as well as they allow orbitals to occupy a larger region of space. Basis sets with diffuse functions are important for systems where electrons are relatively far from the nucleus such as molecules with lone pairs, anions and other systems with significant negative charge, systems in their excited states, system with low ionization potentials, descriptions of absolute acidities and so on. The 6-31+G(d) basis set is the 6-31G(d) basis set with diffuse functions added to non-hydrogen atoms. The double plus version, 6-31++G(d), adds diffuse functions to the hydrogen atom as well. Diffuse functions on hydrogen atoms seldom make a significant difference in accuracy.

It can be noted that the basis sets which are used in this work will be perform in Pople-style nomenclature. The example for basis set and its description are shown in Scheme 2.1.



One of the errors arising from limitations of Hartree-Fock method is the electron correlation which is the correlation between the motions of the electrons within a molecular system, especially that arising between electrons of the opposite spin that make the difference in energy between the HF and the lowest possible energy in a given basis set. To correct the electron correlation problem, there are many different correlated approaches such as *Configuration Interaction (CI)* and *Møller-Plesset Perturbation (MPn)* methods.

### 2.1.5. Møller-Plesset Perturbation Theory

The Møller-Plesset Perturbation theory is the most widely used method. Perturbation theory works on the idea that when an exact answer for one problem is found, an answer for a closely related problem can also be worked out. When the solution of the Schrödinger equation for one problem, i.e. for one Hamiltonian operator were known. A problem with a Hamiltonian operator which is fairly close to the first one, can be solved by treating the difference between the Hamiltonian operators as a small perturbation to the first solution, then, expand the solution to the second problem in terms of the first solution or in terms in various powers of the perturbation. This approach was originally used for problems such as solving for the wave function of an atom in a small electric field where the term in the Hamiltonian arising from the electric field is the perturbation.

Qualitatively, the Møller-Plesset [53] Perturbation theory adds higher excitations to the Hartree-Fock theory as a non-iterative correction, drawing upon techniques from the *many body perturbation theory* introduced by Rayleigh and Schrödinger. The HF problem is treated as the unperturbed wave function and the residual part of the Hamiltonian is treated as a perturbation. Perturbation theory is based upon dividing the Hamiltonian into two parts:

$$H = H_0 + \lambda H^{(1)} \quad (2.23)$$

where  $H_0$  is unperturbed Hamiltonian of the exact problem while  $\lambda H^{(1)}$  is a *perturbation* applied to  $H_0$ , a correction which is assumed to be small in comparison to

$H_0$ .  $\lambda$  is a formal parameter, introduced for technical reasons only. The application of the perturbation theory is justified, if the contribution of electron correlation energy (the “perturbation”) is small. The usual way to treat a small perturbation to  $H_0$  is to express the perturbed wavefunction and energy as a power series in  $H^{(1)}$  in terms of the parameter  $\lambda$ .

From the HF computation, the energy eigenvalues and eigenfunctions are known corresponding to the solution of the unperturbed system with  $H_0$ ,  $\Psi^{(0)}$  (HF Slater determinant) and  $E^{(0)}$ :

$$H_0\Psi^{(0)} = E^{(0)}\Psi^{(0)} \quad (2.24)$$

If the perturbation is small, then  $\Psi^{(0)}$  and  $E^{(0)}$  lie close to the exact wave function,  $\Psi$  and the energy,  $E$ . Assuming these two conditions, a generalized electronic Hamiltonian ( $H_\lambda$ ) can be defined as:

$$H_\lambda = H_0 + \lambda H^{(1)} \quad (2.25)$$

Expanding the wave function ( $\Psi_\lambda$ ) and energy as a power series:

$$\Psi_\lambda = \Psi^{(0)} + \lambda^1\Psi^{(1)} + \lambda^2\Psi^{(2)} + \dots = \sum_{n=0}^{\infty} \lambda^n \Psi^{(n)} \quad (2.26)$$

$$E_\lambda = E^{(0)} + \lambda^1 E^{(1)} + \lambda^2 E^{(2)} + \dots = \sum_{n=0}^{\infty} \lambda^n E^{(n)} \quad (2.27)$$

where  $\lambda$  is an arbitrary parameter to keep track of the orders of perturbation applied.  $\Psi_\lambda$  and  $E_\lambda$  represent the exact (within a given basis set) ground state wave function and energy for a system described by the Hamiltonian,  $H_\lambda$ . Note that for  $\lambda = 0$ ,  $H_\lambda$  equals the unperturbed operator ( $0^{\text{th}}$  power),  $H_0$ .

Now, the following eigenvalue equation has to be solved:

$$H_\lambda \Psi_\lambda = E_\lambda \Psi_\lambda \quad (2.28)$$

The wave function and energy are substituted by the power series:

$$\begin{aligned} (H_0 + \lambda H^{(1)})[\Psi^{(0)} + \lambda^1 \Psi^{(1)} + \lambda^2 \Psi^{(2)} + \dots] = \\ (E^{(0)} + \lambda^1 E^{(1)} + \lambda^2 E^{(2)} + \dots)[\Psi^{(0)} + \lambda^1 \Psi^{(1)} + \lambda^2 \Psi^{(2)} + \dots] \end{aligned} \quad (2.29)$$

Expanding the products and collecting terms with the same  $\lambda^n$  together

$$\begin{aligned} H_0|\Psi^{(0)}\rangle + \lambda H_0|\Psi^{(1)}\rangle + \lambda^2 H_0|\Psi^{(2)}\rangle + \lambda H^{(1)}|\Psi^{(0)}\rangle + \lambda^2 H^{(1)}|\Psi^{(1)}\rangle + \dots = \\ E^{(0)}|\Psi^{(0)}\rangle + \lambda E^{(0)}|\Psi^{(1)}\rangle + \lambda^2 E^{(0)}|\Psi^{(2)}\rangle + \dots \end{aligned} \quad (2.30)$$

$$\begin{aligned} \lambda^0; \quad & H_0|\Psi^{(0)}\rangle = E^{(0)}|\Psi^{(0)}\rangle \\ \lambda^1; \quad & (H_0 - E^{(0)})|\Psi^{(1)}\rangle = E^{(1)}|\Psi^{(0)}\rangle - H^{(1)}|\Psi^{(0)}\rangle \\ \lambda^2; \quad & (H_0 - E^{(0)})|\Psi^{(2)}\rangle = E^{(2)}|\Psi^{(0)}\rangle - E^{(1)}|\Psi^{(1)}\rangle - H^{(1)}|\Psi^{(1)}\rangle \end{aligned} \quad (2.31)$$

and, then, equating them (since  $\lambda$  is arbitrary) the energies setting  $\lambda = 1$  and imposing *orthogonalisation* condition ( $\langle \Psi^{(i)} | \Psi^{(j)} \rangle = \delta_{ij}$ ), one finally has

$$E^{(0)} = \langle \Psi^{(0)} | H_0 | \Psi^{(0)} \rangle, \quad E^{(1)} = \langle \Psi^{(0)} | H^{(1)} | \Psi^{(0)} \rangle, \quad E^{(2)} = \langle \Psi^{(0)} | H^{(1)} | \Psi^{(1)} \rangle, \dots \quad (2.32)$$

All resulting terms can be expressed in terms of  $E^{(0)}$ ,  $\Psi^{(0)}$  and the determinable term  $\langle \Psi^{(0)} | H^{(1)} | \Psi^{(0)} \rangle$ . The unperturbed, ground state wave function and energy can be written in terms of the occupied, one-electron spin orbitals,  $\Psi^b$ , and the energy of any single spin orbital,  $\varepsilon_i$ .

$$\Psi_0 = \Psi^{(0)} \text{ and } E_0 = E^{(0)} = \sum_{i \in \Psi^b} \varepsilon_i \quad (2.33)$$

Møller and Plesset introduced the following expression for the perturbation operator.

$$H_\lambda = H_0 + \lambda H^{(1)} = \sum_i F_i + \lambda \left[ \sum_{i,j,i < j} \frac{1}{r_{ij}} - \frac{1}{2} \sum_i (J_i - K_i) \right] \quad (2.34)$$

Here,  $H_0$  is defined as the sum of the one-electron Fock operators,  $\sum_i F_i$ .  $E^{(0)}$  is the sum of the one-electron energies and therefore, only the sum  $E^{(0)} + E^{(1)}$  represents the HF energy since  $\Psi^{(0)}$  corresponds to the HF wave function.

$$E^{HF} = E^{(0)} + E^{(1)} = \langle \Psi^{(0)} | H_\lambda | \Psi^{(0)} \rangle \quad (2.35)$$

To calculate  $E^{(2)}$  the first order wave function  $\Psi^{(1)}$  has to be known. This is given by:

$$\Psi^{(1)} = \sum_{s>0} (E_0 - E_s)^{-1} P_{s0} \Psi_s \quad (2.36)$$

The energy,  $E_s$ , corresponding to a determinant,  $\Psi_s$ , is the sum of one-electron energies of those spin-orbitals which are occupied.  $P_{s0}$  are the matrix elements of the perturbation operator. It can be shown that  $P_{s0}$  does not become zero, if  $s$  corresponds to a determinant with double substitutions. Thus, only double substitutions contribute to the first order wave function.

Due to the good cost (CPU time) to accuracy ratio, the power expansion is often truncated after the second order, known as MP2 level, for which the energy is:

$$E^{MP2} = E^{(0)} + E^{(1)} + E^{(2)} = E^{HF} + E^{(2)} \quad (2.37)$$

and the explicit formula for the second-order Møller-Plesset correction when indices,  $i$  and  $j$ , correspond to the occupied orbitals and indices,  $a$  and  $b$ , correspond to the unoccupied orbitals,  $E^{(2)}$ , is given by:

$$E^{(2)} = \sum_{i < j}^{occ} \sum_{a < b}^{vir} \frac{|\langle ij|ab\rangle - \langle ij|ba\rangle|^2}{\varepsilon_i + \varepsilon_j - \varepsilon_a - \varepsilon_b} \quad (2.38)$$

A Møller and Plesset computation to a second-order energy correction is called an *MP2* computation, and higher-order energy corrections are called *MP3*, *MP4*, and so on. The MP2 level incorporates contributions from single and double substitutions [54,55] whereas at the MP4 level are additional single, double, triple and quadruple (MP4; SDTQ) substitutions are included [56,57]. The *MPn* method is size-consistent, but not variational. Its principle deficiency is that MP series sometimes converges slowly, especially in systems where the effects of correlation are large corresponding to a large perturbation. The MP method is practical to fourth order, however, it is limited to relatively small systems at MP4 level. The MP2 is relatively economic to evaluate and gives a reasonable proportion of the correlation energy and has been used extensively even for larger systems. In practice, MP2 must be used with reasonable basis sets (e.g. 6-31G\* or better). Higher order terms become more complicated and much more time-consuming. MP3 is commonly used but does not seem to give much improvement over MP2. MP4, with some terms removed to speed things up, is often used. MP4 gives reasonable results but it is much more expensive than MP2. Higher order terms than 4'th order are rarely evaluated.

## 2.2. Density Functional Theory

Density functional theory (DFT) is a powerful formally exact theory proved by Hohenberg and Kohn [58]. The DFT approach makes approximations in both the Hamiltonian and the wavefunction. However, it takes a completely different approach than the HF-based methods. The DFT approach is based upon a strategy of modeling electron correlation via general functionals of the electron density.



DFT has become the most widely used methods in the last decade due to its accuracy and cost effective. In the first stage of DFT, the energy is expressed as a functional of the density of a uniform electron gas ( $E(\rho)$ ) and, then, modified to express the electron density around molecules. Despite its simple origins, DFT works very well in most cases. For about the same cost of doing a Hartree-Fock calculation, DFT includes a significant fraction of the electron correlation. Note that DFT is not a Hartree-Fock method, nor it is a post-Hartree-Fock method. The wave function is constructed in a different way such as the spin and spatial parts are different to those developed in the Hartree-Fock theory and the resulting orbitals are often referred to as “Kohn-Sham” orbitals [59]. Nevertheless, the same SCF procedure is used as in the Hartree-Fock theory.

The advantage of using electron density is that the integrals for Coulomb repulsion need be done only over the electron density, which is a three-dimensional function, thus scaling as  $N^3$ . Furthermore, at least some electron correlation can be included in the calculation. These results in faster calculations than HF calculations (which scale as  $N^4$ ) and computations those are a bit more accurate as well. The better DFT functionals give results with an accuracy similar to that of and MP2 calculation.

### 2.2.1 Basic theory

#### *The Hohenberg-Kohn Theorems*

In 1964, Hohenberg and Kohn proved two theorems that provide the basis for the development of modern DFT.

*Theorem-I:* “For a given external potential  $V_{\text{ext}}(\mathbf{r})$ , the electron density  $\rho(\mathbf{r})$  of the ground state of a system *uniquely determines* the ground state wave function and hence *all properties* of the ground state.”

To prove this theorem, it is assumed that two external potentials,  $V_{\text{ext}}(\mathbf{r})$  and  $V'_{\text{ext}}(\mathbf{r})$  differ by more than a constant and both give the same  $\rho(\mathbf{r})$  for their

respective ground state forming two Hamiltonians,  $\hat{H}$  and  $\hat{H}'$  whose ground state densities were the same while the normalized wave functions  $\psi$  and  $\psi'$  would be different. Taking  $\psi'$  as a trial wave function for the  $\hat{H}$  problem,

$$\begin{aligned} E_0 < \langle \psi' | \hat{H} | \psi' \rangle &= \langle \psi' | \hat{H}' | \psi' \rangle + \langle \psi' | \hat{H} - \hat{H}' | \psi' \rangle \\ &= E'_0 + \int \rho(r) [V_{ext}(r) - V'_{ext}(r)] dr \end{aligned} \quad (2.39)$$

where  $E_0$  and  $E'_0$  are the ground-state energies for the  $\hat{H}$  and  $\hat{H}'$ , respectively. Similarly, taking  $\psi$  as a trial function for the  $\hat{H}'$  problem,

$$\begin{aligned} E'_0 < \langle \psi | \hat{H}' | \psi \rangle &= \langle \psi | \hat{H} | \psi \rangle + \langle \psi | \hat{H}' - \hat{H} | \psi \rangle \\ &= E_0 + \int \rho(r) [V_{ext}(r) - V'_{ext}(r)] dr \end{aligned} \quad (2.40)$$

when sum of equation (2.39) and (2.40), it performs,

$$E_0 + E'_0 < E'_0 + E_0 \quad (2.41)$$

Equation (2.41) shows a contradiction and so there cannot be two different  $V_{ext}(r)$  that give the same  $\rho(r)$  for their ground state.

Therefore,  $\rho(r)$  determines  $N$  and  $V_{ext}(r)$  and hence all the properties of the ground state, for instance the kinetic energy  $T(\rho)$ , the potential energy  $V(\rho)$  and the total energy  $E(\rho)$ . The total energy can be written as

$$E[\rho] = E_{NE}[\rho] + T[\rho] + E_{ee}[\rho] = \int \rho(r) V_{NE}(r) dr + F_{HK}[\rho] \quad (2.42)$$

where  $F_{HK}[\rho] = T[\rho] + E_{ee}[\rho]$ ,  $E_{NE}[\rho]$  is the potential energy due to the electron-nuclei attraction,  $E_{ee}[\rho]$  represents the electron-electron repulsion energy and  $T[\rho]$  is the kinetic energy of the electron. The functional  $F_{HK}$  is an universal functional. If it is

known, the Schrödinger equation can be solved exactly.  $F_{\text{HK}}$  includes the functional for the kinetic energy,  $T[\rho]$  and the electron-electron interaction,  $E_{\text{ee}}[\rho]$ . The explicit form of both of these functionals is unclear. However, the classical part of  $J[\rho]$  can be extracted from the  $E_{\text{ee}}[\rho]$ .

$$E_{ee}[\rho] = \frac{1}{2} \iint \frac{\rho(r_1)\rho(r_2)}{r_{12}} dr_1 dr_2 + E_{ncl} = J[\rho] + E_{ncl} \quad (2.43)$$

$E_{ncl}$  is the non-classical contribution to the electron-electron interaction including self-interaction correction, exchange and coulomb correlation.

**Theorem-II:** “The functional  $F_{\text{HK}}[\rho]$  delivers the ground state energy leading the lowest energy of the system if the input density is the true ground state density.”

$$E_0 \leq E[\tilde{\rho}] = T[\tilde{\rho}] + E_{NE}[\tilde{\rho}] + E_{ee}[\tilde{\rho}] \quad (2.44)$$

when  $\tilde{\rho}$  is trial density. The ground state density can be calculated using the variational principal involving the density.

### ***The Kohn-Sham Equation***

The Kohn-Sham formulation provides for the system of interacting particles to an ensemble of electrons which only interact through their total density. The ground state energy of the system can be rewritten as

$$E_0 = \min_{\rho \rightarrow N} \left( F[\rho] + \int \rho(r) V_{NE} dr \right) \quad (2.45)$$

where the universal functional  $F[\rho]$  contains the contribution of the kinetic energy, the classical Coulomb interaction and the non-classical portion.

$$F[\rho] = T[\rho] + J[\rho] + E_{ncl}[\rho] \quad (2.46)$$

Only  $J[\rho]$  is known whereas the expression for  $T[\rho]$  and  $E_{\text{ncI}}[\rho]$  are not known. According to the solution that Kohn and Sham proposed in 1965, the unknown terms could be described by two following approaches. The first one is *calculating the largest component of the kinetic energy by using the non-interacting reference system.*

$$T_s = -\frac{1}{2} \sum_i^N \langle \psi_i | \nabla^2 | \psi_i \rangle \quad (2.47)$$

$$\rho_s(r) = \sum_i^N \sum_s |\psi_i(r, s)|^2 = \rho(r) \quad (2.48)$$

where  $\psi_i$  are the orbitals of the non-interacting system.  $T_s$  is not equal to the true kinetic energy of the system. The second approach introduces *the separation of the  $F[\rho]$  as following:*

$$F[\rho] = T_s[\rho] + J[\rho] + E_{\text{XC}}[\rho] \quad (2.49)$$

where  $E_{\text{XC}}$  is called “exchange-correlation energy” and which is the functional containing everything that is unknown.

$$E_{\text{XC}} = (T[\rho] - T_s[\rho]) + (E_{\text{ee}}[\rho] - J[\rho]) \quad (2.50)$$

Thus, the expression for the energy of the interacting system can be defined in term of  $E_{\text{XC}}$  as following:

$$E[\rho] = T_s[\rho] + J[\rho] + E_{\text{XC}}[\rho] + E_{\text{NE}}[\rho] \quad (2.51)$$

Equation (2.51) can be rewritten as

$$E[\rho] = T_s[\rho] + \frac{1}{2} \iint \frac{\rho(r_1)\rho(r_2)}{r_{12}} dr_1 dr_2 + E_{\text{XC}}[\rho] + \int V_{\text{NE}} \rho(r) dr - \frac{1}{2} \sum_i^N \langle \psi_i | \nabla^2 | \psi_i \rangle$$

$$= \frac{1}{2} \sum_i^N \sum_j^N \iint |\psi_i(r)|^2 |\psi_j(r)|^2 dr_1 dr_2 + E_{XC}[\rho] - \sum_i^N \int \sum_A^M \frac{Z_A}{r_{iA}} |\psi_i(r)|^2 dr_1 \quad (2.52)$$

The only term for which no explicit form can be given is  $E_{XC}$ . The variational principle (the second Hohenberg-Kohn theorem) is applied in order to minimize this energy expression under the constraint  $\langle \psi_i | \psi_j \rangle = \delta_{ij}$ . The resulting equations are the Kohn-Sham equations.

$$\left( -\frac{1}{2} \nabla^2 + \left[ \int \frac{\rho(r_2)}{r_{12}} + V_{XC}(r_1) - \sum_A^M \frac{Z_A}{r_{1A}} \right] \right) \psi_i = \left( \frac{1}{2} \nabla^2 + V_{KS}(r_1) \right) \psi_i = \epsilon_i \psi_i \quad (2.53)$$

where the exchange correlation potential is given by the functional derivative.

$$V_{XC} = \frac{\partial E_{XC}}{\partial \rho} \quad (2.54)$$

$$V_{KS}(r) = V_{el} + V_{XC} + V_{nuc} \quad (2.55)$$

The exact ground-state density  $\rho(r)$  of an N-electron system is,

$$\rho(r) = \sum_{i=1}^N \psi_i^*(r) \psi_i(r) \quad (2.56)$$

where the single-particle wave function  $\psi_i(r)$  are the N lowest-energy of the Kohn-Sham equation. The theorem of Kohn and Sham can now be formulated as follows:

$$\hat{H}_{KS} \psi_i = \epsilon_i \psi_i \quad (2.57)$$

Note that  $V_{KS}$  depends on the density corresponding to a self-consistency problem and therefore the Kohn-Sham equations have to be solved iteratively.

According to the Kohn-Sham scheme, it was totally apart from the Born-Oppenheimer approximation and no other approximations were made. However, the exact functional form for the exchange-correlation is unknown. Several approximations have been introduced for approximate forms of the exchange-correlation functional.

### 2.2.2 Local Density Methods

In the *Local Density Approximation* (LDA) is the simplest of all approximate exchange-correlation functionals. It is assumed that the density locally can be treated as a uniform electron gas, or equivalently that the density is a slowly varying function in space. The exchange energy for a uniform electron gas is given by the Dirac formula.

$$\begin{aligned} E_x^{\text{LDA}}[\rho] &= -C_x \int \rho^{4/3}(\mathbf{r}) \mathbf{d}\mathbf{r} \\ \varepsilon_x^{\text{LDA}}[\rho] &= -C_x \rho^{1/3} \end{aligned} \quad (2.58)$$

In the more common case, where the  $\alpha$  and  $\beta$  densities are not equal, LDA (where the sum of the  $\alpha$  and  $\beta$  densities is raised to the 4/3 power) has been virtually abandoned and replaced by the *Local Spin Density Approximation* (LSDA) (which is given as the sum of the individual densities raised to the 4/3 power), Equation (2.59).

$$\begin{aligned} E_x^{\text{LSDA}}[\rho] &= -2^{1/3} C_x \int [\rho_\alpha^{4/3} + \rho_\beta^{4/3}] \mathbf{d}\mathbf{r} \\ \varepsilon_x^{\text{LSDA}}[\rho] &= -C_x \rho [\rho_\alpha^{1/3} + \rho_\beta^{1/3}] \end{aligned} \quad (2.59)$$

LSDA may also be written in terms of the total density and the spin polarization.

$$\varepsilon_x^{\text{LSDA}}[\rho] = -\frac{1}{2} C_x \rho^{1/3} [(1 + \zeta)^{4/3} + (1 - \zeta)^{4/3}] \quad (2.60)$$

The correlation energy of a uniform electron gas has been determined by Monte Carlo methods for a number of different densities. In order to use these results in DFT calculations, it is desirable to have a suitable analytic interpolation formula. This has been constructed by Vosko, Wilk and Nusair (VWN) [60] and is in general considered to be a very accurate fit. It interpolates between the unpolarized ( $\zeta = 0$ ) and spin polarized ( $\zeta = 1$ ) limits by the following functional.

$$\varepsilon_c^{\text{VWN}}(r_s, \zeta) = \varepsilon_c(r_s, 0) + \varepsilon_a(r_s) \left[ \frac{f(\zeta)}{f'(0)} \right] [1 - \zeta^4] + [\varepsilon_c(r_s, 1) - \varepsilon_c(r_s, 0)] f(\zeta) \zeta^4$$

$$f(\zeta) = \frac{(1 + \zeta)^{4/3} + (1 - \zeta)^{4/3} - 2}{2(2^{1/3} - 1)} \quad (2.61)$$

The LSDA approximation in general underestimates the exchange energy by  $\sim 10\%$ , thereby creating errors which are larger than the whole correlation energy. Electron correlation is furthermore overestimated, often by a factor close to 2, and bond strengths are, as a consequence, overestimated. Despite the simplicity of the fundamental assumptions, LSDA methods are often found to provide results with accuracy similar to that obtained by wave mechanics HF methods.

### 2.2.3. Gradient Corrected Methods

Improvements over the LSDA approach have to consider a non-uniform electron gas. A step in this direction is to make the exchange and correlation energies dependent not only on the electron density, but also on derivatives of the density. Such methods are known as *Gradient Corrected or Generalized Gradient Approximation* (GGA) methods (a straightforward Taylor expansion does not lead to an improvement over LSDA, it actually makes things worse, thus the name generalized gradient approximation). GGA methods are also sometimes referred to as *non-local* methods, although this is somewhat misleading since the functionals depend only on the density (and derivatives) at a given point, not on a space volume as for example the Hartree-Fock exchange energy.

Perdew and Wang (PW86) [61] proposed to modify the LSDA exchange expression to the form shown in Equation (2.62), where  $x$  is a dimensionless gradient variable, and  $a$ ,  $b$  and  $c$  being suitable constants (summation over equivalent expressions for the  $\alpha$  and  $\beta$  densities is implicitly assumed).

$$\begin{aligned}\epsilon_x^{\text{PW86}} &= \epsilon_x^{\text{LDA}} \left(1 + a x^2 + b x^4 + c x^6\right)^{1/15} \\ x &= \frac{|\nabla\rho|}{\rho^{4/3}}\end{aligned}\quad (2.62)$$

Becke [62] proposed a widely used correction to the LSDA exchange energy, with has the correct  $-r^{-1}$  asymptotic behavior for the energy density (but not for the exchange potential).

$$\begin{aligned}\epsilon_x^{\text{B88}} &= \epsilon_x^{\text{LDA}} + \Delta\epsilon_x^{\text{B88}} \\ \Delta_x^{\text{B88}} &= -\beta\rho^{1/3} \frac{x^2}{1 + 6\beta x \sinh^{-1} x}\end{aligned}\quad (2.63)$$

The  $\beta$  parameter is determined by fitting to known atomic data and  $x$  is defined in Equation 2.62.

Perdew and Wang have proposed an exchange functional similar to B88 to be used in connection with the PW91 correlation functional given below.

$$\epsilon_x^{\text{PW91}} = \epsilon_x^{\text{LDA}} \left( \frac{1 + x a_1 \sinh^{-1}(x a_2) + \left(a_3 + a_4 e^{-bx^2}\right) x^2}{1 + x a_1 \sinh^{-1}(x a_2) + a_5 x^2} \right) \quad (2.64)$$

There have been various gradient corrected functional forms proposed for the correlation energy. One popular functional (not a correction) is due to Lee, Yang and Parr (LYP) [63] and has the form:



$$\begin{aligned}
\varepsilon_c^{\text{LYP}} &= -a \frac{\gamma}{(1+d\rho^{-1/3})} - ab \frac{\gamma e^{-c\rho^{-1/3}}}{9(1+d\rho^{1/3})\rho^{8/3}} \\
&\quad \times \left[ 18(2^{2/3})C_F(\rho_\alpha^{8/3} + \rho_\beta^{8/3}) - 18\rho t_W \right. \\
&\quad \left. + \rho_\alpha(2t_W^\alpha + \nabla^2\rho_\alpha) + \rho_\beta(2t_W^\beta + \nabla^2\rho_\beta) \right] \\
\gamma &= 2 \left[ 1 - \frac{\rho_\alpha^2 + \rho_\beta^2}{\rho^2} \right] \\
t_W^\sigma &= \frac{1}{8} \left( \frac{|\nabla\rho_\sigma|^2}{\rho_\sigma} - \nabla^2\rho_\sigma \right)
\end{aligned} \tag{2.65}$$

where the  $a$ ,  $b$ ,  $c$  and  $d$  parameters are determined by fitting to data for the helium atom. The  $t_W$  functional is known as the local Weizsacker kinetic energy density. Note that the  $\gamma$ -factor becomes zero when all the spins are aligned ( $\rho = \rho_\alpha$ ,  $\rho_\beta = 0$ ), i.e. the LYP functional does not predict any parallel spin correlation in such a case (e.g. The LYP correlation energy in triplet He is Zero). The appearance of the second derivative of the density can be removed by partial integration to give Equation (2.66).

$$\begin{aligned}
\varepsilon_c^{\text{LYP}} &= -4\alpha \frac{\rho_\alpha\rho_\beta}{\rho^2(1+d\rho^{-1/3})} \\
&\quad - ab\omega \left\{ \frac{\rho_\alpha\rho_\beta}{18} \left[ 144(2^{2/3})C_F(\rho_\alpha^{8/3} + \rho_\beta^{8/3}) + (47-7\delta)|\nabla\rho|^2 \right. \right. \\
&\quad \left. \left. - (45-\delta)(|\nabla\rho_\alpha|^2 + |\nabla\rho_\beta|^2) + 2\rho^{-1}(11-\delta)(\rho_\alpha|\nabla\rho_\alpha|^2 + \rho_\beta|\nabla\rho_\beta|^2) \right] \right\} \\
&\quad \left. + \frac{2}{3}\rho^2(|\nabla\rho_\alpha|^2 + |\nabla\rho_\beta|^2 - |\nabla\rho|^2) - (\rho_\alpha^2|\nabla\rho_\beta|^2 + \rho_\beta^2|\nabla\rho_\alpha|^2) \right\} \\
\omega &= \frac{e^{-c\rho^{-1/3}}}{(1+d\rho^{-1/3})\rho^{14/3}} \\
\delta &= c\rho^{1/3} + \frac{d\rho^{-1/3}}{(1+d\rho^{-1/3})}
\end{aligned} \tag{2.66}$$

#### 2.2.4. Hybrid Methods

From the Hamiltonian and the definition of the exchange-correlation energy an exact connection can be made between the exchange-correlation energy and

the corresponding potential connecting the non-interacting reference and the actual system. The resulting equation is called the *Adiabatic Connection Formula* (ACF) and involves an integration over the parameter  $\lambda$  which “turns on” the electron-electron interaction.

$$E_{xc} = \int_0^1 \langle \Psi_\lambda | \mathbf{V}_{xc}(\lambda) | \Psi_\lambda \rangle d\lambda \quad (2.67)$$

In the crudest approximation (taking  $\mathbf{V}_{xc}$  to be linear in  $\lambda$ ) the integral is given as the average of the values at the two end-points.

$$E_{xc} \approx \frac{1}{2} \langle \Psi_0 | \mathbf{V}_{xc}(0) | \Psi_0 \rangle + \frac{1}{2} \langle \Psi_1 | \mathbf{V}_{xc}(1) | \Psi_1 \rangle \quad (2.68)$$

In the  $\lambda = 0$  limit, the electrons are non-interacting and there is consequently no correlation energy, only exchange energy. Furthermore, since the exact wave function in this case is a single Slater determinant composed of KS orbitals, the exchange energy is exactly that given by the Hartree-Fock theory. If the KS orbitals are identical to the HF orbitals, the “exact” exchange is precisely the exchange energy calculated by HF wave mechanics methods.

$$E_{xc}^{B3} = (1-a)E_x^{LSDA} + aE_x^{\text{exact}} + b\Delta E_x^{\text{BSS}} + E_c^{LSDA} + c\Delta E_c^{\text{GGA}} \quad (2.69)$$

Models which include exact exchange are often called *hybrid* methods, the names *Adiabatic Connection Model* (ACM) and *Becke 3 parameter functional* (B3) are examples of such hybrid models defined by Equation (2.69). The  $a$ ,  $b$  and  $c$  parameters are determined by fitting to experimental data and depend on the form chosen for  $E_c^{\text{GGA}}$ , typical values are  $a \sim 0.2$ ,  $b \sim 0.7$  and  $c \sim 0.8$ . Owing to the substantially better performance of such parameterized functionals the Half-and-Half model is rarely used anymore. The B3 procedure has been generalized to include more fitting parameters, however, the improvement is rather small.

## CHAPTER 3

### CALCULATION DETAILS

In this chapter, the investigated models representing interaction between silanol groups on the external surface of silicalite-1 and guest molecules were described. The detailed method and the basis set used in the geometrical optimizations and energetic calculations as well as in the evaluation of spectroscopic frequency were also illustrated.

#### 3.1 Naked Cluster Models

The (010) surface of the silicalite-1 which is perpendicular to the straight channel, was selected and cut from the crystal lattice using the Cerius<sup>2</sup> program. Silanol groups on the surface were generated by adding hydrogen atoms to the cutted O-Si bonds. Due to the size of the silicalite-1 lattice with a crystallographic cell *Pnma* consisting of 96 Si and 192 O atoms, it is not possible to take into account the whole lattice in the quantum chemical calculations. Therefore, the silicalite-1 was represented by three clusters taken from different parts of the (010) surface.

They were, then, named, for simplification, as single silanol (Figure 3.1b, Single), double silanol bridged by -O- group (Figure 3.1c, Double-near) and double silanol bridged by -O-Si-O- group (Figure 3.1d, Double-far). They were, respectively, used to model interactions with the isolated (single) silanol and two possible configurations of the two (double) contacted silanols on the (010) surface. The hydrogen atoms were added to SiO- groups on the surface of the selected fragment, by replacing silicon atoms of the lattice. All O-H bond lengths and Si-O-H angles as well as the rotation of the isolated silanol group around the Si-O bond were optimized, using different levels of quantum chemical calculation. Their chemical compositions, after filling up the remaining valence orbitals of the silicon atoms by the hydrogen atoms, are Si<sub>4</sub>O<sub>13</sub>H<sub>10</sub>, Si<sub>7</sub>O<sub>22</sub>H<sub>16</sub> and Si<sub>9</sub>O<sub>27</sub>H<sub>18</sub>, respectively.

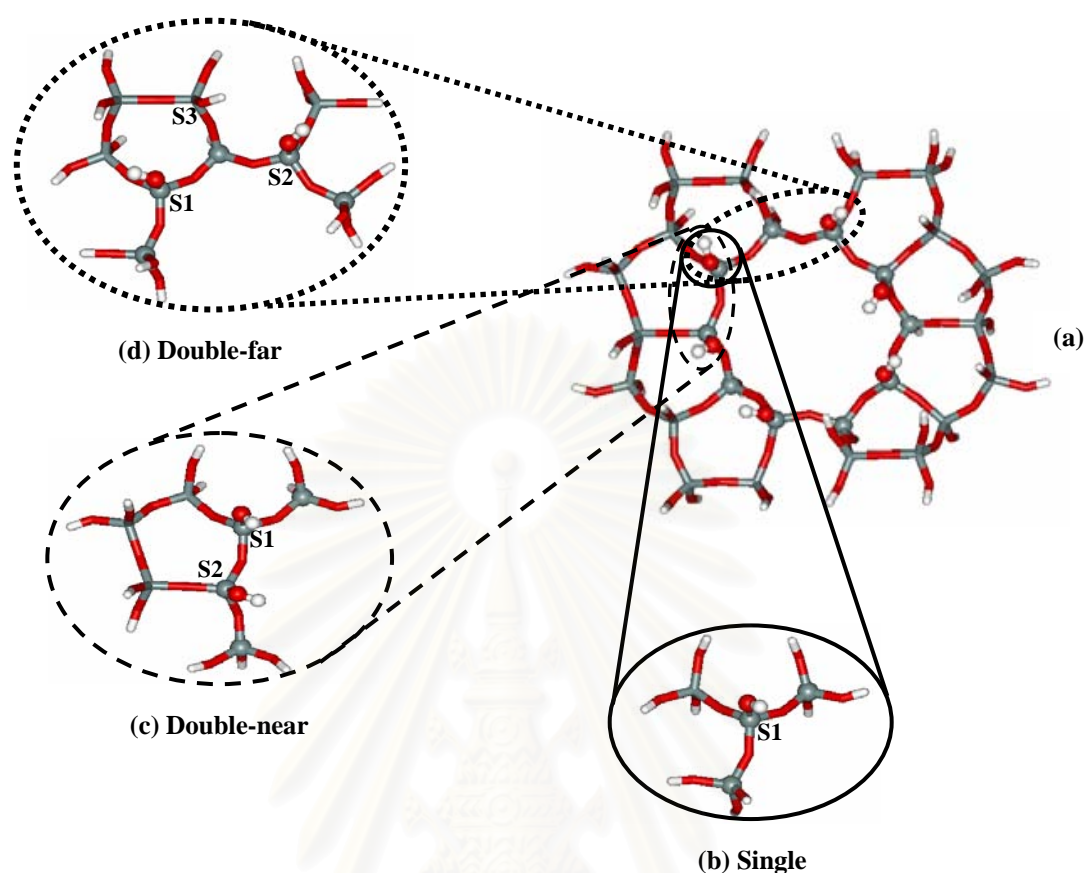


**Figure 3.1** The (010) surface of silicalite-1 (a) and the three  $\text{Si}_4\text{O}_{13}\text{H}_{10}$  (b),  $\text{Si}_7\text{O}_{22}\text{H}_{16}$  (c) and  $\text{Si}_9\text{O}_{27}\text{H}_{18}$  (d) clusters, used to represent the surface in the quantum chemical calculations to evaluate interactions between guest molecules and single (S1), double-near and double-far silanol groups (S1 and S2), respectively (details see text).

### 3.2. Geometries, Interaction Energies and Vibrational Frequencies of the Complexes

#### 3.2.1. Water Molecules

Four possible configurations of a water molecule were assigned to bind to a single silanol group to form mono- (Figures 3.2a-3.2c) and di-hydrated (Figure 3.2d) complexes. They are, then, denoted as Single-I to Single-IV as shown in Figure 3.2.

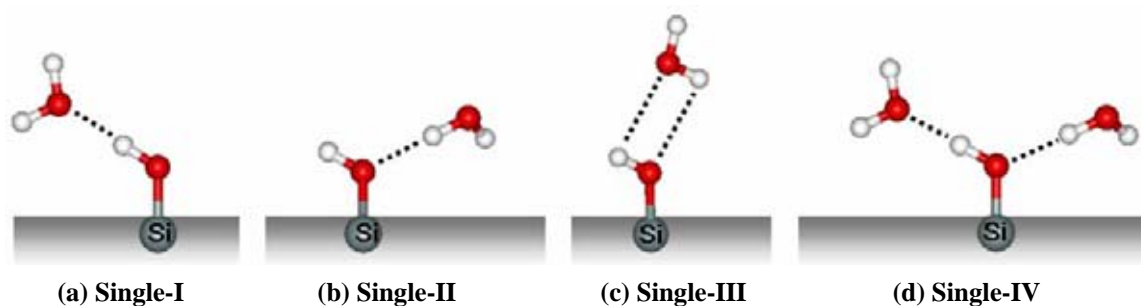


**Figure 3.2** Four investigated conformations representing interaction between single silanol and one (a-c) and two (d) water molecules.

For the case that two silanols with O-O distance of 3.86 Å are bridged by one water molecule, three possible binding configurations, Double-near-I to Double-near-III as in Figures 3.3a-3.3c, were proposed.

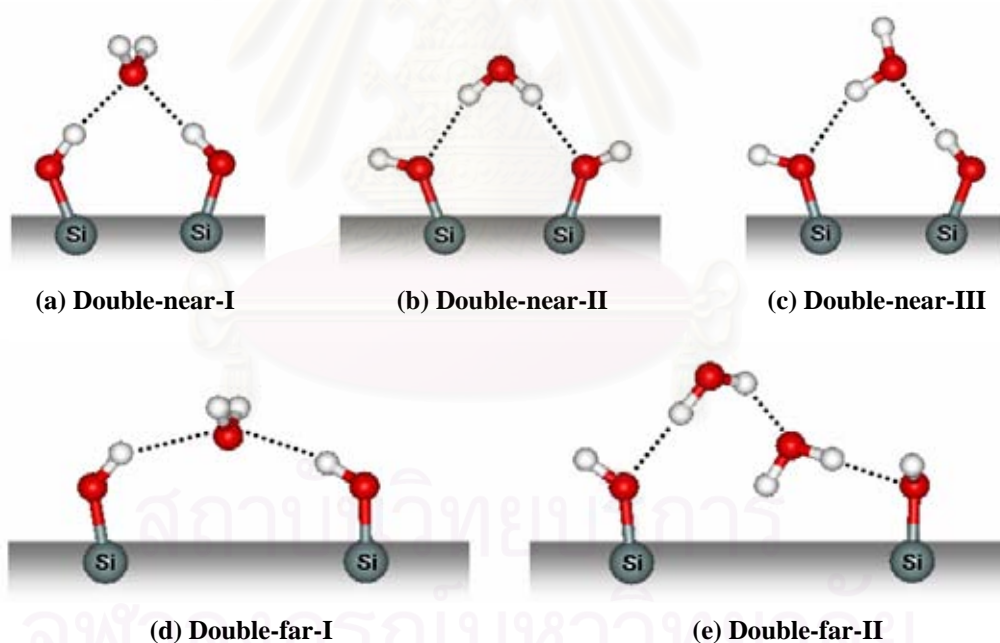


**Figure 3.3** Investigated conformations representing interaction between water molecule and double silanol group: Double-near (a-c) and Double-far (d-e).

The situation is different for the Double-far complex where the O-O distance between the two contacted silanols of 5.75 Å is large enough to accumulate two water molecules. Therefore, the two possible complexes shown in Figures 3.3d-3.3e were examined. Note that the distance between the two silanols in the Double-far system is too large to form complexes with one water molecule as in the configurations shown in Figures 3.3b-3.3c (details were discussed chapter 4).

The intramolecular geometry of the water molecule (O-H bonds and H-O-H angle) and of the silanol group (O-H bond) as well as the intermolecular parameters (distances and orientation of water molecules relative to the silanol group) were fully optimized, using different levels of accuracy. Then, the interaction energy and the vibrational frequencies of the OH stretching of the water molecule and the silanol group were investigated and reported in comparison to the experimental data. The following two procedures were applied for the quantum chemical calculations: (i) optimize the geometry of the complex using the Hartree Fock method with 3-21G\* basis set, HF/3-21G\*, then, performance of the single point calculation using different levels of accuracy, HF/6-31G(d,p), HF/6-31++G(d,p), B3LYP/6-31G(d,p) and B3LYP/6-31++G(d,p), to get the energy and spectroscopic properties of the complexes. (ii) the same method and level of accuracy were applied for both steps, geometry optimizations and energies as well as spectroscopic calculations. For simplification, abbreviations were used, for example HF/3-21G\*/HF/6-31++G(d,p), the HF/3-21G\* and the HF/6-31++G(d,p) were used in the geometry optimization and the single point calculation, respectively.

Binding energies ( $\Delta E_{\text{bind}}$ ) for the single silanol cluster are described by the summation of the two terms,

$$\Delta E_{\text{bind}} = \Delta E_{\text{deform}} + \Delta E_{\text{interact}} \quad (3.1)$$

where  $\Delta E_{\text{deform}}$  is the deformation energy required to change the geometry of water and silanol from their equilibrium configuration in free forms, (water-free) and (cluster-free), to those suitable for complexation, (water-cpx) and (cluster-cpx), defined as

$$\text{for cluster:} \quad \Delta E_{\text{deform}} = E(\text{cluster-cpx}) - E(\text{cluster-free}) \quad (3.2a)$$

$$\text{for water:} \quad \Delta E_{\text{deform}} = E(\text{water-cpx}) - E(\text{water-free}) \quad (3.2b)$$

where  $E(\text{cluster-cpx})$  and  $E(\text{cluster-free})$  are the total energy of the clusters in the configuration given in parenthesis. The same method was also applied for the  $E(\text{water-cpx})$  and  $E(\text{water-free})$ . For the second term in equation (3.1),  $\Delta E_{\text{interact}}$  was defined based on supermolecular approach according to equation (3.3),

$$\Delta E_{\text{interact}} = E(\text{cluster-cpx/water}) - E(\text{cluster-cpx}) - E(\text{water-cpx}) \quad (3.3)$$

here,  $E(\text{cluster-cpx/water})$  stands for the total energy of the complex in its optimal configuration where as  $E(\text{cluster-cpx})$  and  $E(\text{water-cpx})$  are the total energies of the silanol cluster and of the water molecule at the complex configuration obtained from quantum chemical calculations, respectively.

For the double silanol groups complexed with water molecule, the two silanols have to be rotated to the configuration suitable for complexation. The rotational energy required for this process was included into the  $\Delta E_{\text{deform}}$  which defined in equation (3.2a).

### 3.2.2. Methane Molecules

Interaction between methane molecule and the (010) surface of the silicalite-1 was calculated in a similar manner as that of water molecule. As it is known for a weak interaction system such as hydrocarbon that major contribution to the molecular interaction is dispersion forces. Therefore, beside the B3LYP/6-31++G(d,p) calculation which was considered as the appropriate method for water molecule, the second-order Møller-Plesset perturbation (MP2) method which was successfully used in the previous works [64], was also examined. The same method was applied for both geometry optimization and the single point calculation.

Interactions with methane molecule was evaluated in the two configurations, Single and Double-near, shown in Figures 3.4a-3.4b. The same reason as for the water molecule, interaction between methane and surface of the silicalite-1 in the Double-far (see Figure 3.3d or 3.3e) configuration was not taken into consideration.

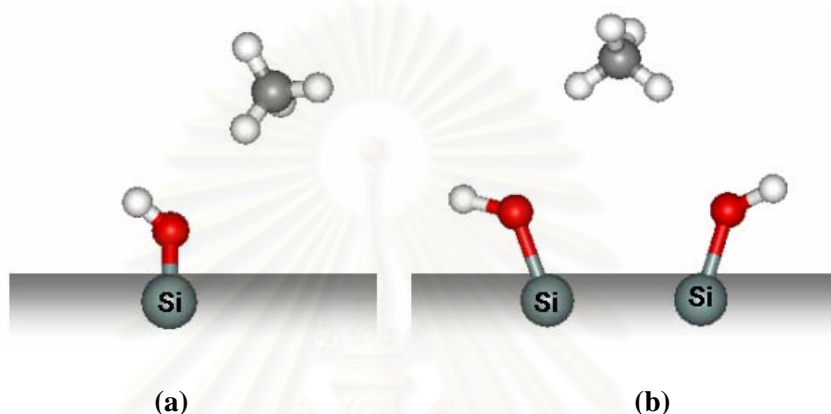


**Figure 3.4** Investigated conformations representing interaction between methane molecules and the single (a) and double (b) silanol groups on the silicalite-1's surface.

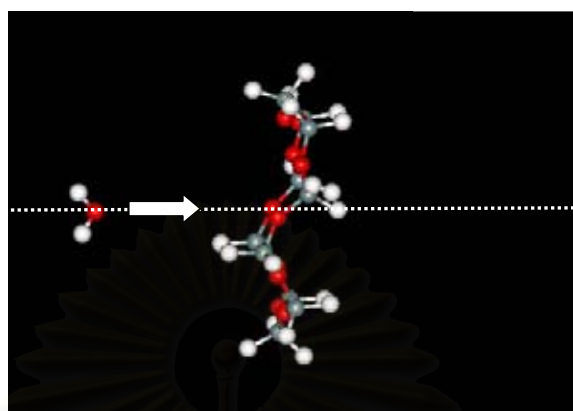
As in the case of water, observed geometry changes via complexation were insignificant. In addition, the molecular geometries were assumed to be much less induced by the hydrophobic molecule, such as hydrocarbons, than by the hydrophilic one. Therefore, intramolecular geometries were kept constant via the optimizations. However, position and orientation of guest molecules as well as their rotation of the OH groups of the silanols were fully optimized. This means that the  $\Delta E_{\text{deform}}$  for the hydrocarbon-surface complex consists of only the energy required to rotate O-H groups of the silanol from their free form to those suitable for complexation.



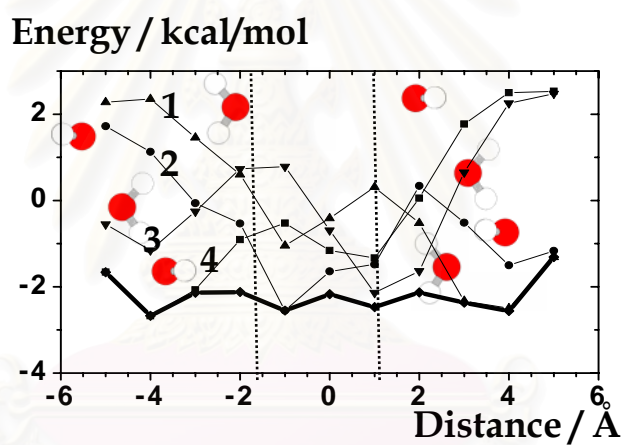
### 3.3. Estimated Energy Barrier

To estimate the energy barrier for guest molecules to enter into the silicalite-1's pore, details of investigation are based on Figure 3.5 taken from Ref. [65]. Here, interaction energies were calculated for a water molecule moving through the straight channel of the silicalite-1. Numerous configurations of water molecules were generated along the vector pointing through the center of the ring and parallel to the inner wall of the straight channel, varying the water orientation around the  $x$ ,  $y$  and  $z$  axes. The rotational step was  $15^\circ$  and the translational step was  $1 \text{ \AA}$ . The interaction energies for the four configurations were given in Figure 3.5a where the optimal route was represented by the dot solid-line. The calculations were based on the HF method with the 6-31G\* basis set. The plot for the optimal route shows very clear that at the distance  $4 \text{ \AA}$  before entering and after leaving to the ring, the average interaction energy is  $\sim -2.5 \text{ kcal/mol}$ . In addition, binding of water molecule to the inner wall of the straight channel of the silicalite-1 leads to the stabilization energy of  $\sim -0.95 \text{ kcal/mol}$ , which is higher than that of  $\sim -2.5 \text{ kcal/mol}$  when water moves along the optimal route (see Ref. [65] for more details).

Based on the above data, guest molecules were placed at the center of the ring. The same fragment as in Ref. [65] was used. The binding energy was calculated using the B3LYP/6-31++G(d,p) method. The obtained data were used as the optimal binding energy when guest molecules locate inside the straight channel of the silicalite-1,  $\Delta E_{\text{bind-in}}$ . In addition, the optimal binding energy outside the channel,  $\Delta E_{\text{bind-out}}$ , was represented by that obtained from section 3.2, for the binding energy between guest molecules and silanol groups. With this criteria, the energy barrier ( $\Delta E_{\text{barrier}}$ ) for guest molecules to enter the straight channel via the adsorption due to the silanol groups on the (010) surface of the silicalite-1 can be estimated from the energetic difference ( $\Delta\Delta E$ ) between the  $\Delta E_{\text{bind-in}}$  and the  $\Delta E_{\text{bind-out}}$  as defined in Figure 3.6.



(b)



(a)

**Figure 3.5** Interaction energy versus water-silicalite-1 distance (a) when a water molecule moves through the center of the straight channel (b) in the four configurations shown in the insert. The dot solid-line represents the optimal route. The results were calculated using the HF method with the 6-31G\* basis set and BSSE corrections and taken from Ref. [65].

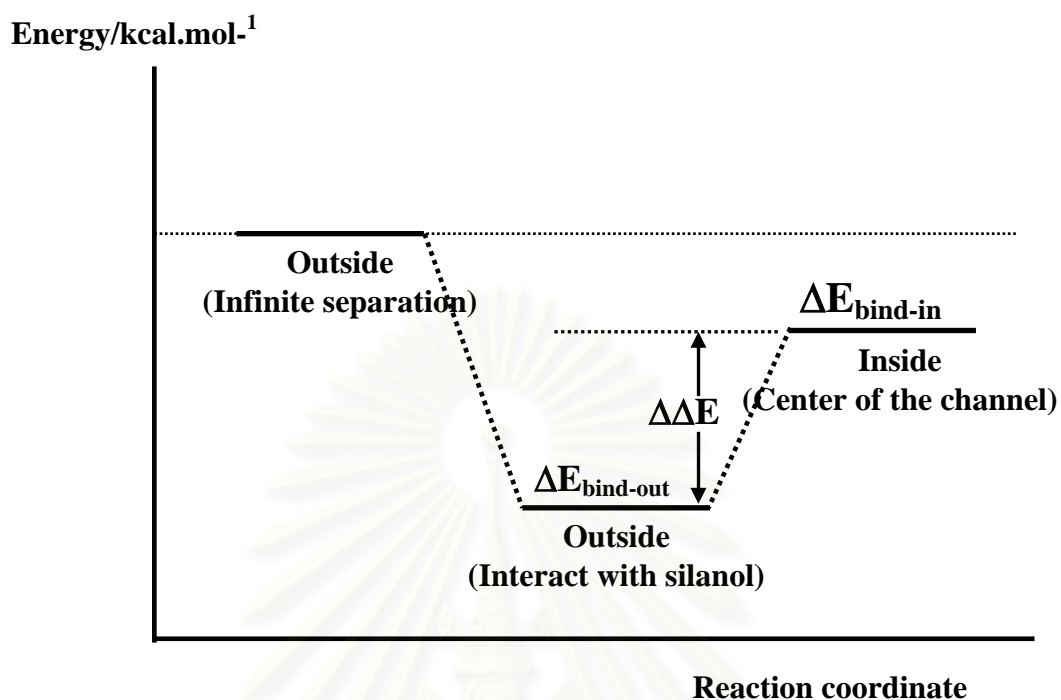


**Figure 3.6** Binding energy when the guest molecule coordinates to the silanol group outside the channel ( $\Delta E_{\text{bind-out}}$ ) and at the center of the channel ( $\Delta E_{\text{bind-in}}$ ) as well as their differences ( $\Delta\Delta E$ ) which were used to estimate the energy barrier ( $\Delta E_{\text{barrier}}$ ) for guest molecule to enter into the straight channel of the silicalite-1 via the (010) surface (see text for more details).

สถาบันวิทยบริการ  
จุฬาลงกรณ์มหาวิทยาลัย

## CHAPTER 4

### RESULTS AND DISCUSSION

#### 4.1. Water-Silanol Complexes

##### 4.1.1. Complexes with Single Silanol

###### 4.1.1.1. Optimal Method, Basis Set and Interaction Energies

For the four selected configurations (Figures 3.2a-3.2d) of the complexes between water molecules and single silanol groups and the surface geometry yielded from the HF/3-21G\* optimization, interactions between a water molecule and a single silanol group were calculated using different levels of accuracy. The results were summarized in Table 4.1. The calculated results lead to the following conclusions: (i) No significant difference was found in terms of deformation energy of the four complexes, due to the change of the geometry of water and silanol via complexation. However, the Single-IV complex requires higher deformation energy than those of the three configurations. (ii) With the same basis set, the interaction energies obtained from the B3LYP method are significantly lower than those of the HF one. (iii) Among the four calculations, the interaction energies in the four configurations are in the following order: B3LYP/6-31G(d,p)  $\ll$  B3LYP/6-31++G(d,p)  $<$  HF/6-31G(d,p)  $\ll$  HF/6-31++G(d,p). (iv) Among the three configurations complexed with one water molecule, the B3LYP/6-31G(d,p) predicts the Single-II (Figure 2a) as the most stable conformation and the stability is in the following order: Single-II  $<$  Single-I  $\ll$  Single-III while the other calculations indicate that the Single-I is more stable than the Single-II. The only reason that can be found for such a discrepancy is that the optimal geometry of the surface yielded from the HF/3-21G\* and used for the single point calculation, is not the optimal form for the other calculations.

**Table 4.1** Interaction and deformation energies (kcal/mol) representing complexation between water and single silanol groups in the configurations shown in Figure 3.2 where the surface geometry (Figure 3.1b) was optimized using the HF/3-21G\* while the energy was calculated using different levels of accuracy (see calculation details).

Cluster type	HF/3-21G*// HF/6-31G(d,p)			HF/3-21G*// HF/6-31++G(d,p)			HF/3-21G*// B3LYP/6-31G(d,p)			HF/3-21G*// B3LYP/6-31++G(d,p)		
	$\Delta E_{\text{deform}}$	$\Delta E_{\text{interact}}$	$\Delta E_{\text{bind}}$	$\Delta E_{\text{deform}}$	$\Delta E_{\text{interact}}$	$\Delta E_{\text{bind}}$	$\Delta E_{\text{deform}}$	$\Delta E_{\text{interact}}$	$\Delta E_{\text{bind}}$	$\Delta E_{\text{deform}}$	$\Delta E_{\text{interact}}$	$\Delta E_{\text{bind}}$
Single-I	1.11	-7.38	-6.27	0.96	-6.26	-5.30	0.76	-9.73	-8.97	0.54	-7.66	-7.12
Single-II	0.45	-6.05	-5.60	0.34	-3.69	-3.35	0.44	-10.30	-9.86	0.26	-5.71	-5.45
Single-III	0.17	-1.10	-0.93	0.13	-0.58	-0.45	0.13	-2.62	-2.49	0.07	-1.42	-1.35
Single-IV*	2.22	-15.00 (-7.50)	-12.78 (-6.39)	1.95	-11.38 (-5.69)	-9.43 (-4.72)	1.54	-22.04 (-11.02)	-20.50 (-10.25)	1.11	-15.13 (-7.56)	-14.02 (-7.01)

\*the interaction and binding energy per water molecule are given in parenthesis, respectively.

In order to examine the above mentioned discrepancy, different methods were applied to optimize the geometry of the silanol cluster. The calculated geometry of the single silanol in the free form (Figure 3.1b) as well as the corresponding atomic net charges were given in Table 4.2.

**Table 4.2** Optimal geometry, O-H bond length (Å) and Si-O-H bond angle (in degree), and atomic net charges (in atomic unit),  $q_i$  where  $i$  denotes H, O and Si atoms, of the single silanol in free form yielded from different calculations.

Parameter	HF/3-21G*	HF/6-31G(d,p)	HF/ 6-31++G(d,p)	B3LYP/ 6-31G(d,p)	B3LYP/ 6-31++G(d,p)
O-H	0.9557	0.9396	0.9399	0.9600	0.9599
< Si-O-H	130.3	121.5	122.5	119.3	121.4
$q_H$	0.426	0.362	0.417	0.330	0.398
$q_O$	-0.778	-0.719	-1.294	-0.568	-1.132
$q_{Si}$	1.573	1.497	3.454	0.990	2.879

The calculated data support the assumption on the discrepancy in the prediction of the most stable configuration of the complexes between the single silanol and the water molecule (Figure 3.2) shown in Table 4.1. The O-H bond length obtained from the HF method of  $\sim 0.94$  Å is slightly shorter than that of  $\sim 0.96$  Å from the B3LYP calculation. The Si-O-H angle of the silanol group of  $130.3^\circ$  yielded from the HF optimization with the small basis set (3-21G\*) is significantly bigger than those between  $119^\circ$  -  $123^\circ$  obtained from the other calculations. Note that the experimental O-H bond length based on the neutron diffraction method [66] and the calculated Si-O-H bond angle based on the coupled pair functional method employing large basis sets, [6s,5p,2d,1f/5s,3p,2d,1f/3s,2p] [67], are  $0.969$  Å and  $117.7^\circ$ , respectively. These data are in good agreement with the B3LYP results. In addition, it was found also that the atomic net charges, especially on the O and Si atoms of the silanol, depend strongly on the method and the basis set used. The calculated atomic net charges shown in Table 4.2 are too acidic. This leads consequently to a red shift of the O-H vibrational frequency (details in section 4.1.1.2).

To overcome the difficulty due to the surface geometry which is not in the optimal configuration for each calculation, the same method and the same level of accuracy were applied to the optimization of the geometry as well as the single point energy calculations. The results were shown in Table 4.3. It can be clearly seen that the data are more reliable than those shown in Table 4.1. Among the three configurations where one water molecule binds to a single silanol group (Figures 3.2a-3.2c), stabilization energies yielded from all models are in the same trend, which is Single-I < Single-II << Single-III. Based on thermal fluctuation at room temperature ( $T$ ), *i.e.*,  $kT \sim 0.6$  kcal/mol where  $k$  denotes Boltzmann's constant, it can be concluded that all models, except B3LYP/6-31G(d,p) suggest Single-I (Figure 3.2a) and Single-IV (Figure 3.2d) as the preferential conformations for the silanol-water complex. The calculated binding energy is ranging between -7 and -10 kcal/mol. However, the B3LYP/6-31++G(d,p) binding energy is proposed to be the optimal value because of the following reasons. (i) The B3LYP method is superior to the HF calculation because the electron correlation was included. (ii) The 6-31++G(d,p) basis set is more reliable than the 6-31G(d,p) because the electron diffusion is taken into account. This leads to the conclusion that the two predicted conformations where one water forms hydrogen bonding by pointing the O atom to the silanol (Figure 3.2a) and two water molecules bind to one silanol in the configuration shown in Figure 3.4d yield the binding energy of  $\sim -8$  kcal/mol (Table 4.3).

In terms of the deformation energy, the data for all models in Table 4.3 are roughly higher than those in Table 4.1. This indicates clearly that in comparison to the conformations yielded from the HF/3-21G\* optimization (Table 4.1), the equilibrium geometry of the water molecule and the cluster in the free forms, (water-free) and (cluster-free), shown in Table 4.2 are closer to those suitable for complexation, (water-cpx) and (cluster-cpx).

**Table 4.3** Interaction and deformation energies (kcal/mol) representing complexation between water and single silanol groups in the configurations shown in Figure 3.2 where the surface optimization and the energy calculations were performed using the same levels of accuracy (see calculation details).

Cluster type	HF/6-31G(d,p)// HF/6-31G(d,p)			HF/6-31++G(d,p)// HF/6-31++G(d,p)			B3LYP/6-31G(d,p)// B3LYP/6-31G(d,p)			B3LYP/6-31++G(d,p)// B3LYP/6-31++G(d,p)		
	$\Delta E_{\text{deform}}$	$\Delta E_{\text{interact}}$	$\Delta E_{\text{bind}}$	$\Delta E_{\text{deform}}$	$\Delta E_{\text{interact}}$	$\Delta E_{\text{bind}}$	$\Delta E_{\text{deform}}$	$\Delta E_{\text{interact}}$	$\Delta E_{\text{bind}}$	$\Delta E_{\text{deform}}$	$\Delta E_{\text{interact}}$	$\Delta E_{\text{bind}}$
Single-I	0.11	-8.34	-8.23	0.05	-7.43	-7.38	0.62	-10.76	-10.14	0.14	-8.39	-8.25
Single-II	0.05	-6.33	-6.28	0.02	-4.78	-4.76	0.45	-10.11	-9.66	0.03	-6.03	-6.00
Single-III	0.02	-1.91	-1.89	0.01	-1.54	-1.53	0.39	-3.31	-2.92	0.01	-2.04	-2.03
Single-IV*	0.20	-16.05 (-8.02)	-15.85 (-7.92)	0.11	-13.54 (-6.77)	-13.43 (-6.72)	0.85	-22.39 (-11.20)	-21.54 (-10.77)	0.28	-16.15 (-8.08)	-15.87 (-7.94)

\*the interaction and binding energy per water molecule is given in parenthesis, respectively.



#### 4.1.1.2. Geometries and Vibrational Frequencies

**Table 4.4** Bond length, bond angle and stretching frequency ( $\nu$ ) of water, naked surface and complex between water and single silanol group (Figure 2) using different methods of calculation where subscript “s” and “w” stand for surface and water molecule, respectively. The B3LYP/6-31++G(d,p) data, bold line, were proposed to be the optimal values.

Structure	Method	$r(\text{O}_s\text{-H}_s)$ (Å)	$r(\text{O}_s\cdots\text{O}_w)$ (Å)	$r(\text{O}_w\text{-H}_w)$ (Å)	$\langle\text{H}_w\text{-O}_w\text{-H}_w\rangle$ (degree)	$\nu\text{O}_s\text{-H}_s$ ( $\text{cm}^{-1}$ )	sym. $\nu\text{O}_w\text{-H}_w$ ( $\text{cm}^{-1}$ )
<b>Water:</b>							
Exp.	Ref. [68]	-	-	0.9576	104.48	-	3345
Calc.	HF/6-31G(d,p)	-	-	0.9431	106.04	-	3732
	B3LYP/6-31G(d,p)	-	-	0.9653	103.71	-	3420
	HF/6-31++G(d,p)	-	-	0.9433	107.12	-	3731
	<b>B3LYP/6-31++G(d,p)</b>	-	-	<b>0.9652</b>	<b>105.73</b>	-	<b>3426</b>
<b>Naked Surface:</b>							
Exp.	Ref. [7]	-	-	-	-	3750	-
Calc.	HF/6-31G(d,p)	0.9396	-	-	-	3834	-
	B3LYP/6-31G(d,p)	0.9600	-	-	-	3545	-
	HF/6-31++G(d,p)	0.9399	-	-	-	3833	-
	<b>B3LYP/6-31++G(d,p)</b>	<b>0.9599</b>	-	-	-	<b>3551</b>	-
<b>Complex:</b>							
Exp.	Ref. [69]	0.956-1.000	2.70-2.90	-	-	-	-
Single-I	HF/6-31G(d,p)	0.9494	2.8477	0.9434	107.45	3664	3734
	B3LYP/6-31G(d,p)	0.9758	2.7464	0.9640	106.56	3271	3441
	HF/6-31++G(d,p)	0.9485	2.8883	0.9441	107.87	3681	3726
	<b>B3LYP/6-31++G(d,p)</b>	<b>0.9736</b>	<b>2.7958</b>	<b>0.9651</b>	<b>107.34</b>	<b>3310</b>	<b>3434</b>
Single-II	HF/6-31G(d,p)	0.9417	2.9459	0.9442	107.40	3807	3713
	B3LYP/6-31G(d,p)	0.9620	2.8933	0.9675	105.87	3522	3380
	HF/6-31++G(d,p)	0.9422	2.9405	0.9445	107.97	3804	3707
	<b>B3LYP/6-31++G(d,p)</b>	<b>0.9623</b>	<b>2.8772</b>	<b>0.9679</b>	<b>106.91</b>	<b>3524</b>	<b>3371</b>
Single-III	HF/6-31G(d)	0.9438	2.8900	0.9428	106.34	3786	3738
	B3LYP/6-31G(d)	0.9651	2.7200	0.9646	104.67	3489	3430
	HF/6-31++G(d,p)	0.9439	2.9470	0.9432	107.17	3783	3735
	<b>B3LYP/6-31++G(d,p)</b>	<b>0.9649</b>	<b>2.8090</b>	<b>0.9652</b>	<b>106.03</b>	<b>3495</b>	<b>3430</b>

In Table 4.5, intra- and intermolecular geometries as well as spectroscopic properties of water, naked surface and surface-water complexes in the four configurations shown in Figure 3.2 were summarized. Here, the same method was used to optimize water, naked surface and complex geometries.

For the free water molecule, the geometry yielded from the four models, HF and B3LYP methods with 6-31G(d,p) and 6-31++G(d,p) basis sets, is in good agreement with the experimental measurements [66]. The Hartree-Fock O-H bond length of  $\sim 0.943 \text{ \AA}$  is slightly shorter than the experimental one while the B3LYP value of  $\sim 0.965 \text{ \AA}$  is longer than the experimental data. (This shorter one arises from lacking of electron correlation of the HF method.)

In addition, no significant difference of the O-H bond was found among the two basis sets used. In terms of the H-O-H angle, the B3LYP method is slightly better than the HF in representing the experimental data ( $104.48 \text{ \AA}$ ). The values for the frequencies corresponding to two symmetrical O-H stretchings of the water molecule obtained from the B3LYP calculations ( $3420$  and  $3426 \text{ cm}^{-1}$ ) are in good agreement with the  $3345 \text{ cm}^{-1}$  obtained experimentally. This is not the case for the HF method from which a frequency of more than  $3700 \text{ cm}^{-1}$  was calculated. The above finding leads to the conclusion that the B3LYP method is appropriate for geometry optimization and still good enough to reproduce the experimental frequency.

Considering the naked (010) surface (Table 4.4) represented by the  $\text{Si}_4\text{O}_{13}\text{H}_{10}$  fragment as shown in Figure 3.1b, the predicted O-H bond of the silanol group is in the range  $0.94\text{-}0.96 \text{ \AA}$ . The OH stretchings of  $3545 \text{ cm}^{-1}$  and  $3551 \text{ cm}^{-1}$  determined from the B3LYP method are significantly lower than the experimental vibrational frequencies of the stretching mode of the isolated OH groups located on the external surface of nonporous silica (Aerosil) of  $3750 \text{ cm}^{-1}$  [7]. This discrepancy can be due to a too acidic atomic charges of the silicon atom in the framework shown in Table 4.2. Note that there is no significant difference in the vibrational frequencies arising from the same method using different basis sets.

For the silanol-water complex, the attention focused to the Single-I complex where the most stable conformation of the complex was detected. The experimental O-H bond length of the silanol ( $0.956\text{-}1.000 \text{ \AA}$ ) and the intermolecular distance between oxygen atoms of silanol and water molecule,  $\text{O}_s\text{---O}_w$ , ( $2.70\text{-}2.90 \text{ \AA}$ )

cover broad ranges, that include all calculated data. The calculated O-H bond length of the silanol in free form was detected to be slightly larger than that in the complex. This fact is true for all calculated methods and basis sets used. However, such change was not clearly observed for the O-H bond length and the H-O-H angle of the water molecule. In terms of the stretching frequency, the complexation leads to red shift of the O-H stretching of the silanol group, approximately  $150\text{ cm}^{-1}$  and  $270\text{ cm}^{-1}$  for the HF and B3LYP calculations, respectively. This event was not detected for the O-H bond of the water molecule. Taking into account the data and conclusions summarized above including the discrepancy among the methods and the basis sets used, the data obtained from the B3LYP/6-31++G(d,p) were proposed to be the optimal values.

## 4.1.2. Double Complexes

### 4.1.2.1. Interaction Energies

For the sake of accuracy, as stated in the case of Single-I, only the B3LYP/6-31++G(d,p)//B3LYP/6-31++G(d,p) calculations were applied to investigate interaction and optimal configuration between water and the two nearest silanol groups (Figure 3.2). The optimal values are summarized in Table 4.5. Note that binding between two silanols and one water molecule requires an additional step in rotating of the silanol groups to the configuration suitable for complexation. The rotational energy was included in the  $\Delta E_{\text{deform}}$  of the cluster, defined in Equation (3.2a) which was added to the interaction energy in equation (3.1).

Some comments could be made concerning the final geometry of the Double-far-I complex. With the initial configuration shown in Figure 3.3d, the B3LYP/6-31++G(d,p) fully optimization procedure brings the water molecule to the configuration shown in Figure 4.1 where the water molecule prefers to coordinate to S3 (see Figure 3.1d) rather than to S2. Here, the distance from the O atom of water to the O atom of silanol S1 or S3 is  $2.90\text{ \AA}$  while that of S2 is  $3.75\text{ \AA}$ . This result supports our assumption made in section 3.2 (Calculation details) that the distance between the two silanols, S1 and S2, in the Double-far is too large to be coordinated by a single water molecule.

In terms of complex stability, the most stable complex takes place via the Double-far-I complex. The corresponding binding energy is -13.84 kcal/mol. This value is significantly lower than those of -9.05 kcal/mol for the Double-far-II and -7.82 kcal/mol for the Double-near-III complexes. In addition, the deformation energies for the double silanol complexes shown in Table 4.5 are higher than those of the single silanol one in Table 4.3 due to the addition of the rotational energy into the  $\Delta E_{\text{deform}}$  term, as defined in equation (3.2a).

The rotational energy for the Double-far configurations is much lower than that of the Double-near complexes due to a larger O-O distance between the two silanols which amount to 5.75 Å and 3.86 Å, respectively. Strong repulsion between the two OH groups leads to the  $\Delta E_{\text{deform}}$  in the Double-near-I configuration (Figure 3.3a) of 8.36 kcal/mol. This energy decreases to 5.68 kcal/mol when the two OH groups turn away from each other (Double-near-II, Figure 3.3b). In addition, the repulsion is lower when the H atom of one OH points toward the O atom of the other OH groups (Figure 3.3c).

**Table 4.5** The deformation energy and binding energy (kcal/mol) representing interaction between water and two silanol groups in the configurations shown in Figure 3 where the surface optimization and the energy calculations were performed using B3LYP/6-31++G(d,p) (see calculation details).

Cluster type	$\Delta E_{\text{deform}}$	$\Delta E_{\text{interact}}$	$\Delta E_{\text{binding}}$
Double-near-I	8.36	-14.02	-5.66
Double-near-II	5.68	-3.65	2.03
Double-near-III	2.28	-10.10	-7.82
Double-far-I	0.62	-14.45	-13.84
Double-far-II*	0.25	-17.85	-18.10 (-9.05)

\*with the initial configuration shown in Figure 3.3d, the optimal structure in Figure 4.1b was yielded.

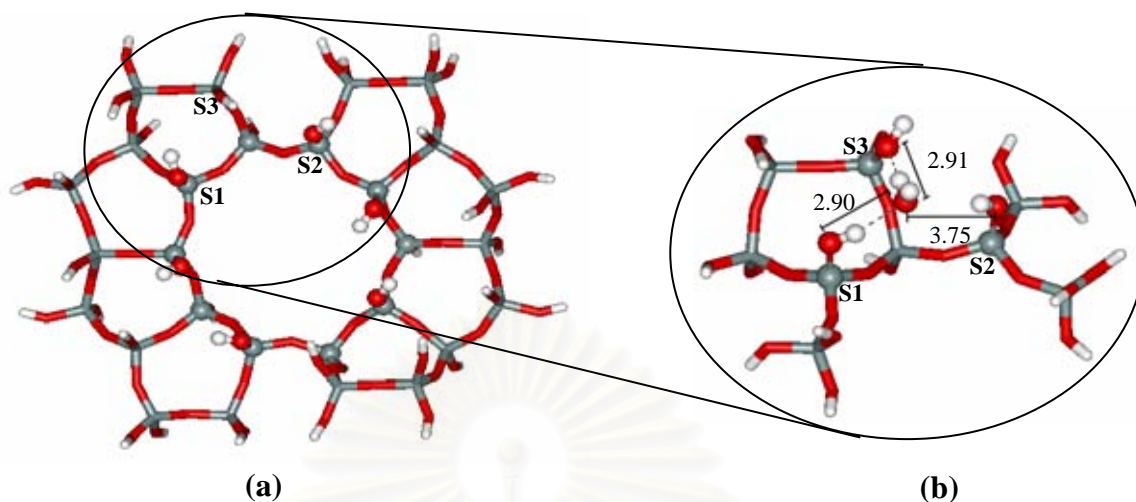


**Figure 4.1** (a) The (010) surface of silicalite-1 and (b) with the initial configuration shown in Figure 3d, the B3LYP/6-31++G(d,p) fully optimization procedure brings the water molecule to the new configuration where water molecule prefers more to coordinate to S3 (see Figure 1d) than that to S2.

Taking into account all the data summarizing above, the B3LYP/6-31++G(d,p) binding energies are in the following order: Double-far-I < Double-far-II ~ Single-I ~ Single-IV ~ Double-near-III. Since the stability of -13.84 kcal/mol for the Double-far-I complex (Figure 3d) is significantly lower than the other configurations, therefore, these areas on the (010) surface of the silicalite-1 are supposed to be the first binding sites which have to be covered when water molecule approaches the surface. In the other words, the most stable conformation takes place when a water molecule forms two hydrogen bonds with two silanols, only one lies on the opening pore of the straight channel. When the water loading increases, the next favorable silanols are those of the pore opening in which the complex conformations are Double-far-II, Single-I, Single-II and Double-near-III where the corresponding binding energy for those coordinations are ~ -8 kcal/mol.

## 4.2. Methane-Silanol Complexes

**Table 4.6** The deformation energy and binding energy (kcal/mol) representing interaction between methane and silanol groups in the configurations are shown in Figure 3.2 where the surface optimization and the energy calculations were performed using HF/6-31++G(d,p), B3LYP/6-31++G(d,p) and MP2/6-31++G(d) (see calculation details).

Cluster type	HF/6-31++G(d,p)// HF/6-31++G(d,p)			B3LYP/6-31++G(d,p)// B3LYP/6-31++G(d,p)			MP2/6-31++G(d)// MP2/6-31++G(d)		
	$\Delta E_{\text{deform}}$	$\Delta E_{\text{interact}}$	$\Delta E_{\text{bind}}$	$\Delta E_{\text{deform}}$	$\Delta E_{\text{interact}}$	$\Delta E_{\text{bind}}$	$\Delta E_{\text{deform}}$	$\Delta E_{\text{interact}}$	$\Delta E_{\text{bind}}$
Single	-	-0.30	-	-	-0.26	-	-	-1.28	-
Double	-	-0.16	-	5.68	-0.10	5.58	5.40	-0.67	4.73

For the same reason as in the case of water, the orientation of the silanol group was not taken into consideration for the single silanol group. In contrast to the water/ligand system, the interaction energy for the hydrocarbon/ligand system where the dispersion forces are dominant is very low. The  $\Delta E_{\text{bind}}$  yielded from the HF/6-31++G(d,p) and B3LYP/6-31++G(d,p) calculations are within thermal fluctuation,  $kT$ , at room temperature. No significant difference was found for the interaction energy obtained from the two methods. The MP2/6-31++G(d,p) energy for both single and double clusters are slightly lower than the other two methods.

For the methane-surface interaction in the double-near configuration (Figure 3.4b), the rotational energy of 5.68 kcal/mol and 5.40 kcal/mol obtained from B3LYP/6-31++G(d,p) and MP2/6-31++G(d,p) are much higher than the corresponding interaction energy of -0.10 kcal/mol and -0.67 kcal/mol, respectively. These lead to a strong positive binding energy.

The results mentioned above for both single and double silanol clusters lead to a clear conclusion that the methane molecule does not absorb on the (010) surface of the silicalite-1.

### 4.3. The Energy Barrier for Guest Molecules to Enter into Silicalite-1's channel

Corresponding to the calculation details given in section 3.3, the optimal binding energy on the surface ( $\Delta E_{\text{bind-out}}$ ), the optimal binding energy inside the pore ( $\Delta E_{\text{bind-in}}$ ) and the energy barrier ( $\Delta E_{\text{barrier}}$ ), estimated from the  $\Delta\Delta E$  in Figure 3.6, yielded from the B3LYP/6-31++G(d,p) calculations were summarized in Table 4.7 and shown in Figure 4.2a and 4.2b for water and methane molecule, respectively. It can be seen that strong silanol/water binding leads to a high barrier of 9.08 kcal/mol for water molecules to enter into the straight channel via the (010) surface. In contrast, methane molecule moves from higher energy state (-0.26 kcal/mol) on the (010) surface to the lower energy one (-3.87 kcal/mol) inside the pore. Therefore, the entering process for methane molecules is barrier free.

Experimentally, the sample has to be activated by keeping under high vacuum at 473 K for 20 hours in order to bring water molecules into the pore of silicalite-1 [68]. This fact supports the data shown in Table 4.7 where the energy barrier, due to the silanol/water binding on the (010) surface, of 9.08 kcal/mol was required.

**Table 4.7** Optimal binding energy (kcal/mol) on the surface ( $\Delta E_{\text{bind-out}}$ ), optimal binding energy inside the pore ( $\Delta E_{\text{bind-in}}$ ),  $\Delta\Delta E$  (see Figure 3.6) and the estimated energy barrier ( $\Delta E_{\text{barrier}}$ ) for H<sub>2</sub>O and CH<sub>4</sub> molecules to enter into the straight channel via the (010) surface of the silicalite-1 (see section 3.3 for more details).

Guest molecule	$\Delta E_{\text{bind-out}}$	$\Delta E_{\text{bind-in}}$	$\Delta\Delta E$	$\Delta E_{\text{barrier}}$
H <sub>2</sub> O	-13.84	-4.76	9.08	9.08
CH <sub>4</sub>	-0.26	-3.87	-3.61	0.00 (barrier free)

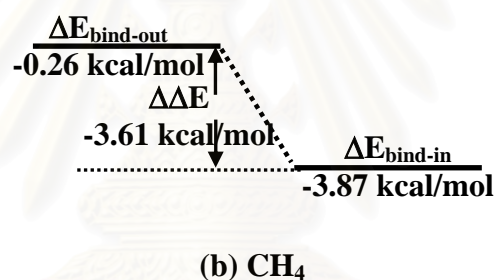
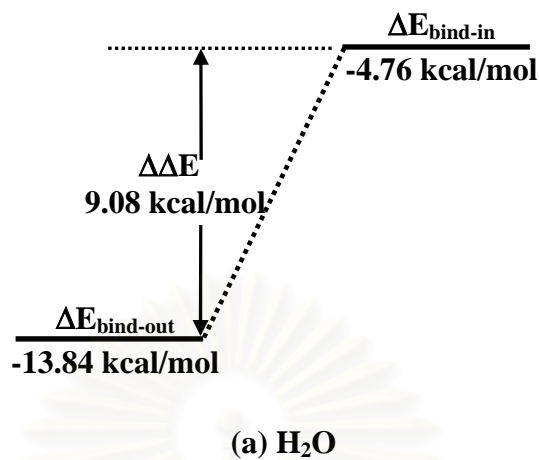


**Figure 4.2** Binding energy when the guest molecule coordinates to the silanol group outside the channel ( $\Delta E_{\text{bind-out}}$ ) and at the center of the channel ( $\Delta E_{\text{bind-in}}$ ) as well as their differences ( $\Delta\Delta E$ ) which were used to estimate the energy barrier ( $\Delta E_{\text{barrier}}$ ) for water (a) and methane molecule (b) to enter into the straight channel of the silicalite-1 via the (010) surface (see text for more details).



## CHAPTER 5

### CONCLUSION

It was known that the key elements determining the adsorption and diffusion behaviors of guest molecules on the external surfaces are silanol groups. Aim of this study is to investigate role of the silanol group in preventing guest molecule to enter into the pore of silicalite-1. Interest is focused on the silanol groups lying around the pore of the straight channel. Therefore, the (010) surface which is perpendicular to the straight channel, was selected. Interaction as well as spectroscopic properties of the systems were calculated for different conformations of guest molecules on the (010) surface of silicalite-1. Quantum chemical calculations were performed using different levels of accuracy.

Based on the B3LYP method with the 6-31++G(d,p) basis set, water molecule was observed to bind tightly by forming 2 hydrogen bonds with the two silanols, one O-H bond of water binds to the silanol located on the open pore of the straight channel while the other one points away from the pore. The corresponding interaction energy is -13.84 kcal/mol. The next preferential binding sites cover broad regions consisting of 4 possible configurations of the complex with the interaction energy of 8 kcal/mol, approximately.

The calculated O-H bond length of the silanol in free form was detected to be slightly larger than that in the complex. However, such change was not clearly observed for the O-H bond length and the H-O-H angle of the water molecule.

In terms of the stretching frequency, the complexation leads to red shift of the O-H stretching of the silanol group, approximately  $150\text{ cm}^{-1}$  and  $270\text{ cm}^{-1}$  for the HF and B3LYP calculations, respectively. This event was not detected for the O-H bond of the water molecule.

For the methane/silicalite-1 complex, the methane-surface interaction is within thermal fluctuation. This is much lower than the energy required to rotate the silanol group. This event leads to a clear conclusion that methane molecule does not absorb on (010) surface of silicalite-1.

The strong silanol/water binding leads to the energy barrier of 9.08 kcal/mol for water molecule to enter into the straight channel via the (010) surface. In contrast, the entering process for methane molecule is barrier free.



สถาบันวิทยบริการ  
จุฬาลงกรณ์มหาวิทยาลัย

## REFERENCES

1. Turro, N. J. From Boiling Stones to Smart Crystals: Supramolecular and Magnetic Isotope Control of Radical-Radical Reactions in Zeolites *Acc. Chem. Res.* **2000**, *33*, 637-646.
2. Turro, N. J.; Lei, X.; Li, W.; Liu, Z.; Ottaviani, M. F. Adsorption of Cyclic Ketones on the External and Internal Surfaces of a Faujasite Zeolite (CaX). A Solid-State  $^2\text{H}$  NMR,  $^{13}\text{C}$  NMR, FT-IR, and EPR Investigation *J. Am. Chem. Soc.* **2000**, *122*, 12571-12581.
3. Park, S. H.; Rhee, H. K. Shape selective conversion of 1,2,4-trimethylbenzene over zeolite NU-87 *Catal. Today* **2000**, *63*, 267-273.
4. Klemm, E.; Scheidat, H.; Emig, G. A study of shape selectivity on zeolites in ethylbenzene disproportionation [Simulation and experiment] *Chem. Eng. Sci.* **1997**, *52*, 2757-2768.
5. Aguilar, J.; Corma, A.; Melo, F. V.; Sastre, E. Alkylation of biphenyl with propylene using acid catalysts *Catal. Today* **2000**, *55*, 225-232.
6. Denayer, J. F.; Baron, G. V.; Vanbutsele, G.; Jacobs, P. A.; Martens, J. H. Modeling of adsorption and bifunctional conversion of n-alkanes on Pt/H-ZSM-22 zeolite catalyst *Chem. Eng. Sci.* **1999**, *54*, 3553-3561.
7. Zecchina, A.; Bordiga, S.; Spoto, G.; Marchese, L. Silicallite Characterization. 2. IR Spectroscopy of the Interaction of CO with Internal and External Hydroxyl Groups *J. Phys. Chem.* **1992**, *96*, 4991-4997.
8. Trombetta, M.; Busca, G.; Lenarda, M.; Storaro, L.; Pavan, M. An investigation of the surface acidity of mesoporous Al-containing MCM-41 and of the external surface of ferrierite through pivalonitrile adsorption *Appl. Catal. A* **1999**, *182*, 225-235.
9. Armaroli, T.; Bevilacqua, M.; Trombetta, M.; Milella, F.; Alejandre, A. G.; Ramírez, J.; Notari, B.; Willey, R. J.; Busca, G. A study of the external and internal sites of MFI-type zeolitic materials through the FT-IR investigation of the adsorption of nitriles *Appl. Catal. A* **2001**, *216*, 59-71.

10. Trombetta, M.; Armaroli, T.; Alejandre, A. G.; Solis, J. R.; Busca, G. An FT-IR study of the internal and external surfaces of HZSM5 zeolite *Appl. Catal. A* **2000**, *192*, 125-136.
11. Armaroli, T.; Trombetta, M.; Alejandre, A. G.; Solis, J. R.; Busca, G. FTIR study of the interaction of some branched aliphatic molecules with the external and internal sites of H-ZSM5 zeolite *Phys. Chem. Chem. Phys.* **2000**, *2*, 3341-3348.
12. Kawai, T.; Tsutsumi, K. Reactivity of silanol groups on zeolite surfaces *Colloid Polym. Sci.* **1998**, *276*, 992-998.
13. Olson, D. H.; Haag, W. O.; Borghard, W. S. Use of water as a probe of zeolitic properties: interaction of water with HZSM-5 *Micropor. Mesopor. Mat.* **2000**, *35*, 435-446.
14. Trombetta, M.; Busca, G. On the Characterization of the External Acid Sites of Ferrierite and Other Zeolites *J. Catal.* **1999**, *187*, 521-523.
15. Cronstedt, A. F. *Akad. Handl. Stockholm*, **1756**, *18*, 120.
16. Breck, D. W. *Zeolite Molecular Sieves: Structure, Chemistry, and Use*; New York: Wiley, 1974.
17. Kärger, J.; Ruthven, D. M. *Diffusion in Zeolites and Other Microporous Solids*; New York: Wiley, 1992.
18. Galarneau, A.; Di Renzo, F.; Fajula, A.; Vindrine, J. *Zeolites and Mesoporous Materials at the Dawn of the 21st Century*, 13<sup>th</sup> International Zeolite Conference Montpellier, France; Elsevier Science: Amsterdam, 2001.
19. Dryer, A. *An Introduction to Zeolite Molecular Sieves*. Chichester, New York, Brisbane, Toronto, Singapore: Wiley, 1988.
20. Meier, W. M.; Olson, D. M. *Atlas of Zeolite Structure Types*. 3<sup>th</sup> ed. London: Butterworth-Heinemann, 1992.
21. Vaughan, D. E. W., *Natural Zeolites: Occurrence, Properties and Use*; Sand, L. B. and Mumpton, F. A. Eds.: London Pergamon, 1978.
22. Meier, W. M.; Moeck, H. J. The topology of three-dimensional 4-connected nets: Classification of zeolite framework types using coordination sequences *J. Solid State Chem.* **1979**, *27*, 349-355.

23. Szostak, R. *Zeolite Molecular Sieves. Principles of Synthesis and Identification*. New York: Van Nostrand Reinhold, 1989.
24. Tsai, T.; Liu, S.; Wang, I. Disproportionation and transalkylation of alkylbenzenes over zeolite catalysts *Appl. Catal. A: General* **1999**, *181*, 355-398.
25. McBain, J. W. *The Sorption of Gases and Vapors by Solids*. London: Rutledge, 1932.
26. Csicsery, S. M. Shape-selective catalysis in zeolites *zeolites* **1984**, *4*, 202-213.
27. Meier, W. M.; Olson, D. M. Preface *zeolites* **1996**, *17*, 1-2.
28. Weitkamp, J.; Puppe, L.; *Catalysis and Zeolites (Fundamentals and Applications)*. Berlin Heidenberg: Springer-Verlag, 1999.
29. Jolimaitre, E.; Tayakout-Fayolle, M.; Jallut, C.; Ragil, K. Determination of Mass Transfer and Thermodynamic Properties of Branched Paraffins in Silicalite by Inverse Chromatography Technique *Ind. Eng. Chem. Res.* **2001**, *40*, 914-926.
30. Sano, T.; Ejiri, S.; Yamada, K.; Kawakami, Y.; Yanagishita, H. Separation of acetic acid-water mixtures by pervaporation through silicalite membrane *J. Membr. Sci.* **1997**, *123*, 225-233.
31. Sano, T.; Hasegawa, M.; Kawakami, Y.; Yanagishita, H. Separation of methanol/*tert*-butyl ether mixture by pervaporation using silicalite membrane *J. Membr. Sci.* **1995**, *107*, 193-196.
32. Morow, B. A.; McFarlan, A. J. Surface vibrational modes of silanol groups on silica *J. Phys. Chem.* **1992**, *96*, 1395-1400.
33. Turro, N. J.; Lei, X.-G.; Li, W.; Liu, Z.; McDermott, A.; Ottaviani, M. F.; Abrams, L. Photochemical and Magnetic Resonance Investigations of the Supramolecular Structure and Dynamics of Molecules and Reactive Radicals on the External and Internal Surface of MFI Zeolites *J. Am. Chem. Soc.* **2000**, *122*, 11649-11659.
34. Kawai, T.; Tsutsumi, K. A Study on the Surface Silanol Groups Developed by Hydrothermal and Acid Treatment of Faujasite Type Zeolites *J. Colloid Interf. Sci.* **2000**, *212*, 310-316.
35. Corma, A. From Microporous to Mesoporous Molecular Sieve Materials and Their Use in Catalysis *Chem Rev.* **1997**, *97*, 2373.

36. Bellussi, G. *Zeolite catalysts for the production of Chemical Commodities: BTX Derivatives in Abstracts and Full Papers of Plenary and Keynote Lectures of the 14<sup>th</sup> International Zeolite Conference*, edited by Van Steen, E.; Callanan, L. H.; Claeys, M.; The Catalysis Society of South Africa: Cape Town, South Africa, 2004.
37. Theodorou D. N.; Snurr. R.; Bell, A. T. *Molecular dynamics and diffusion in microporous materials in Comprehensive Supermolecular Chemistry*: edited by Bein T.; Oxford: Pergamon Press, **1996**, 7, 507.
38. Demontis, P.; Suffritti G. B. Structure and Dynamics of Zeolites Investigated by Molecular Dynamics *Chem. Rev.* **1997**, 97, 2845-2878.
39. Kärger, J. *Molecular transport in zeolites (miracles, insights and practical issues, in Proceedings of the 13<sup>th</sup> International Zeolite Conference*, Materials Research Society: Warrendale, 1999, Baltimore, 1998.
40. Auerbach, S. M.; Jousse, F.; Vercauteren D. P. *Dynamics of sorbed molecular, Computer Modelling of Microporous and Mesoporous Materials*, 2001.
41. Haberlandt, R.; Fritzsche, S.; Vörtler, H. L. *Simulation of microporous systems: confined fluids in equilibrium and diffusion in zeolites in Handbook of Surfaces and Interfaces of Materials*. London, Boston, New York, Sydney, Tokyo, Toronto: Academic Press, **2001**, 5.
42. Kärger, J.; Vasenkov, S.; Auerbach, S. M. *Diffusion in zeolites, Handbook of Zeolite Science and Technology*; Marcel Dekker Inc.: New York, 2003.
43. Vlught, T. J. H.; Krishna, R.; Smit, B. Molecular Simulations of Adsorption Isotherms for Linear and Branched Alkanes and Their Mixtures in Silicalite *J. Phys. Chem. B* **1999**, 103, 1102-1118.
44. Haberlandt, R. Transport processes in porous media: diffusion in zeolites *Thin Solid Films* **1998**, 330, 34-45.
45. Mikhailenko, S. D.; Kaliaguine, S.; Ghali, E. Water-assisted ionic conductance of zeolites with ZSM-5 structure *Microporous Mater.* **1997**, 11, 37-44.
46. Komiyama, M.; Kobayashi, M. Geometry and Energetics of Pyridine Base Adsorption at Water-Zeolite Interfaces: A Simulation Study *J. Phy. Chem. B* **1999**, 103, 10651-10656.

47. Levine, I. N. *Quantum Chemistry*, 5<sup>th</sup> edition; Prentice-Hall, Inc.: New Jersey, 2000.
48. Schaefer, H. F. *Methods of Electronic Structure Theory. Modern Theoretical Chemistry Vol.3* New York: Plenum, 1977.
49. Schaefer, H. F. *Methods of Electronic Structure Theory. Modern Theoretical Chemistry Vol.4* New York: Plenum, 1977.
50. Hehre, W. J.; Random, L.; Schleyer, P. V. R.; Pople, J. A. *Ab Initio Molecular orbital Theory*. New York: Wiley, 1986.
51. Lawley, K. P. *Ab Initio Methods in Quantum Chemistry-I*. New York: Wiley, 1987.
52. Lawley, K. P. *Ab Initio Methods in Quantum Chemistry-II*. New York: Wiley, 1987.
53. Møller, C.; Plesset, M. S. Note on an Approximation Treatment for Many-Electron Systems *Phys. Rev.* **1934**, *46*, 618-622.
54. Bartlett, R. J.; Silver, D. M. Many-body perturbation theory applied to electron pair correlation energies. I. Closed-shell first-row diatomic hydrides *J. Chem. Phys.* **1975**, *62*, 3258-3268.
55. a) Pople, J. A.; Binkley, J. S.; Seeger, R. Theoretical Models Incorporating Electron Correlation *Int. J. Quant. Chem., Quant. Chem. Symp.* **1976**, *10*, 1;  
b) Pople, J. A.; Seeger, R.; Krishnan, R. Variational Configuration Interaction Methods and Comparison with Perturbation Theory *ibid., Symp.* **1977**, *11*, 149.
56. Bartlett, R. J.; Shavitt, I. Comparison of high-order many-body perturbation theory and configuration interaction for H<sub>2</sub>O *Chem. Phys. Lett.* **1977**, *50*, 190-198.
57. Krishnan, R.; Pople, J. A. An Approximate Fourth Order Perturbation Theory of the Electron Correlation Energy *Int. J. Quant. Chem.* **1978**, *14*, 91.
58. Hohenberg P.; Kohn, W. Inhomogeneous Electron Gas *Phys. Rev.*, **1964**, *136*, B864-B871.
59. Kohn, W.; Sham, L. J. Self-Consistent Equations Including Exchange and Correlation Effects *Phys Rev.*, **1965**, *140*, A1133-A1138.

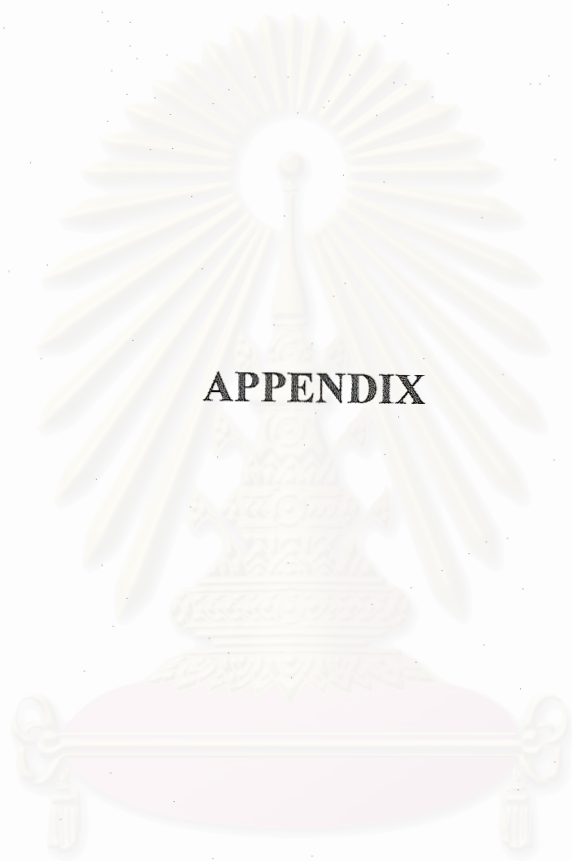
60. Vosko, S. J.; Wilk L.; Nusair, M. Accurate spin-dependent electron liquid correlation energies for local spin density calculations: a critical analysis *Can. J. Phys.*, **1980**, *58*, 1200-1211.
61. Perdew J. D.; Wang, Y. Accurate and simple density functional for the electronic exchange energy: Generalized gradient approximation *Phys Rev.*, B, **1986**, *33*, 8800-8802.
62. Becke, A. D. Density-functional exchange-energy approximation with correct asymptotic behavior *Phys Rev.*, A, **1988**, *38*, 3098-3100.
63. Lee, C.; Yang, W.; Parr, R. G. Development of the Colle-Salvetti correlation-energy formula into a functional of the electron density *Phys. Rev. B*, **1988**, *37*, 785-789.
64. Bussai, C. *Study of Diffusion of Guest Molecules Through Zeolite Pores Using Methods of Quantum Chemistry, Computer Simulations, and Pulse Field Gradient-Nuclear Magnetic Resonance Experiments*; A Ph. D. Dissertation in chemistry: Department of Chemistry, Faculty of Science, Chulalongkorn University, 2002.
65. Bussai, C.; Hannongbua, S.; Haberlandt, R. Understanding the Movement, Encapsulation, and Energy Barrier of Water Molecule Diffusion into and in Silicalites Using Ab Initio Calculations *J. Phy. Chem. B* **2001**, *105*, 3409-3414.
66. Ceccarelli, C.; Jeffrey, G. A.; Taylor, R. A survey of O-H...O hydrogen bond geometries determined by neutron diffraction *J. Mol. Struct.* **1981**, *70*, 255-271.
67. Sauer, J.; Ahlrichs, R. Gas phase acidities and molecular geometries of H<sub>3</sub>SiOH, H<sub>3</sub>COH, and H<sub>2</sub>O *J. Chem. Phys.* **1990**, *93*, 2575-2583.
68. Murphy, W. F.; Bernstein, H. J. Raman spectra and an assignment of the vibrational stretching region of water *J. Phys. Chem.* **1972**, *76*, 1147-1152.
69. Nyfeler, D.; Armbruster, T.; Silanol groups in minerals and inorganic compounds *American Mineralogist* **1998**, *83*, 119-125.
70. Bussai, C.; Liu, H.; Vasenkov, S.; Hannongbua, S.; Fritzsche, S.; Haberlandt, R.; Kaerger, J. On the Diffusion of Water in Silicalite: PFG-NMR



Measurements and MD Simulations using Fully Ab initio Potential *J. App. Cat.* **2002**, 232, 59-66.



สถาบันวิทยบริการ  
จุฬาลงกรณ์มหาวิทยาลัย



**APPENDIX**

สถาบันวิทยบริการ  
จุฬาลงกรณ์มหาวิทยาลัย

**APPENDIX A****MANUSCRIPT**

**Structure and Energetic of Water-Silanol Binding on the Surface of  
Silicalite-1: Quantum Chemical Calculations**

**Oraphan Saengsawang, Tewun Remsungnen, Siegfried Fritzsche,  
Reinhold Haberlandt and Supot Hannongbua**

*To be submitted.*

สถาบันวิทยบริการ  
จุฬาลงกรณ์มหาวิทยาลัย

## Structure and Energetic of Water-Silanol Binding on the Surface of Silicalite-1: Quantum Chemical Calculations

O. Saengsawang<sup>1</sup>, T. Remsungnen<sup>1</sup>, (Jörg Kärger)<sup>2</sup>, S. Fritzsche<sup>2</sup>,  
R. Haberlandt<sup>2</sup> and S. Hannongbua<sup>1\*</sup>

<sup>1</sup>*Department of Chemistry, Faculty of Science, Chulalongkorn University, Bangkok 10330, Thailand*

<sup>2</sup>*Department of Molecular Dynamics/Computer Simulation, Faculty of Physics and Geoscience, Institute for Theoretical Physics (ITP), University of Leipzig, Augustplatz 10-11, 04109 Leipzig, Germany*

### Abstract

Quantum mechanical calculations have been carried out to investigate structural properties and interaction between water molecule and silanol group on the surface of silicalite-1. The (010) surface which is perpendicular to the straight channel, has been selected and represented by three fragments taken from different parts of the surface. Calculations have been performed using different levels of accuracy: HF/6-31G(d,p), B3LYP/6-31G(d,p), HF/6-31++G(d,p), and B3LYP/6-31++G(d,p). The geometry of the silanol groups as well as those of the water molecules have been fully optimized. The results show that the most stable conformation takes place when a water molecule forms two hydrogen bonds with two silanols, only one silanol lying on the opening of the pore of the straight channel. The corresponding binding energy is -13.84 kcal/mol. These areas are supposed to be the first binding sites which have to be covered when the water molecule approaches the surface. When the water loading increases, the next favorable silanols are those of the opening of the pore in which the three possible complex conformations yield the binding energy of  $\sim$ -8 kcal/mol. It was also found that the calculated O-H bond length of the silanol in the free form was slightly larger than that in the complex. In terms of the stretching frequency, the complexation leads to red shift of the O-H stretching of the silanol group.

**Keywords:** *silanol, water, quantum chemical calculation, binding energy, optimal conformation*

---

\*To whom correspondence should be sent  
E-mail address: supot.h@chula.ac.th (Supot Hannongbua)

## 1. Introduction

Zeolites are microporous aluminosilicate materials which have numerous properties that are appropriate for catalysis and separation. The high porosity and the regular system of nanosize pores lead to beneficial characteristics of these materials as for example shape selectivity and catalytic properties. However, before the activities in the pore can take place, the guest molecules have to diffuse into the pore opening of the zeolite that means they have to interact with the external surface. Only recently [1-3] the problem of approach and penetration of guest molecules at the zeolite surface started to be investigated. There exists experimental evidence which shows the significant role of external and internal surfaces and the very complicated nature of their interplay in the shape-size selected catalysis. Turro and coworkers used a combination of different spectroscopic techniques to show the very complicated nature of the shape-size selected catalysis of photolysis reactions of many ketone molecules by FAU and MFI as caused by the external and internal surface (4,5). Isomerization of 1, 2, 4-trimethylbenzene over zeolite NU-87 was observed to take place mainly on the external surface (6) while alkylation of biphenyl over various zeolites was observed only on the external surfaces (7,8). The external surface also contributes to adsorption of C<sub>6</sub>-C<sub>9</sub> *n*-alkanes on Pt/H-ZSM-22 (9).

It is known that the key elements determining the adsorption and diffusion behavior of guest molecules on the external surfaces are silanol groups. Most of the information regarding characteristics of silanol on the external surface of zeolites arises from FTIR experiments (10). It was found that the open surfaces of most of the zeolitic and amorphous silica materials are covered by the silanol groups.

Non-cationic zeolites, in particular silicalite-1 are widely used in the separation of mixtures of light hydrocarbons with water or other polar solvents. It should be noted that the internal surface of perfect silicalite-1 is hydrophobic whereas the external surface is hydrophilic attributable to terminal silanol groups which can interact with guest molecules. Several FTIR experiments expose that the O-H bond of silanol groups is softened when interacting with nitriles (11,12,13,14), alcohols (15), water (16), pyridine (17) and even with aliphatic and aromatic hydrocarbons (13). However, most of the experimental and theoretical works focus on the internal surface that

means the pore or channel whereas much less is known about the details of the external surface.

In this study, the interaction between the silanol groups on the external surface of silicalite-1 and water molecules has been investigated. The energetic and geometric optimizations have been performed using quantum chemical calculations at the Hartree-Fock (HF) as well as at the DFT levels. In addition, the calculated vibrational frequencies have been evaluated and compared with the experimental data.

## 2. Details of Calculations

### 2.1 Naked cluster models

The (010) surface of the silicalite-1 which is perpendicular to the straight channel, was selected and cut from the crystal lattice using the Cerius<sup>2</sup> program. Silanol groups on the surface were generated by adding hydrogen atoms to the cutted O-Si bonds. Due to the size of the silicalite-1 lattice with a crystallographic cell *Pnma* consisting of 96 Si and 192 O atoms, it is not possible to take into account the whole lattice in the quantum chemical calculations. Therefore, the silicalite-1 was represented by three clusters taken from different parts of the (010) surface. They were named, for simplification, as single silanol (Figure 1b, Single), double silanol bridged by -O- group (Figure 1c, Double-near) and double silanol bridged by -O-Si-O- group (Figure 1d, Double-far). They were, respectively, used to model interactions with the isolated (single) silanol and two possible configurations of the two (double) contacted silanols on the (010) surface. The hydrogen atoms were added to SiO- groups on the surface of the selected fragment, by replacing silicon atoms of the lattice. All O-H bond lengths and Si-O-H angles as well as the rotation of isolated silanol groups around the Si-O bond were optimized, using different levels of quantum chemical calculation. Their chemical compositions, after filling up the remaining valence orbitals of the silicon atoms by the hydrogen atoms, are Si<sub>4</sub>O<sub>13</sub>H<sub>10</sub>, Si<sub>7</sub>O<sub>22</sub>H<sub>16</sub> and Si<sub>9</sub>O<sub>27</sub>H<sub>18</sub>, respectively.

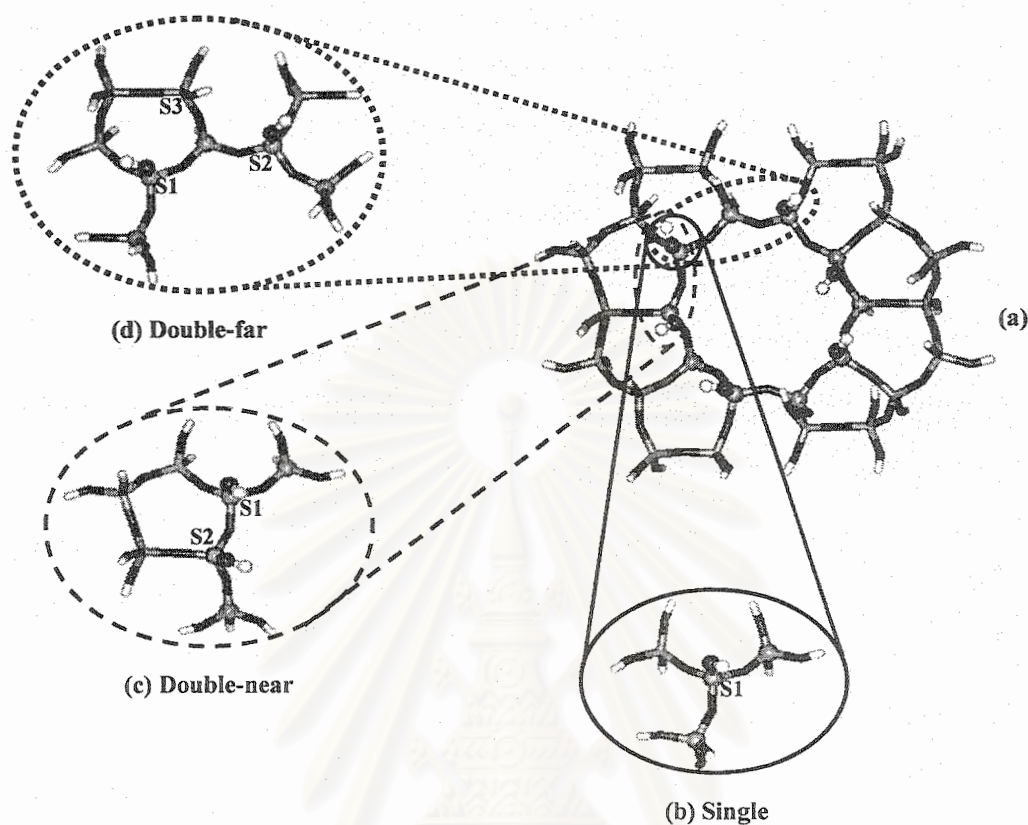


**Figure 1** The (010) surface of silicalite-1 (a) and the three  $\text{Si}_4\text{O}_{13}\text{H}_{10}$  (b),  $\text{Si}_7\text{O}_{22}\text{H}_{16}$  (c) and  $\text{Si}_9\text{O}_{27}\text{H}_{18}$  (d) clusters, used to represent the surface in the quantum chemical calculations to evaluate interactions between water molecules and single (S1), double-near and double-far silanol groups (S1 and S2), respectively (details see text).

## 2.2 Geometries, interaction energies, and vibrational frequencies of the complexes

Four possible configurations of water molecules were assigned to bind to a single silanol group to form mono- (Figures 2a-2c) and di-hydrated (Figure 2d) complexes. They are, then, denoted as Single-I to Single-IV, as shown in Figure 2. For the two contacted silanols bridged by -O- group (Double-near) where the O-O distance between the two silanols is 3.86 Å, three possible binding configurations, Double-near-I to Double-near-III as in Figures 3a-3c, were proposed. The situation is different for the Double-far complex where the O-O distance between the two contacted silanols of 5.75 Å is large enough to accumulate two water molecules. Therefore, the two possible

complexes shown in Figures 3d-3e were examined. Note that the distance between the two silanols in the Double-far system is too large to form complexes with water molecules as in the configurations shown in Figures 3b-3c (details are discussed later).

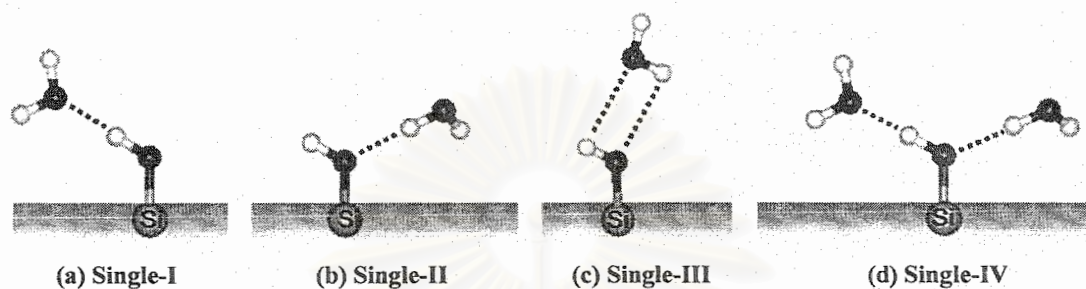


**Figure 2** Four investigated conformations representing interaction between single silanol and one (a-c) and two (d) water molecules.

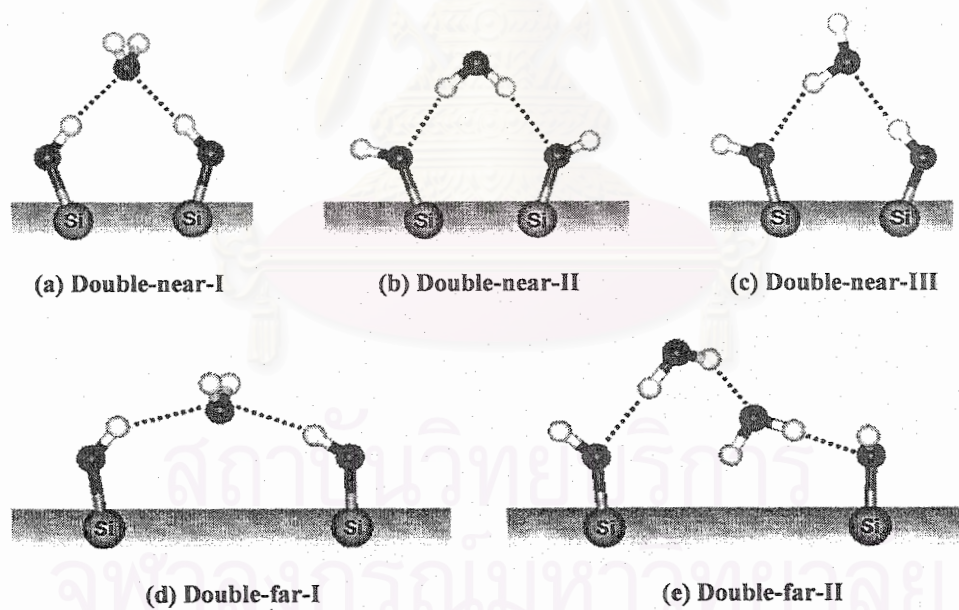


**Figure 3** Investigated conformations representing interaction between water molecule and double silanol group: Double-near (a-c) and Double-far (d-e).



The intramolecular geometry of the water molecule (O-H bonds and H-O-H angle) and of the silanol group (O-H bond) as well as the intermolecular parameters (distances and orientation of water molecules relative to the silanol group) were fully optimized, using different levels of accuracy. Then, the interaction energy and the vibrational frequencies of the OH stretching of the water molecule and the silanol group were investigated and reported in comparison to the experimental data. The following two procedures were applied to the quantum chemical calculations: (i) optimization of the geometry of the complex using the Hartree Fock method with 3-21G\* basis set, HF/3-21G\*, then, performance of the single point calculation using different levels of accuracy, HF/6-31G(d,p), HF/6-31++G(d,p), B3LYP/6-31G(d,p) and B3LYP/6-31++G(d,p), to get the energy and spectroscopic properties of the complexes. (ii) The same method and level of accuracy were applied to both steps, geometry optimizations and energies as well as spectroscopic calculations. For simplification, abbreviations were used, for example HF/3-21G\*/HF/6-31++G(d,p), the HF/3-21G\* and the HF/6-31++G(d,p) were used in the geometry optimization and the single point calculation, respectively.

Binding energies ( $\Delta E_{\text{bind}}$ ) for the single silanol cluster are described by the summation of the two terms,

$$\Delta E_{\text{bind}} = \Delta E_{\text{deform}} + \Delta E_{\text{interact}} \quad (1)$$

where,  $\Delta E_{\text{deform}}$  is the deformation energy required to change the geometry of water and silanol from their equilibrium configuration in free forms, (water-free) and (cluster-free), to those suitable for complexation, (water-cpx) and (cluster-cpx), defined as:

$$\text{for cluster: } \Delta E_{\text{deform}} = E(\text{cluster-cpx}) - E(\text{cluster-free}) \quad (2a)$$

$$\text{for water: } \Delta E_{\text{deform}} = E(\text{water-cpx}) - E(\text{water-free}) \quad (2b)$$

where,  $E(\text{cluster-cpx})$  and  $E(\text{cluster-free})$  are the total energy of the clusters in the configuration given in parenthesis. The same manner was also applied for the  $E(\text{water-cpx})$  and  $E(\text{water-free})$ . For the second term in equation (1),  $\Delta E_{\text{interact}}$  was defined based on supermolecular approach according to equation (3):

$$\Delta E_{\text{interact}} = E(\text{cluster-cpx/water}) - E(\text{cluster-cpx}) - E(\text{water-cpx}) \quad (3)$$

here,  $E(\text{cluster-cpx/water})$  stands for the total energy of the complex in its optimal configuration where as  $E(\text{cluster-cpx})$  and  $E(\text{water-cpx})$  are the total energies of the silanol cluster and of the water molecule at the complex configuration obtained from quantum chemical calculations, respectively.

For the double silanol groups complexed with one or two water molecules, the two silanol clusters have to be rotated to the configuration suitable for complexation. The rotational energy required for this process was included into the  $\Delta E_{\text{deform}}$  which is defined in equation (2a).

### 3. Results and Discussion

#### 3.1 Single silanol complexes

With the four selected configurations (Figures 2a-2d) and the surface geometry yielded from the HF/3-21G\* optimization, the interactions between a water molecule and a single silanol group were calculated using different levels of accuracy. The results were summarized in Table 1 leading to the following conclusions: (i) No significant difference was found in terms of deformation energy of the four complexes, due to the change of the geometry of water and silanol via complexation. However, the Single-IV complex requires higher deformation energy than those of the three other configurations. (ii) With the same basis set, the interaction energies obtained from the B3LYP method are significantly lower than those of the HF one. (iii) Among the four calculations, the interaction energies in the four configurations are in the following order:  $\text{B3LYP/6-31G(d,p)} \ll \text{HF/6-31G(d,p)} < \text{B3LYP/6-31++G(d,p)} \ll \text{HF/6-31++G(d,p)}$ . (iv) Among the three configurations complexed with one water molecule, the B3LYP/6-31G(d,p) predicts the Single-II (Figure 2a) as the most stable conformation and the stability is in the following order:  $\text{Single-II} < \text{Single-I} \ll \text{Single-III}$  while the other calculations indicate that the Single-I is more stable than the Single-II. The only reason that can be found for such a discrepancy is that the optimal geometry of the surface yielded from the HF/3-21G\* and used for the single point calculation, is not the optimal form for the other calculations.

In order to examine the above mentioned discrepancy, different methods were applied to optimize the geometry of the silanol cluster. The calculated geometry of the single silanol in the free form (Figure 1b) as well as the corresponding atomic net charges were given in Table 2. The calculated data support our assumption on the discrepancy in prediction of the most stable configuration of the complexes between the single silanol and the water molecule (Figure 2) shown in Table 1. The O-H bond length obtained from the HF method of  $\sim 0.94 \text{ \AA}$  is slightly shorter than that of  $\sim 0.96 \text{ \AA}$  from the B3LYP calculation. The Si-O-H angle of the silanol group of  $130.3^\circ$  yielded from the HF optimization with the small basis set is significantly larger than those between  $119^\circ - 123^\circ$  obtained from the other calculations. In addition, it was found also that the atomic net charges, especially on the O and Si atoms of the silanol, depend strongly on the method and the basis set used.

**Table 1** Interaction and deformation energies (kcal/mol) representing complexation between water and single silanol groups in the configurations shown in Figure 2 where the surface geometry (Figure 1b) was optimized using the HF/3-21G\* while the energy was calculated using different levels of accuracy (see calculation details).

Cluster type	HF/3-21G*// HF/6-31G(d,p)		HF/3-21G*// HF/6-31++G(d,p)		HF/3-21G*// B3LYP/6-31G(d,p)		HF/3-21G*// B3LYP/6-31++G(d,p)	
	$\Delta E_{\text{deform}}$	$\Delta E_{\text{interact}}$	$\Delta E_{\text{deform}}$	$\Delta E_{\text{interact}}$	$\Delta E_{\text{deform}}$	$\Delta E_{\text{interact}}$	$\Delta E_{\text{deform}}$	$\Delta E_{\text{interact}}$
Single-I	1.11	-7.38	0.96	-6.26	0.76	-9.73	0.54	-7.66
Single-II	0.45	-6.05	0.34	-3.69	0.44	-10.30	0.26	-5.71
Single-III	0.17	-1.10	0.13	-0.58	0.13	-2.62	0.07	-1.42
Single-IV*	2.22	-15.00 (-7.50)	1.95	-11.38 (-5.69)	1.54	-22.04 (-11.02)	1.11	-15.13 (-7.56)

\*the interaction energy per water molecule is given in parenthesis.

**Table 2** Optimal geometry, O-H bond length (Å) and Si-O-H bond angle ( in degree), and atomic net charges (in atomic unit),  $q_i$  where  $i$  denotes H, O and Si atoms, of the single silanol in free form yielded from different calculations.

Parameter	HF/3-21G*	HF/6-31G(d,p)	HF/6-31++G(d,p)	B3LYP/ 6-31G(d,p)	B3LYP/ 6-31++G(d,p)
O-H	0.9557	0.9396	0.9399	0.9600	0.9599
< Si-O-H	130.3	121.5	122.5	119.3	121.4
$q_H$	0.426	0.362	0.417	0.330	0.398
$q_O$	-0.778	-0.719	-1.294	-0.568	-1.132
$q_{Si}$	1.573	1.497	3.454	0.990	2.879

To overcome the difficulty due to the surface geometry which is not in the optimal configuration for each calculation, the same method and the same level of accuracy were applied to the optimization of the geometry as well as the single point energy calculations. The results were shown in Table 3. It can be clearly seen that the data are more reliable than those shown in Table 1. Among the three configurations where one water molecule binds to a single silanol group (Figures 2b-2d), the stabilization energies yielded from all models have the same trend, which is Single-I < Single-II << Single-III. Based on thermal fluctuation at room temperature ( $T$ ), *i.e.*,  $kT \sim 0.6$  kcal/mol where  $k$  denotes Boltzmann's constant, it can be concluded that all models, except B3LYP/6-31G(d,p) suggest Single-I (Figure 2a) and Single-IV (Figure 2d) as the preferential conformations for the silanol-water complex. The calculated binding energy is ranging between -7 and -10 kcal/mol. However, the B3LYP/6-31++G(d,p) binding energy is proposed to be the optimal value because of the following reasons. (i) The B3LYP method is superior to the HF calculation because the electron correlation was included. (ii) The 6-31++G(d,p) basis set is more reliable than the 6-31G(d,p) because the electron diffusion is taken into account. This leads to the conclusion that the two predicted conformations where one water forms hydrogen bonding by pointing the O atom to the silanol (Figure 2a) and two water molecules bind to one silanol in the configuration shown in Figure 4d yield the binding energy of  $\sim 8$  kcal/mol (Table 3).

In terms of the deformation energy, the data for all models in Table 3 are roughly higher than those in Table 1. This indicates clearly that in comparison to the conformations yielded from the HF/3-21G\* optimization (Table 1), the equilibrium geometry of the water molecule and the cluster in the free forms, (water-free) and (cluster-free), shown in Table 2 are closer to those suitable for complexation, (water-cpx) and (cluster-cpx).

**Table 3** Interaction and deformation energies (kcal/mol) representing the complexation between water and single silanol groups in the configurations shown in Figure 2 where the surface optimization and the energy calculations were performed using the same levels of accuracy (see calculation details).

Cluster type	HF/6-31G(d,p)// HF/6-31G(d,p)		HF/6-31++G(d,p)// HF/6-31++G(d,p)		B3LYP/6-31G(d,p)// B3LYP/6-31G(d,p)		B3LYP/6-31++G(d,p)// B3LYP/6-31++G(d,p)	
	$\Delta E_{\text{deform}}$	$\Delta E_{\text{interact}}$	$\Delta E_{\text{deform}}$	$\Delta E_{\text{interact}}$	$\Delta E_{\text{deform}}$	$\Delta E_{\text{interact}}$	$\Delta E_{\text{deform}}$	$\Delta E_{\text{interact}}$
Single-I	0.11	-8.34	0.05	-7.43	0.62	-10.76	0.14	-8.39
Single-II	0.05	-6.33	0.02	-4.78	0.45	-10.11	0.03	-6.03
Single-III	0.02	-1.91	0.01	-1.54	0.39	-3.31	0.01	-2.04
Single-IV*	0.20	-16.05 (-8.02)	0.11	-13.54 (-6.77)	0.85	-22.39 (-11.20)	0.28	-16.15 (-8.08)

\*the binding energy per water molecule is given in parenthesis.

### 3.2 Double silanol complexes

For the sake of accuracy, as stated in the case of Single-I, only the B3LYP/6-31++G(d,p)//B3LYP/6-31++G(d,p) calculations were applied to investigate interaction and optimal configuration between water and the two nearest silanol groups (Figure 3). The optimal values are summarized in Table 4. Note that, the binding between two silanols and one water molecule requires an additional step in rotating of the silanol groups to the configuration suitable for complexation. The rotational energy was included in the  $\Delta E_{\text{deform}}$  of the cluster, defined in equation (2a) which was added to the interaction energy in equation (1).

Some comments should be made concerning the final geometry of the Double-far-I complex. With the initial configuration shown in Figure 3d, the B3LYP/6-

31++G(d,p) fully optimization procedure brings the water molecule to the configuration shown in Figure 4b where the water molecule prefers to coordinate to S3 (see Figure 1d) rather than to S2. Here, the distance from the O atom of water to the O atom of silanol S1 or S3 is 2.90 Å while that of S2 is 3.75 Å. This result supports our assumption made in section 2 (calculation details) that the distance between the two silanols, S1 and S2, in the Double-far is too large to be coordinated by a single water molecule.

In terms of complex stability, the most stable complex takes place via the Double-far-I complex. The corresponding binding energy is -13.84 kcal/mol. This value is significantly lower than those of -9.05 kcal/mol for the Double-far-II and -7.82 kcal/mol for the Double-near-III complexes. In addition, the deformation energies for the double silanol complexes shown in Table 4 are higher than those of the single silanol one in Table 3 due to the addition of the rotational energy into the  $\Delta E_{\text{deform}}$  term, as defined in equation (2a).

The rotational energy for the Double-far configurations is much lower than that of the Double-near complexes due to a larger O-O distance between the two silanols which amounts to 5.75 Å and 3.86 Å, respectively. The strong repulsion between the two OH groups leads to the  $\Delta E_{\text{deform}}$  in the Double-near-I configuration (Figure 3a) of 8.36 kcal/mol. This energy decreases to 5.68 kcal/mol when the two OH groups turn away from each other (Double-near-II, Figure 3b). In addition, the repulsion is lower when the H atom of one OH points toward the O atom of the other OH groups (Figure 3c).

**Table 4** Deformation energy and binding energy (kcal/mol) representing interaction between water and two silanol groups in the configurations shown in Figure 3 where the surface optimization and the energy calculations were performed using B3LYP/6-31++G(d,p) (see calculation details).

Cluster type	$\Delta E_{\text{deform}}$	$\Delta E_{\text{interact}}$	$\Delta E_{\text{binding}}$
Double-near-I	8.36	-14.02	-5.66
Double-near-II	5.68	-3.65	2.03
Double-near-III	2.28	-10.10	-7.82
Double-far-I	0.62	-14.45	-13.84
Double-far-II*	0.25	-17.85	-18.10 (-9.05)

\*with the initial configuration shown in Figure 3d, the optimal structure in Figure 4b was yielded.

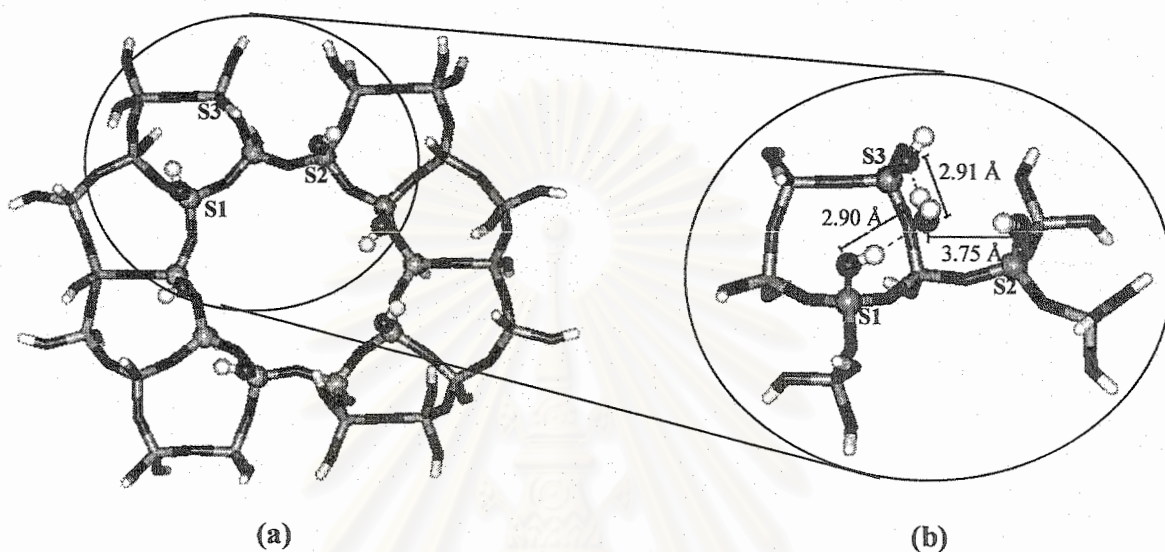


**Figure 4** (a) The (010) surface of silcalite-1 and (b) with the initial configuration shown in Figure 3d, the B3LYP/6-31++G(d,p) fully optimization procedure brings the water molecule to the new configuration where water molecule prefers to coordinate to S3 (see Figure 1d) than that to S2.

Taking into account all the data summarizing above, the B3LYP/6-31++G(d,p) binding energies are in the following order: Double-far-I < Double-far-II ~ Single-I ~ Single-IV ~ Double-near-III. Since the stability of -13.84 kcal/mol for the Double-far-I complex (Figure 3d) is significantly lower than for the other configurations, therefore, these areas on the (010) surface of the silicalite-1 are supposed to be the first binding sites which have to be covered when the water molecule approaches the surface. In the other words, the most stable conformation takes place when a water molecule forms two hydrogen bonds with two silanols, only one lies on the opening pore of the straight channel. When the water loading increases, the next favorable silanols are those of the opening pore in which the complex conformations are Double-far-II, Single-I, Single-

II and Double-near-III where the corresponding binding energy for those coordinations are  $\sim 8$  kcal/mol.

### *3.3 Geometries and vibrational frequencies of single silanol complexes*

In Table 5, intra- and intermolecular geometries as well as spectroscopic properties of water, naked surface and surface-water complexes in the four configurations shown in Figure 2 were summarized. Here, the same method was used to optimize water, naked surface and complex geometries.

For the free water molecule, the geometry yielded from the four models, HF and B3LYP methods with 6-31G(d,p) and 6-31++G(d,p) basis sets, is in good agreement with the experimental measurements (18). The Hartree-Fock O-H bond of  $\sim 0.943$  Å is slightly shorter than the experimental one while the B3LYP value of  $\sim 0.965$  Å is longer than the experimental data. In addition, no significant difference of the O-H bond was found among the two basis sets used. In terms of the H-O-H angle, the B3LYP method is slightly better than the HF in representing the experimental data ( $104.48$  Å). The values for the two symmetrical O-H stretchings of the water molecule obtained from the B3LYP calculations ( $3420$  and  $3426$   $\text{cm}^{-1}$ ) are in good agreement with the  $3345$   $\text{cm}^{-1}$  obtained experimentally. This is not the case for the HF method from which a frequency of more than  $3700$   $\text{cm}^{-1}$  was calculated. The above finding leads to the conclusion that the B3LYP method is appropriate for the geometry optimization and still good enough to reproduce the experimental frequency.



**Table 5** Bond length, bond angle and stretching frequency ( $\nu$ ) of water, naked surface and complex between water and single silanol group (Figure 2) using different methods of calculation where subscripts “s” and “w” stand for surface and water molecule, respectively. The B3LYP/6-31++G(d,p) data, bold character, were proposed to be the optimal values.

Structure	Method	$r(\text{O}_s\text{-H}_s)$ (Å)	$r(\text{O}_s\text{-O}_w)$ (Å)	$r(\text{O}_w\text{-H}_w)$ (Å)	$\langle \text{H}_w\text{-O}_w\text{-H}_w$ (degree)	$\nu\text{O}_s\text{-H}_s$ ( $\text{cm}^{-1}$ )	sym. $\nu\text{O}_w\text{-H}_w$ ( $\text{cm}^{-1}$ )
<b>Water:</b>							
Exp.	Ref. 18	-	-	0.9576	104.48	-	3345
Calc.	HF/6-31G(d,p)	-	-	0.9431	106.04	-	3732
	B3LYP/6-31G(d,p)	-	-	0.9653	103.71	-	3420
	HF/6-31++G(d,p)	-	-	0.9433	107.12	-	3731
	<b>B3LYP/6-31++G(d,p)</b>	-	-	<b>0.9652</b>	<b>105.73</b>	-	<b>3426</b>
	<b>Naked Surface:</b>						
Exp.	Ref. 10	-	-	-	-	3800-3650	-
Calc.	HF/6-31G(d,p)	0.9396	-	-	-	3834	-
	B3LYP/6-31G(d,p)	0.9600	-	-	-	3545	-
	HF/6-31++G(d,p)	0.9399	-	-	-	3833	-
	<b>B3LYP/6-31++G(d,p)</b>	<b>0.9599</b>	-	-	-	<b>3551</b>	-
<b>Complex:</b>							
Exp.	Ref. 19	0.956-1.000	2.70-2.90	-	-	-	-
Calc.							
Single-I	HF/6-31G(d,p)	0.9494	2.8477	0.9434	107.45	3664	3734
	B3LYP/6-31G(d,p)	0.9758	2.7464	0.9640	106.56	3271	3441
	HF/6-31++G(d,p)	0.9485	2.8883	0.9441	107.87	3681	3726
	<b>B3LYP/6-31++G(d,p)</b>	<b>0.9736</b>	<b>2.7958</b>	<b>0.9651</b>	<b>107.34</b>	<b>3310</b>	<b>3434</b>
Single-II	HF/6-31G(d,p)	0.9417	2.9459	0.9442	107.40	3807	3713
	B3LYP/6-31G(d,p)	0.9620	2.8933	0.9675	105.87	3522	3380
	HF/6-31++G(d,p)	0.9422	2.9405	0.9445	107.97	3804	3707
	<b>B3LYP/6-31++G(d,p)</b>	<b>0.9623</b>	<b>2.8772</b>	<b>0.9679</b>	<b>106.91</b>	<b>3524</b>	<b>3371</b>
Single-III	HF/6-31G(d)	0.9438	2.8900	0.9428	106.34	3786	3738
	B3LYP/6-31G(d)	0.9651	2.7200	0.9646	104.67	3489	3430
	HF/6-31++G(d,p)	0.9439	2.9470	0.9432	107.17	3783	3735
	<b>B3LYP/6-31++G(d,p)</b>	<b>0.9649</b>	<b>2.8090</b>	<b>0.9652</b>	<b>106.03</b>	<b>3495</b>	<b>3430</b>

Considering the naked (010) surface (Table 5) represented by the  $\text{Si}_4\text{O}_{13}\text{H}_{10}$  fragment as shown in Figure 1b, the predicted O-H bond of the silanol group is in the range 0.94-0.96 Å. Both O-H stretchings determined from the HF and the B3LYP method are in agreement. The OH stretching modes yielded from the silica and siliceous surfaces are in a broad range ( $3650\text{-}3800\text{ cm}^{-1}$ ) (15) and that of the silicalite-1

surface is not available. Therefore, based on theoretical criteria and the evidence detected for pure water, it can be concluded that the calculated O-H stretching of the silanol group on the (010) surface of the silicalite-1 is  $\sim 3500\text{ cm}^{-1}$ . This value is expected to be slightly higher than the experimental frequency, as in the case of pure water. Note, that there is no significant difference in the vibrational frequencies arising from the same method using different basis sets.

For the silanol-water complex, the attention focused to the Single-I complex where the most stable conformation of the complex was detected. The experimental O-H bond length of the silanol (0.956-1.000 Å) and the intermolecular distance between oxygen atoms of silanol and water molecule,  $O_s\cdots O_w$ , (2.70-2.90 Å) cover broad ranges, including all calculated data. The calculated O-H bond length of the silanol in free form was detected to be slightly larger than that in the complex. This fact is true for all calculated methods and basis sets used. However, such change was not clearly observed for the O-H bond length and the H-O-H angle of the water molecule. In terms of the stretching frequency, the complexation leads to red shift of the O-H stretching of the silanol group, approximately  $150\text{ cm}^{-1}$  and  $270\text{ cm}^{-1}$  for the HF and B3LYP calculations, respectively. This event was not detected for the O-H bond of the water molecule. Taking into account the data and conclusions summarized above including the discrepancy among the methods and the basis sets used, the data obtained from the B3LYP/6-31++G(d,p) were proposed to be the optimal values.

### Acknowledgements

Computing facilities provided by the Computational Chemistry Unit Cell and Computer Center for Advance Research at Faculty of Science, Chulalongkorn University and the Computing Center at the Leipzig University, Germany are gratefully acknowledged. This work was financially supported by the National Research Council of Thailand (NRCT), the Deutsche Forschungsgemeinschaft (DFG) and the Thailand Research Fund (TRF). We thank Dr. Teerakiat Kerdcharoen and Mr. Arthorn Loisruangsin for discussions.

## References

1. M. Chandress, E. B. Webb III, G. S. Grest, M. G. Martin, A. P. Thompson, M. W. Roth, *J. Phys. Chem. B* 105 (2001) 5700.
2. J. A. Z. Pieterse, S. Veefkind-Reyes, K. Seshan, J. A. Lercher, *J. Phys. Chem. B* 104 (2000) 5715.
3. H. Tanaka, S. Zheng, A. Jentys and J. A. Lercher, *Studies of Surface Science and Catalysis* 142 (2002) 1619.
4. N. J. Turro, *Acc. Chem. Res.* 33 (2000) 637.
5. N. J. Turro, X. Lei, W. Li, Z. Liu, M. F. Ottaviani, *J. Am. Chem. Soc.* 122 (2000) 12571.
6. S. H. Park, H. K. Rhee, *Catal. Today* 63 (2000) 267.
7. E. Klemm, H. Scheidat, G. Emig, *Chem. Eng. Sci.* 52 (1997) 2757.
8. J. Aguilar, A. Corma, F. V. Melo, E. Sastre, *Catal. Today* 55 (2000) 255.
9. J. F. Denoyer, G. V. Baron, G. Vanbutsele, P. A. Jacobs, J. H. Martens, *Chem. Eng. Sci.* 54 (1999) 3553.
10. A. Zecchina, S. Bordiga, G. Spoto, L. Marchese, *J. Phys. Chem.* 96 (1992) 4991.
11. M. Trombetta, G. Busca, M. Lenarda, L. Storaro, M. Pavan, *Appl. Catal. A* 182 (1999) 225.
12. T. Armaroli, M. Bevilacqua, M. Trombetta, F. Milella, A. G. Alejandre, J. Ramírez, B. Notari, R. J. Willey, G. Busca, *Appl. Catal. A* 216 (2001) 59.
13. M. Trombetta, T. Armaroli, A. G. Alejandre, J. R. Solis, G. Busca, *Appl. Catal. A* 192 (2000) 125.
14. T. Armaroli, M. Trombetta, A. G. Alejandre, J. R. Solis, G. Busca, *Chem. Phys.* 2 (2000) 3341.
15. T. Kawai, K. Tsutsumi, *Colloid Polym. Sci.* 276 (1998) 992.
16. D. H. Olson, W. O. Haag, W. S. Borghard, *Micropor. Mesopor. Mat.* 35 (2000) 435.
17. M. Trombetta, G. J. Busca, *Catal.* 187 (1999) 521.
18. W. F. Murphy, H. J. Bernstein, *J. Phys. Chem.* 76 (1972) 1147.
19. D. Nyfeler, T. Armbruster, *American Mineralogist* 83 (1998) 119.

## VITAE

**NAME:** Oraphan Saengsawang

**DATE AND PLACE OF BIRTH:** 14 December 1979 in Samut Sakhon, Thailand

**ELEMENTARY SCHOOL:**

1987-1993: Somrudee School, Samut Sakhon

**SECONDARY SCHOOL:**

1993-1996: Sirindhorn Ratchawittalai School, Nakorn Pathom

1996-1998: Mahidolwitthayanusorn School, Nakorn Pathom

**UNIVERSITY EDUCATION:**

1998-2002: B. Sc. in Chemistry, Department of Chemistry, Faculty of Science,  
Chulalongkorn University, Bangkok

2002-2004: M. Sc. in Physical Chemistry, Department of Chemistry, Faculty of  
Science, Chulalongkorn University, Bangkok

สถาบันวิทยบริการ  
จุฬาลงกรณ์มหาวิทยาลัย